UNIVERSITY OF ALBERTA

Elemental Speciation by Negative Ion Electrospray Mass Spectrometry

BY

David Barnett

A thesis submitted to the Faculty of Graduate Studies and Research in partial fulfillment of the requirements for the degree of **Doctor of Philosophy**.

DEPARTMENT OF CHEMISTRY

Edmonton, Alberta, Canada

Spring, 1999

National Library of Canada
Acquisitions and Bibliographic Services
395 Wellington Street
Ottawa ON K1A 0N4
Canada

Bibliothèque nationale du Canada
Acquisitions et services bibliographiques
395, rue Wellington
Ottawa ON K1A 0N4
Canada

Your file Votre référence

Our file Notre référence

The author has granted a non-exclusive licence allowing the National Library of Canada to reproduce, loan, distribute or sell copies of this thesis in microform, paper or electronic formats.

L'auteur a accordé une licence non exclusive permettant à la Bibliothèque nationale du Canada de reproduire, prêter, distribuer ou vendre des copies de cette thèse sous la forme de microfiche/film, de reproduction sur papier ou sur format électronique.

The author retains ownership of the copyright in this thesis. Neither the thesis nor substantial extracts from it may be printed or otherwise reproduced without the author's permission.

L'auteur conserve la propriété du droit d'auteur qui protège cette thèse. Ni la thèse ni des extraits substantiels de celle-ci ne doivent être imprimés ou autrement reproduits sans son autorisation.

0-612-39502-2

Canada

UNIVERSITY OF ALBERTA

LIBRARY RELEASE FORM

NAME OF AUTHOR:	**David Barnett**
TITLE OF THESIS:	**Elemental Speciation by Negative Ion Electrospray Mass Spectrometry**
DEGREE:	**Doctor of Philosophy**
YEAR THIS DEGREE GRANTED:	**1999**

Permission is hereby granted to the University of Alberta Library to reproduce single copies of this thesis and to lend or sell such copies for private, scholarly or scientific research purposes only.

The author reserves all other publication rights and other rights in association with the copyright in the thesis, and except as hereinbefore provided neither the thesis nor any substantial portion thereof may be printed or otherwise reproduced in any material form whatever without the author's prior written permission.

RR#1 Dorchester

New Brunswick

Canada, E0A 1M0

Date: November 27, 1998

UNIVERSITY OF ALBERTA

FACULTY OF GRADUATE STUDIES AND RESEARCH

The undersigned certify that they have read, and recommend to the Faculty of Graduate Studies and Research for acceptance, a thesis entitled **Elemental Speciation by Negative Ion Electrospray Mass Spectrometry** submitted by **David Barnett** in partial fulfillment of the requirements for the degree of **Doctor of Philosophy**.

Dr. Gary Horlick, supervisor

Dr. Frederick Cantwell

Dr. Mark McDermott

Dr. Arthur Mar

Dr. Xiao-Chun Le

Dr. Gary Hieftje

Date: November 24, 1998

Abstract

The use of Electrospray Mass Spectrometry, ESMS, for elemental speciation of anionic solution components is presented. Halogenic ions were detected at the part-per-billion level in methanolic solution by employing 0.1 mM levels of inert electrolyte to establish a stable electrospray phenomenon. The stabilizing electrolyte was also used as an internal standard to account for changes in the ES source, variations in solvent composition, and analyte suppression caused by high background electrolyte concentrations. Application of standard additions methodology and matrix matching were necessary to correct for large deviations in analyte sensitivity in the presence of cationic surfactants, caused by changes to droplet surface characteristics and ion pair formation.

Analysis of several cationic metal species was accomplished by converting metal ions to anionic complexes of EDTA. Mass spectra were significantly simplified by eliminating species observed in positive-ion spectra of multiply charged metal ions, including gas phase charge reduction, metal oxide formation and metal-counter ion interactions. Collision induced dissociation, CID, in the mass spectrometer vacuum interface was an important variable used to affect the desolvation, charge state, aggregation, and fragmentation of EDTA complexes.

Direct determination of inorganic and organic forms of selenium in methanol resulted in identification of a selenite derived methyl seleno-ester. Isotopic overlaps of this species with biselenate poses a severe spectral interference. Sensitive determination of seleno-amino acids is shown to require careful optimization of solution acidity or

basicity, depending on the ionic form of interest. Development of an aqueous electrospray interface was investigated to simplify the selenium spectral interference and pH control of sample solutions. Preliminary results for positive ions, using a sheath electric field, analogous to the sheath gas used for ion spray, resulted in comparable sensitivity and stability previously observed for methanolic solutions.

Acknowledgements

I would like to thank my supervisor, Dr. Gary Horlick, my parents Allan and Joyce and my Aunt Dorothy for their support and encouragement over the last few years.

Financial support provided by the Department of Chemistry at the University of Alberta, and the National Science and Engineering Research Council (NSERC) is also gratefully acknowledged.

Table of Contents

Chapter		Page
1	**Introduction**	
1.1	Objective	2
1.2	Electrospray	4
	1.2.1 Electrospray Mechanism	5
	1.2.2 Electrospray Current	7
	1.2.3 Electrolytic Nature of Electrospray	11
	1.2.4 Generation of Gas Phase Ion-Solvent Clusters	11
	1.2.5 Ionspray	13
1.3	Electrospray Mass Spectrometry	15
	1.3.1 Electrospray Interface	15
	1.3.2 Collision Induced Dissociation	15
1.4	References	19
2	**Instrumentation**	26
2.1	Introduction	27
2.2	Electrospray	27
	2.2.1 Source	27
	2.2.2 Interface	29
	2.2.3 Curtain Gas	32
2.3	Mass Spectrometer	34
2.4	Spectrum and Data Acquisition	36
2.5	References	38

3	**Quantitative Electrospray Mass Spectrometry of Halides and Halogenic Anions**	39
3.1	Introduction	40
3.2	Experimental	41
	3.2.1 Reagents	42
3.3	Results and Discussion	42
	3.3.1 Halide Spectra	42
	3.3.2 Quantitation	46
	3.3.3 Solvent Composition	49
	3.3.4 Effect of Multiply Charged Ions	53
	3.3.5 Chlorine Speciation	55
	3.3.6 Bromate Analysis	58
	3.3.7 Detection Limits	60
	3.3.8 Fluoride Analysis	60
3.4	Conclusions	70
3.5	References	71
4	**Determination of Metals as EDTA Complexes**	74
4.1	Introduction	75
4.2	Ethylenediaminetetraacetic Acid (EDTA)	77
4.3	Experimental	82
	4.3.1 Mass Spectrometry	82
	4.3.2 Quantitation	82
	4.3.3 Atomic Emission Spectrometry	82
	4.3.4 Reagents	84
	4.3.5 Sample Preparation	84
4.4	Results and Discussion	84
	4.4.1 EDTA Spectra	84
	4.4.2 Divalent Metal Complexes	91
	4.4.2.1 Alkaline Earth Metals	92

4.4.2.2 Copper Sulfate and Cobalt Bromide 92
4.4.2.3 Zinc Nitrate 95
4.4.2.4 Mercuric Nitrate 97
4.4.2.5 Vanadium (VO^{2+} *versus* VO_2^+) 97
4.4.3 Trivalent Metal Complexes 101
4.4.3.1 Aluminum Nitrate 101
4.4.3.2 Praseodymium, Gadolinium and Lutetium 106
4.4.3.3 Samarium and Dysprosium 106
4.4.3.4 Iron (Fe^{2+} *versus* Fe^{3+}) 110
4.4.4 Quantitation of Calcium 112
4.5 Conclusions 119
4.6 References 121

5 Direct Speciation of Selenium 123

5.1 Introduction 124
5.2 Experimental 126
5.2.1 Reagents 126
5.3 Results and Discussion 128
5.3.1 Inorganic Selenium 128
5.3.1.1 Selenate 128
5.3.1.2 Selenite 132
5.3.1.3 Solvent Study: Confirmation of Seleno-Ester Formation 132
5.3.1.4 Analysis of a Mixture of Selenate and Selenite 138
5.3.1.5 Mass Spectral Dependence on Solution pH: Inorganic Selenium 141
5.3.1.6 High Energy Collision Induced Dissociation 141
5.3.2 Organic Sulfur Compounds 144
5.3.2.1 Methionine 144
5.3.2.2 Cysteine 146
5.3.3 Organoselenium Compounds: Seleno-Amino Acids 153

5.3.3.1 Selenomethionine 153
5.3.3.2 Selenocysteine 160
5.4 Conclusions 160
5.5 References 163

6 Aqueous Electrospray Mass Spectrometry 166

6.1 Introduction 167
6.2 Experimental 169
6.2.1 Aqueous Electrospray Design 170
6.3 Results and Discussion 174
6.3.1 Operational Parameters 174
6.3.2 Lithium and Potassium Chloride 175
6.3.3 Cobalt Bromide 177
6.3.4 Lanthanum Nitrate 180
6.4 Conclusions 182
6.5 References 184

7 Conclusions 185

7.1 Summary 186
7.2 Future Work 189
7.2.1 Instrument Modifications 189
7.2.2 Qualitative Analysis 190
7.2.3 Quantitative Analysis 190
7.3 References 192

List of Tables

Table		Page
2.01	Operating parameters for positive and negative ion electrospray mass spectrometry on the modified ELAN 250 ICP-MS.	33
3.01	Prominent background species observed for negative ion electrospray mass spectrometry using methanol/water solvent.	47
3.02	Detection limits and analytical figures of merit for several anionic species by electrospray mass spectrometry.	63
3.03	Determination of fluoride in various synthetic and commercial mouthwash samples.	66
4.01	Formation constants, K_f, for several metal-EDTA complexes.	79
4.02	Fraction of EDTA in Y^{4-} form at various pH values.	80
4.03	Electrospray interface operating conditions for the modified ELAN 250 ICP-MS and the API 100 LC/MS.	83
4.04	Determination of calcium by EDTA complexation coupled with electrospray mass spectrometric detection and by flame atomic emission spectrometry in tap water and a commercial calcium supplement.	120

List of Figures

Figure		Page
1.01	Schematic profile of a stainless steel electrospray capillary with (a) low and (b) high applied voltage relative to a ground planar electrode.	6
1.02	Current response as a function of applied potential for negative ion electrospray of 0.1 mM KCl solution.	9
1.03	Schematic illustration of the mechanism responsible for generation of gas-phase ion solvent species from electrosprayed droplets.	14
1.04	Schematic diagram of the electrospray interface to the mass spectrometer.	16
2.01	Electrospray needle design (not drawn to scale).	28
2.02	Schematic diagram of the electrospray interface to the mass spectrometer.	30
2.03	Electrospray interface components I) front plate, II) spacer, III) sampling plate and IV) skimmer cone.	31
2.04	Schematic diagram of the modified ELAN 250 ICP-MS.	35
3.01	Electrospray mass spectra of a 0.1mM methanolic solution of fluoride, chloride, bromide and iodide acquired with varying ΔV settings: (a) -15 V, (b) -20 V and (c) -40 V.	43
3.02	Cartoon depicting relative ionic and hydrated radii of fluoride and iodide ions.	45
3.03	Attempted analytical curve for bromide in methanol using the ^{79}Br isotope, $\Delta V = -35$ volts.	48
3.04	Signal intensities of bromide (▲, ^{79}Br) and 0.1mM iodide (△, ^{127}I) plotted as a function of increasing bromide concentration, ΔV = -35 volts.	50
3.05	Analytical curves for (a) bromide and (b) fluoride employing 0.1mM iodide as an electrospray stabilizer and internal standard, ΔV = -35 volts.	51
3.06	Effect of increasing water content on signal intensities of bromide (△) iodide (◇) and the signal ratio (◆) in methanolic solution, ΔV = -35 volts.	52

Figure		Page
3.07	Effect of multiply charged metal ions on free gas-phase chloride ion concentrations: (a) 0.1 mM calcium chloride, (b) 0.1 mM ferric chloride and (c) 0.1 mM potassium chloride in the presence of 0.1mM zinc nitrate (ΔV = –45 volts).	54
3.08	Electrospray mass spectra of a 0.1 mM methanolic solution of chloride, chlorate, and perchlorate acquired at varying values of ΔV: (a) -34V, (b) -54 V and (c) -74 V.	56
3.09	Effect of increasing sampling plate to skimmer potential difference, ΔV, (skimmer cone voltage = -5 volts) on (a) perchlorate ion speciation and (b) oxygen radical ion signal intensity.	57
3.10	Multiple component analytical curves for chlorine (▲), chlorate (▽) and perchlorate (◆). A 0.1 mM level of iodide was employed as the electrospray stabilizer and internal standard, (ΔV = -34 volts).	59
3.11	Fractional composition diagram for 0.1 mM bromate (BrO_3^-) as a function of increasing sampling plate to skimmer potential (skimmer = -6 volts).	61
3.12	(a) Signal intensities of bromate (◆, $^{79}BrO_3^-$) and 0.1 mM formate (◇, HCO_2^-) ions as a function of increasing bromate concentration and (b) Analytical curve for bromate employing formate as the electrospray stabilizer and internal standard.	62
3.13	Analytical curve for fluoride employing 0.1mM level of iodide as internal standard and electrospray stabilizer.	64
3.14	Standard addition calibration plots for the two commercial mouthwash samples (◆, Oral-B®) and (◇, Cepacol®) employing iodide as the internal standard and electrospray stabilizer.	67
3.15	(a) Structure of cetylpyridinium chloride and (b) the predicted droplet structure and liberated fluoride ion species in the presence of a cationic surfactant.	69
4.01	(a) Structure of ethylenediaminetetraacetic acid, EDTA, and (b) fractional composition diagrams for EDTA species as a function of aqueous pH.	78
4.02	Mass spectra of 0.1 mM of the disodium salt of EDTA acquired on the ELAN 250 with (a) no sodium hydroxide added and (b) 0.1mM sodium hydroxide added, ΔV = –45 volts.	85
4.03	Mass spectrum of 0.1mM of the disodium salt of EDTA acquired on the ELAN 250 with 0.1mM potassium hydroxide added, ΔV = –35 volts.	87

Figure		Page
4.04	Series of mass spectra of the disodium salt of EDTA (0.1mM) with varying levels of sodium hydroxide added (a) 0.2 mM, (b) 0.02 mM and (c) 0.0 mM in methanol. Spectra were acquired on the SCIEX API-100 LCMS with $\Delta V = -50$ volts.	89
4.05	Series of mass spectra of the disodium salt of EDTA acquired on the SCIEX API-100 LCMS at ΔV settings of: (a) 0 volts, (b) -20 volts and (c) -50 volts.	90
4.06	Mass spectrum of the alkaline earth metals (0.02mM Be, Ca, Mg, Sr and Ba) in 0.12mM Na_2EDTA and 0.1mM NaOH in methanol, $\Delta V = -40$ volts.	93
4.07	Mass spectra of a) 0.08 mM cobalt bromide and b) 0.08 mM copper sulfate with 0.1mM Na_2EDTA at approximately pH 9.5 in methanol.	94
4.08	Mass spectrum of (a) 0.1 mM zinc nitrate and 0.01 mM Na_2EDTA and (b) 0.1mM zinc nitrate and 0.12 mM Na_2EDTA in methanol, $\Delta V = -35$ volts.	96
4.09	Mass spectrum of 0.08 mM $Hg(NO_3)_2$ and 0.1 mM Na_2EDTA acquired on the SCIEX API-100 LCMS, $\Delta V = -20$ volts.	98
4.10	Mass spectra of (a) 0.08 mM sodium vanadate and (b) 0.08mM vanadyl sulfate in 0.1 mM Na_2EDTA. $\Delta V = -35$ volts.	100
4.11	Mass spectrum of 0.08 mM aluminum nitrate and 0.1 mM Na_2EDTA acquired on the SCIEX API-100 LCMS, $\Delta V = 0$ volts.	102
4.12	Series of mass spectra of 0.08 mM aluminum nitrate and 0.1mM Na_2EDTA acquired on the SCIEX API-100 LCMS at varying ΔV settings: (a) -20 volts, (b) -50 volts and (c) -100 volts.	104
4.13	Mass spectrum of an equimolar mixture (0.03 mM) of aluminum, gallium and indium in 0.1mM Na_2EDTA acquired on the SCIEX API-100 LCMS, $\Delta V = -20$ volts.	105
4.14	Mass spectra of (a) 0.2 mM of each of the three metals acquired under bare metal ion conditions on the Elan 250 (adapted from Anal. Chem. 66 (22) **1996**, 3983-3993) and (b) 0.02 mM praseodymium, 0.04 mM gadolinium and 0.02 mM lutetium with 0.1 mM Na_2EDTA acquired on the SCIEX API-100 LCMS.	107
4.15	Mass spectra of a) 0.1mM samarium and b) 0.1mM dysprosium prepared by 1000-fold dilution of ICP standards containing 2% nitric acid into methanol with 0.1mM Na_2EDTA present. Spectra acquired on SCIEX API-100 LCMS, $\Delta V = -20$ volts.	108

Figure		Page
4.16	Mass spectrum of 0.04 mM ferric chloride, 0.04 mM ferrous ammonium sulfate and 0.1mM Na_2EDTA acquired on the SCIEX API-100 LCMS, ΔV = -20 volts.	111
4.17	Mass spectrum of 0.08 mM calcium chloride, 0.1 mM sodium hydroxide and 0.1mM Na_2EDTA acquired on the SCIEX API-100 LCMS, ΔV = –45 volts.	113
4.18	a) Observed signal intensities of chloride and CaY^{2-} as a function of increasing sodium hydroxide concentration and (b) signal intensity ratio of CaY^{2-} to chloride for a mixture of 0.05mM $CaCl_2$ and 0.1mM Na_2EDTA.	114
4.19	Structure and acid equilibria of calmagite indicator	116
4.20	Electrospray mass spectrum of 0.01 mM calmagite indicator in the HIn^{2-} form acquired on the Elan 250 with 0.15 mM sodium hydroxide and 0.1 mM Na_2EDTA.	117
4.21	Simulated titration of 0.1 mM calcium chloride with EDTA in the presence of calmagite indicator with ESMS detection.	118
5.01	Natural isotope abundance of elemental selenium.	127
5.02	Chemical structures of the selenium compounds of interest in this study.	129
5.03	(a) Mass spectrum of 0.1 mM sodium selenate in methanol, ΔV = -29 volts (b) pH dependent fractional composition plot for selenate.	130
5.04	(a) Mass spectrum of 0.1 mM sodium selenite in methanol, ΔV = -29 volts (b) pH dependent fractional composition plot for selenite.	131
5.05	Electrospray mass spectra of 0.1 mM sodium selenite in (a) deuterated methanol, (b) ethanol and (c) isopropanol.	133
5.06	Mass spectrum of 0.1 mM sodium sulfite and sodium sulfate in methanolic solution, ΔV = –29 volts.	135
5.07	Calculated isotopic overlap between selenate ($HSeO_4^-$) and the methyl seleno-ester ($CH_3OSeO_2^-$).	136
5.08	Mass spectrum of 0.1 mM sodium selenite and 0.3 mM sodium selenate in ethanol.	137
5.09	Mass spectrum of a mixture of 0.2 mM sodium selenite and sodium selenate in methanol, ΔV= –24 volts.	139
5.10	Electrospray mass spectra of a mixture of 0.2 mM sodium selenite and 0.2 mM sodium selenate in methanol with ΔV set to (a) –19 volts, (b) –14 volts.	140

Figure		Page
5.11	Electrospray mass spectra of a mixture of 0.2 mM sodium selenite and sodium selenate in methanol at high values of ΔV; (a) –96 volts and (b) –194 volts.	142
5.12	Fractional composition diagrams for (a) methionine and (b) cysteine as a function of pH.	145
5.13	Negative and positive mode electrospray mass spectra of 0.1 mM methionine, ΔV = ± 29 volts.	147
5.14	Negative and positive mode electrospray mass spectra of 0.1 mM cysteine hydrochloride, ΔV = ± 29 volts.	148
5.15	Mass spectra of 0.1 mM cysteine hydrochloride with varying levels of sodium hydroxide added; (a) 0.1 mM, (b) 0.2 mM and (c) 0.35 mM, ΔV = ± 29 volts.	150
5.16	Diagram showing various forms of cysteine present in solution as a function of varying pH.	151
5.17	Mass spectra of 0.1mM cysteine hydrochloride with various levels of sodium hydroxide added.	152
5.18	Fractional composition diagrams for (a) selenomethionine and (b) selenocysteine as a function of pH.	154
5.19	Mass spectra of (a) 0.26 mM selenomethionine and (b,c) fragment ions acquired with ΔV = 34 volts.	155
5.20	Negative ion mass spectrum of 0.26 mM selenomethionine in methanol, ΔV = – 29 volts.	156
5.21	Effect of hydrochloric acid and sodium hydroxide on the determination of selenomethionine by (a) positive and (b) negative mode electrospray mass spectrometry.	158
5.22	Diagram of various forms of selenomethionine present in solution (A,B,C) and in the gas-phase (D,E,F,G) as a function of varying aqueous solution pH.	159
5.23	Positive mode electrospray mass spectrum of 0.22 mM selenocysteine.	162
6.01	(A) Modified electrospray design and (B) expanded view of the plumbing within the Valco tee union.	170
6.02	Expanded view of the electrospray tip and support capillary arrangement.	172
6.03	The syringe to fused silica capillary connection.	173

Figure		Page
6.04	Mass spectra of (a) 1 mM lithium chloride and (b) 1 mM potassium chloride in distilled, deionized water, ΔV = 18 volts.	176
6.05	(a) Mass spectra of 1 mM potassium chloride in distilled, deionized water, (ΔV = 193 volts) (b) an expanded spectrum for the 10 to 70 *m/z* range.	178
6.06	Mass spectrum of 1 mM cobalt bromide in distilled, deionized water, (ΔV = 55 volts).	179
6.07	Mass spectra of 1 mM lanthanum nitrate in distilled, deionized water at ΔV settings of (a) 73 and (b) 293 volts.	181

Chapter 1

Introduction

1.1 Objective

The importance of elemental speciation in toxicity, bioavailability and transport through soil and water systems has become increasingly apparent within the last decade. Requirements for elemental speciation have resulted in coupling of element selective detectors with a wide variety of separation techniques, of which high performance liquid chromatography, HPLC, has been the most widely used. Separation techniques may be used to effectively remove analytes from complex matrices and separate inert forms of the same element prior to detection. Commonly used element-selective detectors are based on atomic absorption, atomic emission and mass spectrometry.

The inductively coupled plasma, ICP, is the predominant ion source for emission and mass spectrometric analyses [1-5] because of relatively few chemical interferences and insensitivity to difficult sample matrices. Although combinations such as HPLC-ICP-MS offer high element selectivity and trace detection capabilities, species identification is based solely on comparison of chromatographic retention times with those of available standards [6-8]. When the composition of samples is unknown, instances in which chromatographic peaks are not successfully identified are common [9, 10]. Solutions to this problem have involved development of extensive libraries of chemical substances or collection of separated fractions of the unknown species and analyzing the fractions by other methods when possible. A less tedious solution to the problem of species identification is the development of more flexible ion sources, which are capable of providing both elemental and molecular detection capabilities. A successful example of such an approach that has been widely adopted for volatile, thermally stable organometallic samples is gas chromatography coupled to mass spectrometry [11]. In comparison, electrospray mass spectrometry is a technique with similar potential that is still in its infancy for speciation in elemental analysis.

Electrospray mass spectrometry is a technique that was first introduced concurrently by Fenn [12, 13] and Aleksandrov [14] in 1984. During the last decade, electrospray has been used extensively and relatively exclusively for the identification of large

polar organic compounds of low volatility. However, a survey of recent literature reveals an increasing number of reports of the use of both electrospray and ionspray, a pneumatically assisted version of electrospray, as sources for mass spectrometric analyses of several monatomic and molecular species [15-21]. Kebarle and co-workers [22-25] pioneered the field of elemental analysis by electrospray with their observations of divalent and trivalent metal ions in the gas phase. Following their initial observations, several other studies of uncomplexed metal ions have appeared in the literature [16, 26-37]. In addition, there have been several recent studies related to speciation, including various inorganic anions [38-41], transition metal complexes [19, 42-49], metal ions coordinated to biological molecules [50-55] and organometallics [20, 56-58]. The recent explosive growth of ESMS in characterization of synthetic inorganic complexes also suggests that ESMS may soon rival nuclear magnetic resonance spectroscopy, NMR, and X-ray crystallography as a characterization method for inorganic species.

In addition to the tremendous potential of electrospray to perform speciation analysis, it offers other advantages over classical atomic detection methods. Presently, the most widely used atomic source is the argon-based ICP, which despite its widespread applications in mass spectrometry has several limitations. High levels of plasma generated background ions can result in severe spectral interferences for several elements with atomic masses lower than 80 amu. For example, the presence and intensity of argides (e.g. ArC^+, ArO^+ and $ArCl^+$) can vary significantly between sample matrices, which can lead to erroneous analytical results in the analysis of chromium, iron and arsenic, respectively. In addition, the efficiency of analyte ionization is highly dependent on ionization potential, which results in poor detection capabilities for several nonmetals including the halogens [59, 60]. On a practical note, conventional plasma mass spectrometry generally requires high sample volumes, of which up to 98% is lost as waste, resulting in equally large volumes of waste to be disposed. The plasma also requires large quantities of argon gas resulting in an operational expense that may be a prohibitive factor for small analysis labs, particularly those located in remote locations.

The objective of this study was to use electrospray to target what have been regarded classically as problem elements for analysis by conventional sources. Unlike an ICP source, which produces ions from a nebulized sample solution *via* the energetic processes of desolvation, atomization and ionization in a harsh thermal environment, electrospray transfers pre-existing ions from solution directly to the gas phase. This rather gentle ion transfer process eliminates losses in sensitivity caused by poor ionization efficiencies and at the same time affords direct identification of molecular ions of these elements without recourse to chromatographic separation. Electrospray is often referred to as an ion source though it is not in the classical atomic sense. With that said, it is important to point out that many polar, neutral molecules may become charged *via* proton or cation attachment in the gas-phase [61-64] or by redox reactions within the ES capillary [65-68].

1.2 Electrospray

The phenomenon of electrospray has been known for several years and used for a multitude of applications. The first published report detailing the observation of electrospray is attributed to Zeleny [69] in 1914. Another publication by Zeleny in 1917 [70] included impressive photographs and details of various operational modes of electrospray. Several fundamental studies [71-95] of the ES phenomenon have ensued from his preliminary work and have been instrumental in its development as both a liquid spraying technique and an ion source for mass spectrometry and ion mobility. Among the more notable industrial applications of electrospray in this century are paint and crop spraying, electrostatic printing and fuel atomization.

Dole and co-workers [96] were the first to attempt to measure charged particles produced by electrospray in 1968. Their goal was to produce a molecular beam of macro-ions and characterize it by ion mobility spectrometry. It was not, however, until Fenn and co-workers [97] reported convincing results for large thermally labile molecules in 1989 that ESMS gained widespread attention. The high sensitivity of the electrospray technique and compatibility with liquid separation methods gave rise to much interest in ESMS. The explosion of interest in electrospray however was

initiated by the observation that high molecular mass compounds could be multiply charged with great efficiency and readily detected on instrumentation previously considered to be of low mass range. Since 1989, the volume of research in organic ESMS has risen exponentially. The field of inorganic ESMS has attracted much less attention for analytical applications. This is due primarily to the fact that there are already several established methods for elemental analysis that have proven to be sensitive, reliable and widely applicable for metal analyses including ICP-OES and ICP-MS. However, since electrospray is tuned to impart only the energy necessary to disperse a low flow of electrolytic solution into a mist of fine droplets, this source may be used to preserve chemical information about solution components including valence state, complexation and molecular form of both cations and anions.

1.2.1 Electrospray Mechanism

Electrospray consists of pumping a low flow of electrolytic solution through a narrow bore stainless steel capillary that is biased to a high potential relative to a counter electrode. A schematic of a generic electrospray configuration is shown in Figure 1.01. When a potential is applied to the capillary, an electric field exists between the capillary tip and counter electrode. The magnitude of the electric field (E) at the capillary tip may be approximated by Equation 1.01.

$$E \approx \frac{2V}{r_c \ln(4d/r_c)} \qquad 1.01$$

where V is the potential applied to the capillary, r_c is the outer radius of the capillary and d is the capillary to counter electrode separation. Under the influence of an electric field, the liquid surface will become charged by an electrophoretic mechanism [98]. Electrophoresis is defined as the migration of ions in solution due to an electric field. The result of electrophoretic migration of solution ions is a partial separation of charge at the liquid surface. When a negative voltage is applied to the capillary, negative ions will migrate towards low field, i.e. the liquid surface, and positive ions will migrate away from the surface, toward the capillary. The resulting

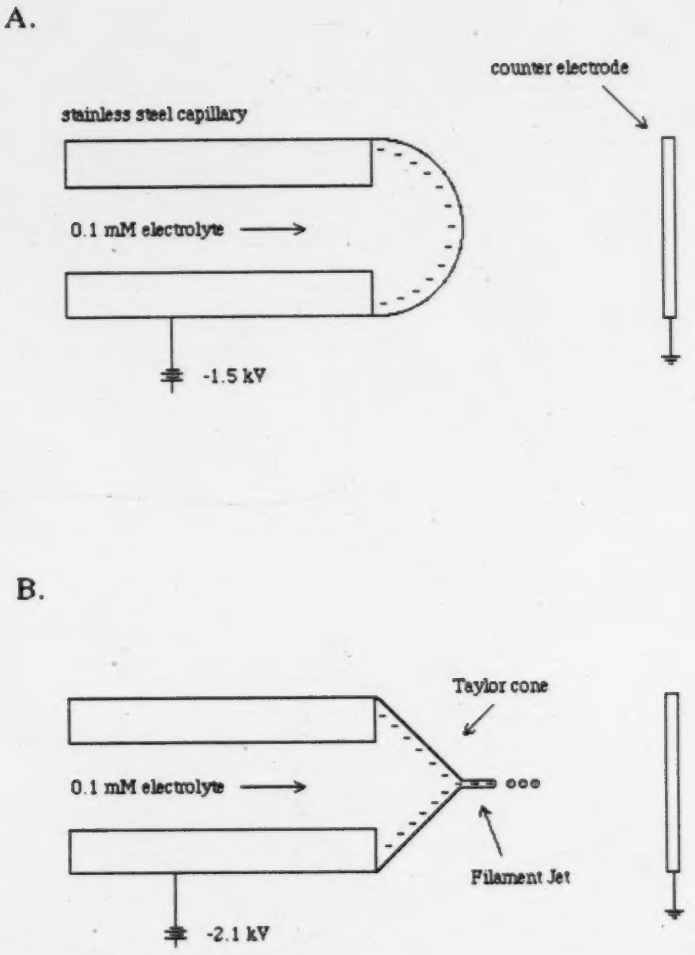

Figure 1.01 Schematic profile of a stainless steel electrospray capillary with (a) low and (b) high applied voltage relative to a ground planar electrode.

excess of negative ions on the surface of the liquid leaving the capillary is shown in Figure 1.01a. When the applied voltage is sufficiently high, the magnitude of charge separation causes a large enough excess of negative ions at the liquid surface to destabilize the surface and lead to emission of negatively charged droplets from the apex of a well-defined cone, shown in Figure 1.01b. Taylor [81] was the first to describe this cone in detail. The voltage required to obtain the Taylor cone and droplet emission in electrolytic solutions is designated V_{on}, and may be approximated by equation 1.02.

$$V_{on} \approx -\left(\frac{\gamma r_c \cos\theta}{2\varepsilon_o}\right)^{1/2} \ln\left(\frac{4d}{r_c}\right) \qquad 1.02$$

where γ is the liquid surface tension, θ is the Taylor cone angle and ε_o is the relative permittivity of vacuum or "free space". It is important to make note of the effect of liquid surface tension from this equation. It is observed that charged droplets emanate from the apex of the cone only when the repulsive forces due to the surface charge excess exceed the binding forces of surface tension. For this reason, polar solvents of low surface tension such as acetonitrile, methanol or isopropyl alcohol are generally used as electrospray solvents rather than water. Binary or ternary mixtures of these solvents and water are also commonly used for electrospray.

1.2.2 Electrospray Current

When an electrospray source is operated under stable conditions, which may be characterized by the presence of a Taylor cone, it is capable of delivering a continuous mist of charged droplets to the counter electrode. These charged droplets result in a current, ions or coulombs per unit time, that may be measured at the tip or the counter electrode. Typical values of the current range from 0.05 – 0.1 μA for 10^{-5} – 10^{-3} M dissolved electrolyte in methanolic solution. Fernandez de la Mora and Loscertales [80] have measured the current reaching the counter electrode and related it to experimental parameters given by equation 1.03.

$$I = f\left(\frac{\varepsilon}{\varepsilon_0}\right)\left(\gamma K V_f \frac{\varepsilon}{\varepsilon_0}\right)^{1/2} \qquad 1.03$$

where $f(\varepsilon/\varepsilon_0)$ is a numerical function tabulated by Fernandez de la Mora and Loscertales, K is the conductivity of solution, V_f is the volume flow rate, ε is the permittivity of solution and ε_0 is the permittivity of vacuum.

Stewart and Horlick [99] also measured electrospray current as a function of applied voltage and related the current to various voltage induced electrospray operational modes for a series of potassium chloride solutions in methanol. Figure 1.02 is a plot of measured current reaching the counter electrode as a function of the applied potential for a 0.1 mM solution of potassium chloride, reproduced from that work. From the figure it is observed that the current emitted in the form of solution ions from a charged capillary increases in rather discrete steps with increasing applied voltage. By observing the electrospray visually while measuring the current, the authors identified several separate functioning modes of the electrospray source that matched the observed changes in current. At low voltages, large droplets were emitted periodically from the capillary tip in what was referred to as a pulsed droplet mode. Moderate increases in the applied voltage increased the frequency of the droplets while decreasing their relative size. A further increase in the applied voltage resulted in a sharp increase in the observed current as the electrospray was observed to abruptly take the shape of a Taylor cone. The Taylor cone mode results in much higher current since it produces smaller droplets with higher surface charge to volume ratios. The cone was observed to be stable over a 300V window. However the cone's length decreased with increasing voltage. The result of further increases in the applied voltage is a bifurcated mode, which consists of two spray origins positioned on opposite sides of the capillary. The discharge condition results in the highest current but a rather unstable spray of liquid. Discharge consists of direct emission of electrons from the capillary tip, which ionize ambient gaseous molecules including atmospheric gases such as oxygen and volatile electrospray solvent. It is generally a greater concern for negative rather than positive ion studies since the capillary is

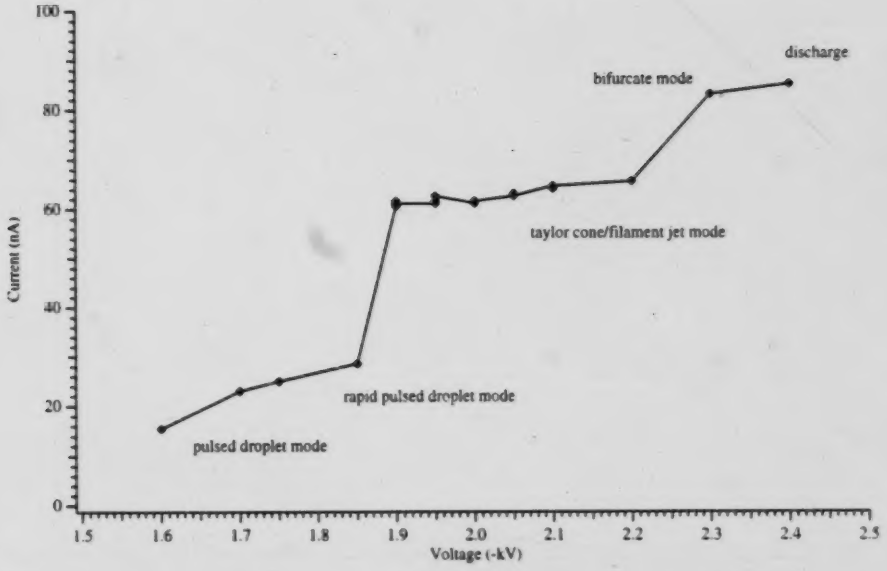

Figure 1.02 Current response as a function of applied potential for negative ion electrospray of 0.1 mM KCl solution (reproduced with permission from [99]).

biased to a high negative potential and is thus electron rich. Reduction of the tendency towards discharge generally involves using smooth, uniform capillary tips, volatile solvents and low voltages. There have also been reports of the addition of such discharge suppressing gases as O_2, CO_2, and SF_6 to the region surrounding the electrospray capillary with varied levels of success in preventing discharge [100-102].

While the measurement of current is useful for defining stable operation of the electrospray source, it does not correlate with mass spectrometrically detected ion currents even for pure standard solutions as reported by Kebarle and Tang [95]. The reason for the lack of correlation may be understood by considering the effects of flow rate and solution conductivity on droplet size and charge. Fernandez de la Mora and Loscertales [80] derived expressions to approximate the initial droplet radius and the charge resulting from stable Taylor cone operation of electrospray. These expressions are given below as equations 1.04 and 1.05,

$$R \approx \left(\frac{V_f \varepsilon}{K}\right)^{1/3} \qquad 1.04$$

$$q \approx 0.7[8\pi(\varepsilon_o R^3 \gamma)^{1/2}] \qquad 1.05$$

where R is the droplet radius and q is the droplet charge. These equations show that droplet volume, $V_d = 4/3\pi R^3$, increases linearly with flow rate and is inversely proportional to conductivity, while the initial droplet charge increases with $V_d^{1/2}$. This means that charge densities will decrease with increasing flow rates. The efficiency of ion liberation from charged droplets decreases with decreasing charge densities, leading to lower mass spectrometric ion currents. Typical electrospray droplets generated from a stable Taylor cone have diameters in the range of 1-2 μm and overall charges of approximately 10^{-14}C.

1.2.3 Electrolytic Nature of Electrospray

In order to explain how charge neutrality is maintained in the analyte bulk solution, Kebarle et al. [103] proposed that electrospray operates as an electrolytic cell of a special kind, owing to the fact that half of the cell occurs in the gas phase. In a fashion analogous to a conventional controlled current electrolytic cell, the accumulation of one polarity of ion at the working electrode (ES capillary) as a result of the selective loss of the opposite polarity ion in the form of charged droplets must be balanced. A charge balancing reaction would involve electrochemical oxidation or reduction of either the metal capillary or a species in solution, or perhaps both. If electrospray is operated in the negative ion mode, i.e. it produces negatively charged droplets, it is assumed that an equal amount of positive ions must be reduced within the capillary to retain charge neutrality in the solution bulk. Alternatively, neutral species may be reduced to negative ions to account for the excess negative charge leaving the capillary.

Van Berkel and Zhou [66] have used this electrolytic nature for *in situ* oxidation of nickel (II) octaethylporphyrin to its radical cation for MS detection. A separate study reported changes in bulk solution pH in excess of 4 pH units as a result of oxidation reactions inside a metal electrospray capillary [104]. Electrospray has since been employed for generation of radical ions from neutral metallocenes and as a detector for electrochemical studies [66, 67, 105-108].

1.2.4 Generation of Gas-Phase Ion Solvent Clusters

At atmospheric pressure, the jet that forms as a result of instability at the apex of a Taylor cone quickly disperses into charged droplets of roughly 1 μm in diameter. These droplets will undergo solvent evaporation. The rate of droplet evaporation will follow the surface evaporation limit law for relatively volatile solvents, such as methanol or water and small droplet sizes [95] which leads to the dependence of droplet radius on time, t, expressed in equation 1.06.

$$r = r_o - \frac{\alpha \bar{\upsilon} \rho^o M}{4 \rho R_g T} t = r_o - 1.0 \times 10^{-3} t \qquad 1.06$$

where r_o is the initial droplet radius, α is the condensation coefficient, υ is the average thermal velocity of the solvent, ρ^o is the saturation vapour pressure of the solvent at the droplet temperature T, M is the molar mass of the solvent, ρ is the density of the solvent and R_g is the gas constant. As the initial droplet shrinks due to evaporation, the level of excess non-volatile ions on the droplet surface will remain the same, resulting in an increase in the surface charge density. An increase in surface charge density will eventually lead to droplet instability and subsequent fission. An equation that predicts the relative charge density at which fission will occur is referred to as the Rayleigh criterion, given in equation 1.07 and was formulated by Lord Rayleigh in 1882 [109].

$$q_r^2 = 64\pi^2 \varepsilon_o \gamma r_r^3 \qquad 1.07$$

When the radius of a charged droplet falls below a critical value determined by this equation for a constant charge, the droplet is unstable. It will experience an asymmetric fission event in which several highly charged offspring droplets are produced in a direction normal to the applied electric field. Gomez and Tang [84] observed that fission actually occurs at 80% of the Rayleigh limit, resulting in approximately 20 offspring droplets. The offspring droplets are approximated to account for 2% of the parent droplet's original mass and 15% of its charge. Both the residual parent droplet and its progeny may be expected to undergo the same sequence of solvent evaporation and fission until gas phase ion clusters, $M(solvent)_m^{n+}$ or $X(solvent)_m^{n-}$, are ultimately produced. Based on equations 1.06 and 1.07, Kebarle [95] has estimated that the time necessary to complete this sequence under normal atmospheric conditions is roughly 700 µs. It is gas phase ion-solvent clusters that are sampled and detected by a mass spectrometer. The degree of solvation of the ions may, in turn, be controlled by mass spectrometric interface parameters that will be

discussed in detail in subsequent chapters. A simple schematic of the ion-solvent cluster liberation mechanism is shown in Figure 1.03.

The precise mechanism by which ion solvent clusters are liberated from charged droplets is controversial. The first attempt to explain the process was proposed by Dole and co-workers [96] who described a "charged residue" model which was later renamed by Kebarle and Tang as the "single ion in droplet theory" or SIDT. This theory is based on successive Rayleigh fission events culminating in the formation of an offspring micro-droplet containing a single charged species. Iribarne and Thomson [93, 110] proposed an alternative mechanistic explanation for ion transfer called the "ion evaporation theory" or IET. The IET is based on direct electrostatic desorption of a solvated ion from the surface of a small highly charged droplet. After much discussion, no consensus has been achieved on which, if either, ion liberation mechanism is correct [98, 111, 112]. However, the detection of such involatile "residues" as $NaCl_2^+$ and Na_2Cl^+ by mass spectrometry lends credence to the SIDT while the IET may explain differences in analyte sensitivities associated with preferential liberation of volatile or surface active compounds.

1.2.5 Ionspray

Ionspray, also referred to as pneumatically assisted electrospray, has become a popular alternative to conventional electrospray in recent years [16, 18, 21, 113-116]. Ionspray employs a concurrent flow of nitrogen gas to enshroud a charged capillary and disrupt the liquid surface, much like a charged Meinhard nebulizer arrangement. This source was originally developed to accommodate higher solution flow rates than possible with electrospray in order to simplify the coupling of electrospray with liquid chromatography [21, 115, 117]. It has since gained widespread application for the nebulization of aqueous solution and is considered to be more rugged for routine use than electrospray. Unfortunately, mass spectra acquired with an ionspray source tend to be very dependent on the relative position of the source [16] and suffer from high levels of ion adducts. In addition, ionspray sources must be positioned off-axis to the mass spectrometer to avoid penetration of liquid solvent into the vacuum chamber.

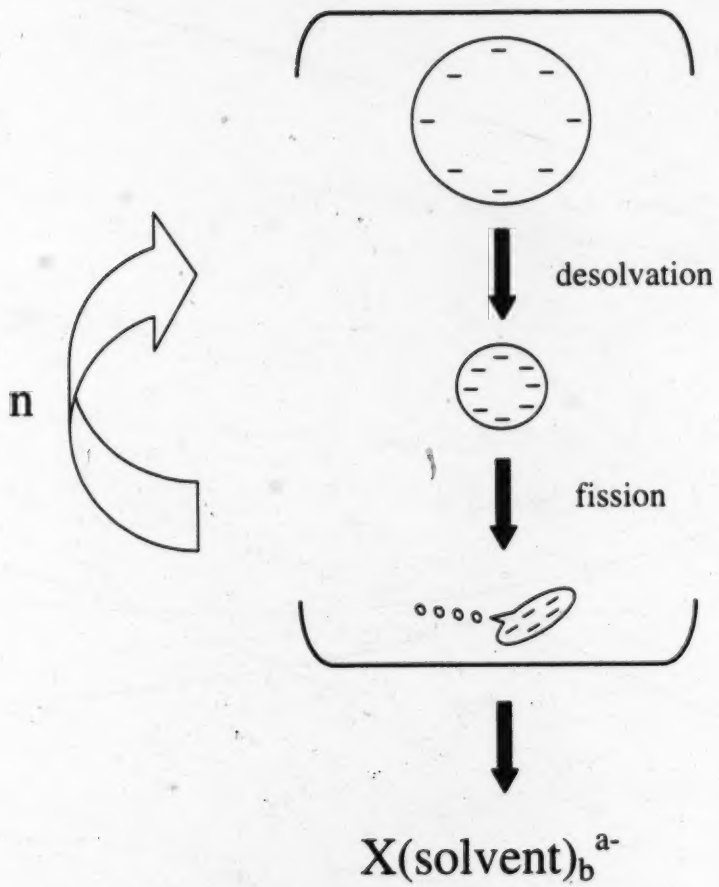

Figure 1.03 Schematic illustration of the mechanism responsible for generation of gas-phase ion solvent species from electrosprayed droplets.

1.3 Electrospray Mass Spectrometry

1.3.1 Electrospray Interface

A schematic of the electrospray interface to the mass spectrometer is shown in Figure 1.04. The interface serves two main functions, the production of charged droplets from the electrospray capillary and sampling of electrospray generated ions from atmosphere into the high vacuum of the mass spectrometer. The atmospheric pressure interface involves a two stage pumping system. The interface consists of a narrow diameter orifice in the sampling plate through which atmospheric gas and analyte vapour is expanded into a low pressure region in front of the skimmer. The expansion is then sampled by the skimmer and guided through the main vacuum chamber to a quadrupole mass analyzer by an ion optical arrangement. The specifics of the interface and mass spectrometer will be discussed in the following chapter; however, it is necessary to highlight the region between the sampling plate and skimmer since its function as a collision cell is of paramount importance throughout the body of this work.

1.3.2 Collision Induced Dissociation (CID)

The expansion region located between the sampling plate and skimmer in Figure 1.04 is of utmost analytical importance and utility for at least two reasons. The first reason is a result of incomplete analyte desolvation and the second reason is that this region may be used as a relatively efficient collision cell for generation of fragment ions. Initially, let us consider the origin of collisions in the expansion region. Analyte ion-solvent clusters or "nano-droplets" from the ES source will be introduced into this region along with atmospheric gases (predominantly N_2 curtain gas) as a result of the pressure differential across the sampling plate. Both neutral species and ions will be accelerated equally into the free jet expansion; however, if a potential difference is applied between the sampling plate and skimmer, charged species may be further accelerated with respect to neutral species, resulting in collisions between ions and

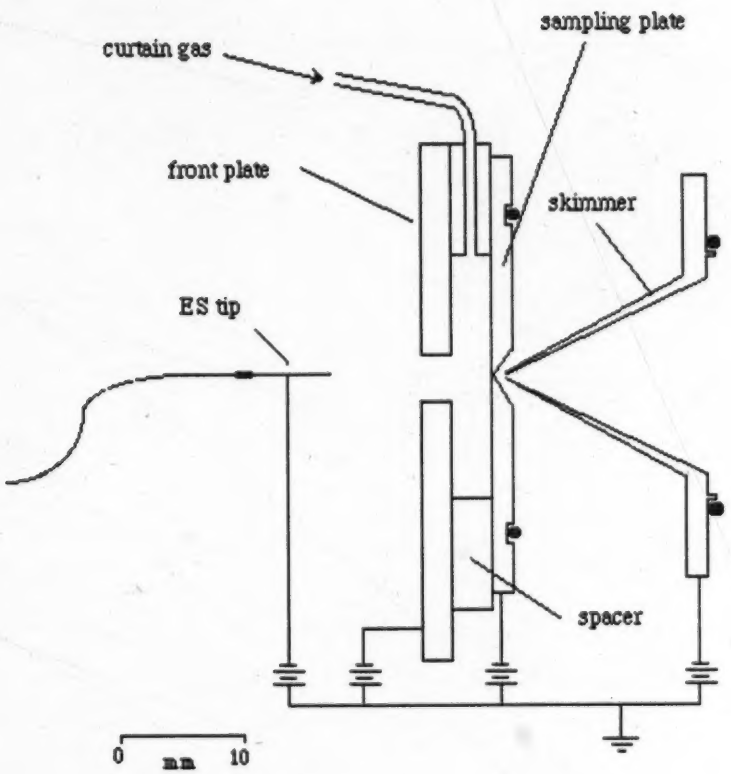

Figure 1.04 Schematic diagram of the electrospray interface to the mass spectrometer.

neutrals. The energy and number of collisions will scale with the magnitude of the applied potential difference.

In the case of ion-solvent interactions (dipole-dipole, van der Waals), relatively low potential differences, 5-30 volts, will result in efficient removal of solvent to produce bare ions. The magnitude of the voltage required for desolvation will vary with analyte charge density or polarizability. In other words, higher declustering voltages are required for small, highly charged ions of low polarizability. When the interface is operated at mild desolvating conditions, observed spectra for monovalent inorganic ions are simple and identification is based on characteristic isotope profiles. Confirmation of identity may be accomplished by resorting to mild sampling conditions to generate solvated distributions. Incremental increases in sampling potential are then used to sequentially reduce solvation until only the bare ion is present in the spectrum. The desolvation steps of monovalent anions and cations is summarized by the following equations:

$$X^-(H_2O)_n + N_2 \rightarrow X^- + n(H_2O) + N_2 \qquad 1.09$$

$$M^+(H_2O)_n + N_2 \rightarrow M^+ + n(H_2O) + N_2 \qquad 1.10$$

where X^- and M^+ are simple anions (e.g. halides) and metal cations (e.g. alkali metals), respectively. At higher potential differences, 30-60 volts, the collisions between ions and neutral species will be more energetic and may result in the following charge separation or reduction reactions for multiply charged analyte ions.

$$X^{2-}(H_2O)_n + N_2 \rightarrow HX^- + OH^- + n(H_2O) + N_2 \qquad 1.11$$

$$M^{2+}(H_2O)_n + N_2 \rightarrow MOH^+ + H^+ + n(H_2O) + N_2 \qquad 1.12$$

The extent of charge separation or charge reduction may be predicted based on relative electron affinities or ionization potentials of analyte and solvent [32, 118].

High collisional voltages may thus be used to completely remove an analyte solvent sheath although they may also result in fragmentation of ionic molecular species:

$$MO_n^- + N_2 \rightarrow MO_{n-1}^- + O^- + N_2 \qquad 1.13$$

$$ML_n^{x+} + N_2 \rightarrow ML_{n-1}^{x+} + L + N_2 \qquad 1.14$$

where MO_4^- and ML_n^{x+} are generic oxo-anions and metal ligand complexes. For the majority of inorganic species, the application of collisional voltages in excess of 100 volts generally results in the observation of relatively simple spectra consisting of bare X^- (e.g. Cl^-, I^- or Se^-) or M^+, M^{2+}, MO^+, MX^+ (e.g. Ba^+, Ba^{2+}, BaO^+ or $BaCl^+$) species. Collision induced dissociation performed in the interface region can produce spectra that are very similar to those observed by tandem mass spectrometry (MS/MS) in a triple quadrupole mass spectrometer or quadrupole storage ion trap (QUISTOR). Interface CID is, however, less versatile since there is no means to isolate or pre-scan for a particular parent ion, which can result in very complex spectra for multi-component solutions. Manipulation of interface voltages does, however, enable electrospray to be operated as a multiple mode source since it provides the ability to easily generate both atomic and molecular spectra from the same sample components. Chromatographic separation methodology may also be used to simplify collisional spectra by reducing the number of analyte species in the CID region at a particular time.

1.4 References

1. Horlick, G., *Spectroscopy*, **1992,** 7, 22-9.

2. Horlick, G., *J. Anal. At. Spectrom.*, **1994,** 9, 593-7.

3. Hieftje, G. M., *J. Anal. At. Spectrom.*, **1992,** 7, 783-90.

4. Broekaert, J. A. C., *Mikrochim. Acta*, **1995,** 120, 21-38.

5. VanLoon, J. C.; Barefoot, R. R., *Analyst*, **1992,** 117, 563-70.

6. Byrdy, F. A.; Caruso, J. A., *Environ. Sci. Technol.*, **1994,** 28, 528A-34A.

7. Lobinski, R., *Appl. Spectrosc.*, **1997,** 51, 260A-78A.

8. Vela, N. P.; Caruso, J. A., *J. Anal. At. Spectrom.*, **1993,** 8, 787-94.

9. Larsen, E. H.; Pritzl, G.; Hansen, S. H., *J. Anal At. Spectrom.*, **1993,** 8, 1075-84.

10. Al-Rashdan, A.; Vela, N. P.; Caruso, J. A.; Heitkemper, D. T., *J. Anal. At. Spectrom.*, **1992,** 7, 551-5.

11. *Gas chromatography/Mass Spectrometry*; Springer-Verlag: New York, 1986.

12. Yamashita, M.; Fenn, J. B., *J. Phys. Chem.*, **1984,** 88, 4451-9.

13. Yamashita, M.; Fenn, J. B., *J. Phys. Chem.*, **1984,** 88, 4671-5.

14. Aleksandrov, M. L.; Gall, L. N.; Krasnov, N. V.; Nikolaev, V. I.; Pavlenko, V. A.; Shkurov, V. A., *Int. J. Mass Spectrom. Ion Proc.*, **1984,** 54, 231-5.

15. Gwizdala, A. B.; Johnson, S. K.; Mollah, S.; Houk, R. S., *J. Anal. At. Spectrom.*, **1997,** 12, 503-6.

16. Olesik, J. W.; Thaxton, K. K.; Olesik, S. V., *J. Anal . At. Spectrom.*, **1997,** 12, 507-16.

17. Pergantis, S. A.; Winnik, W.; Betowski, D., *J. Anal. At. Spectrom.*, **1997,** 12, 531.

18. Corr, J. J., *J. Anal. At. Spectrom.*, **1997,** 12, 537-46.

19. Ross, A. R. S.; Ikonomou, M. G.; Thompson, J. A. J.; Orians, K. J., *in press*, **1998**.

20. Zoorob, G.; Brown, F. B.; Caruso, J., *J. Anal. At. Spectrom.*, **1997,** 12, 517-24.

21. Siu, K. W. M.; Gardner, G. J.; Berman, S. S., *Anal. Chem.*, **1989,** 61, 2320-2.

22. Blades, A. T.; Jayaweera, P.; Ikonomou, M. G.; Kebarle, P., *Int. J. Mass. Spectrom. Ion. Proc.*, **1990,** 102, 251-67.

23. Blades, A. T.; Jayaweera, P.; Ikonomou, M. G.; Kebarle, P., *Int. J. Mass. Spectrom. Ion Proc.*, **1990,** 101, 325-36.

24. Blades, A. T.; Jayaweera, P.; Ikonomou, M. G.; Kebarle, P., *J. Chem. Phys.*, **1990,** 92, 5900-6.

25. Jayaweera, P.; Blades, A. T.; Ikonomou, M. G.; Kebarle, P., *J. Am. Chem. Soc.*, **1990,** 112, 2452-4.

26. Agnes, G. R.; Horlick, G., *Appl. Spectrosc.*, **1992,** 46, 401-6.

27. Agnes, G. R.; Stewart, I. I.; Horlick, G., *Appl. Spectrosc.*, **1994,** 48, 1347 - 59.

28. Agnes, G. R.; Horlick, G., *Appl. Spec.*, **1994,** 48, 655-61.

29. Agnes, G. R. PhD Thesis, University of Alberta, Edmonton, Alberta, 1994.

30. Agnes, G. R.; Horlick, G., *Appl. Spectrosc.*, **1994,** 48, 649-54.

31. Agnes, G. R.; Horlick, G., *Appl. Spectrosc.*, **1995,** 49, 324-34.

32. Stewart, I. I.; Horlick, G., *Anal. Chem.*, **1994,** 66, 3983 - 93.

33. Stewart, I. I.; Horlick, G., *J. Anal. At. Spectrom.*, **1996,** 11, 1203-14.

34. Ketterer, M. E.; John P. Guzowski, J., *Anal. Chem.*, **1996,** 68, 883-7.

35. Brown, F. B.; Olson, L. K.; Caruso, J. A., *J. Anal. At. Spectrosc.*, **1996,** 11, 633-41.

36. Cheng, Z. L.; Siu, K. W. M.; Geuvremont, R.; Berman, S. S., *Org. Mass. Spectrom.*, **1992,** 27, 1370-6.

37. Cheng, Z. L.; Siu, K. W. M.; Geuvremont, R.; Berman, S. S., *J. Am. Soc. Mass. Spectrom.*, **1992,** 3, 281-8.

38. Corr, J. J.; Anacleto, J. F., *Anal. Chem.*, **1996,** 68, 2155-63.

39. Huggins, T. G.; Henion, J. D., *Electrophoresis*, **1993,** 14, 531-9.

40. Raymond, C. C.; Dick, D. L.; Dorhout, P. K., *Inorg. Chem.*, **1997,** 36, 2678-81.

41. Mahoney, P. P.; John P. Guzowski, J.; Ray, S. J.; Hieftje, G. M., *Appl. Spectrosc.*, **1997,** 51, 1464-70.

42. vandenBergen, A.; Colton, R.; Percy, M.; West, B. O., *Inorg. Chem.*, **1993,** 32, 3408-11.

43. Lipshutz, B.; Stevens, K. L.; James, B.; Pavlovich, J. G.; Snyder, J. P., *J. Am. Chem. Soc.*, **1996,** 118, 6796-7.

44. Gatlin, C. L.; Turecek, F.; Vaisar, T., *J. Mass Spectrom.*, **1995,** 30, 1617-27.

45. Horwitz, C. P.; Warden, J. T.; Weintraub, S. T., *Inorg. Chim. Acta*, **1996,** 246, 311-20.

46. Kohler, M.; Leary, J. A., *Int. J. Mass Spectrom. Ion Proc.*, **1997,** 162, 17-34.

47. Katta, V.; Chowdhury, S. K.; Chait, B. T., *J. Am. Chem. Soc.*, **1990,** 112, 5348-9.

48. Arakawa, R.; Jian, L.; Yoshimura, A.; Nozaki, K.; Ohno, T.; Doe, H.; Matsuo, T., *Inorg. Chem.*, **1995,** 34, 3874-8.

49. Burns, T. D.; Spence, T. G.; Mooney, M. A.; Posey, L. A., *Chem. Phys. Lett.*, **1996,** 258, 669-79.

50. Hu, P.; Ye, Q.-Z.; Loo, J. A., *Anal. Chem.*, **1994,** 66, 4190-4.

51. Hu, P.; Loo, J. A., *J. Am. Chem. Soc.*, **1995,** 117, 11314-9.

52. Hu, P.; Loo, J. A., *J. Mass Spectrom.*, **1995,** 30, 1076-82.

53. Yu, X.; Wojciechowski, M.; Fenseleau, C., *Anal. Chem.*, **1993,** 65, 1355-9.

54. Yalcin, T.; Wang, J.; Wen, D.; Harrison, A. G., *J. Am. Soc. Mass Spectrom.*, **1997,** 8, 749-55.

55. Ralph, S. F.; Iannitti, P.; Kanitz, R.; Sheil, M. M., *Eur. Mass Spectrom.*, **1996,** 2/3, 173-9.

56. Ferrer, M.; Reina, R.; Rossell, O.; Seco, M.; Segales, G., *J. Organometallic Chem.*, **1996,** 515, 205-11.

57. Colton, R.; D'Agostino, A.; Traeger, J. C., *Mass Spectrom. Rev.*, **1995,** 14, 79-106.

58. Kane-Maguire, L. A. P.; Kanitz, R.; Sheil, M. M., *Inorg. Chim. Acta*, **1996,** 245, 209-14.

59. Houk, R. S., *Anal. Chem.*, **1986,** 58, 97A-105A.

60. Tan, S. H.; Horlick, G., *Appl. Spectrosc.*, **1986,** 40, 445-59.

61. Peiris, D. M.; Yang, Y.; Ramanathan, R.; Williams, K. R.; Watson, C. H.; Eyler, J. R., *Int. J. Mass Spectrom. Ion Proc.*, **1996,** 157/158, 365-78.

62. Henderson, W.; Nicholson, B. K., *J. Chem. Soc. Chem. Commun.*, **1995,** 24, 2531-2.

63. Saf, R.; Mirtl, C.; Hummel, K., *Tetrahedron Lett.*, **1994,** 35, 6653-6.

64. Crescenzi, C.; Corcia, A. D.; Samperi, R.; Marcomini, A., *Anal. Chem.*, **1995,** 67, 1797-804.

65. VanBerkel, G. J.; McLuckey, S. A.; Glish, G. L., *Anal. Chem.*, **1992,** 64, 1586-93.

66. VanBerkel, G. J.; Zhou, F., *Anal. Chem.*, **1995,** 67, 3958-64.

67. VanBerkel, G. J.; Zhou, F., *Anal. Chem.*, **1995,** 67, 2916-23.

68. VanBerkel, G. J. In *Electrospray Ionization Mass Spectrometry*; Cole, R. B., Ed.; John Wiley & Sons: New York, 1997, pp 65-105.

69. Zeleny, J., *Phys. Rev.*, **1914,** 3, 69.

70. Zeleny, J., *Phys. Rev.*, **1917,** 10, 1-6.

71. Cloupeau, M.; Prunet-Foch, B., *J. Electrostatics*, **1989,** 22, 135-9.

72. Cloupeau, M.; Prunet-Foch, B., *J. Electrostatics*, **1990,** 25, 165-84.

73. Cloupeau, M., *J. Aerosol Sci.*, **1994,** 25, 1143-57.

74. Cloupeau, M.; Prunet-Foch, B., *J. Aerosol Sci.*, **1994,** 25, 1021-36.

75. Ganan-Calvo, A. M.; Lasheras, J. C.; Davila, J.; Barrero, A., *J. Aerosol Sci.*, **1994,** 25, 1121-42.

76. Charbonnier, F.; Rolando, C.; Saru, F.; Hapiot, P.; Pinson, J., **1993**.

77. Kelly, M. A.; Vestling, M. M.; Fenseleau, C. C.; Smith, P. B., *Org. Mass Spectrom.*, **1992,** 27, 1143-7.

78. Kelly, A. J., *J. Aerosol Sci.*, **1994,** 25, 1159-77.

79. Grace, J. M.; Marijnissen, J. C. M., *J. Aerosol Sci.*, **1994,** 25, 1005-19.

80. Mora, J. F. d. l.; Loscertales, I. G., *J. Fluid Mech.*, **1994,** 260, 155-84.

81. Taylor, G. I., *Proc. Roy. Soc. Lond. A.*, **1969,** 313, 453.

82. Hamdam, M.; Curcuruto, O., *Int. J. Mass. Spectrom. Ion. Proc.*, **1991,** 108, 93-113.

83. Bruins, A. P., *J. Chim. Phys.*, **1993,** 90, 1335-44.

84. Gomez, A.; Tang, K., *Phys. Fluids*, **1994,** 6, 404-14.

85. Drozin, V. G., **1954**, 158-64.

86. Chen, D.-R.; Pui, D. Y. H.; Kaufman, S. L., *J. Aerosol Sci.*, **1995,** 26, 963-77.

87. Hayati, I.; Bailey, A.; Tadros, T. F., *J. Coll. Int. Sci.*, **1986,** 117, 222-30.

88. Hayati, I.; Bailey, A.; Tadros, T. F., *J. Coll. Int. Sci.*, **1986,** 117, 205-21.

89. Hayati, I.; Bailey, A. I.; Tadros, T. F., *Nature*, **1986,** 319, 41-3.

90. Taflin, D. C.; Ward, T. L.; Davis, E. J., *Langmuir*, **1989,** 5, 376-84.

91. Grigor'ev, A. I.; Shir'aeva, S. O., *J. Phys. D: Appl. Phys.*, **1990,** 23, 1361-70.

92. Wilm, M. S.; Mann, M., *Int. J. Mass Spectrom. Ion Proc.*, **1994,** 136, 167-80.

93. Thomson, B. A.; Iribarne, J. V., *J. Chem. Phys.*, **1979,** 71, 4451-63.

94. Smith, D. P. H., *IEEE Trans. Ind. Appl.*, **1986,** IA-22, 527-35.

95. Kebarle, P.; Tang, L., *Anal. Chem.*, **1993,** 65, 972A.

96. Dole, M.; Mack, L. L.; Hines, R. L.; Mobley, R. C.; Ferguson, L. D.; Alice, M. B., *J. Chem. Phys.*, **1968,** 49, 2240-9.

97. Fenn, J. B.; Mann, M.; Meng, C. K.; Wong, S. F.; Whitehouse, C. M., *Science*, **1989,** 246, 64-71.

98. Kebarle, P.; Ho, Y. In *Electrospray ionization mass spectrometry*; Cole, R. B., Ed.; John Wiley & Sons: New York, 1997, pp 3-63.

99. Stewart, I. I. PhD Thesis, University of Alberta, Edmonton, Alberta, 1996.

100. Chowdhury, S. K.; Chait, B. T., *Anal. Chem.*, **1991,** 63, 1660-4.

101. Wampler, F. M.; Blades, A. T.; Kebarle, P., *J. Am. Soc. Mass. Spectrom.*, **1993,** 4, 289-95.

102. Ikonomou, M. G.; Blades, A. T.; Kebarle, P., *J. Am. Soc. Mass. Spectrom.*, **1991,** 2, 497-505.

103. Blades, A. T.; Ikonomou, M. G.; Kebarle, P., *Anal. Chem.*, **1991,** 63, 2109-14.

104. VanBerkel, G. J.; Zhou, F.; Aronson, J. T., *Int. J. Mass Spectrom. Ion Proc.*, **1997,** 162, 55-67.

105. VanBerkel, G. J.; Zhou, F., *Anal. Chem.*, **1994,** 66, 3408-15.

106. Zhou, F.; Berkel, G. J. V., *Anal. Chem.*, **1995,** 67, 3643-9.

107. Dupont, A.; Gisselbrecht, J.-P.; Leize, E.; Wagner, L.; Dorsselaer, A. V., *Tetrahedron Lett.*, **1994,** 35, 6083-6.

108. Bond, A. M.; Colton, R.; D'Agostino, A.; Downard, A. J.; Traeger, J. C., *Anal. Chem.*, **1995,** 67, 1691-5.

109. Rayleigh, L., *Philosoph. Mag*, **1882,** 14, 184.

110. Iribarne, J. V.; Thomson, B. A., *J. Chem. Phys.*, **1976,** 64, 2287-94.

111. Ashton, D. S.; Beddell, C. R.; Cooper, D. J.; Green, B. N.; Oliver, R. W. A., *Org. Mass Spectrom.*, **1993,** 28, 721-8.

112. Siu, K. W. M.; Geuvremont, R.; LeBlanc, J. C. Y.; O'Brien, R. T.; Berman, S. S., *Org. Mass. Spectrom.*, **1993,** 28, 579-84.

113. Ikonomou, M. G.; Blades, A. T.; Kebarle, P., *Anal. Chem.*, **1991,** 63, 1989-98.

114. Leblanc, J. C. Y., *J. Anal. At. Spectrom.*, **1997,** 12, 525-30.

115. Bruins, A. P.; Covey, T. R.; Henion, J. D., *Anal. Chem.*, **1987,** 59, 2642-6.

116. Sharp, B. L.; Sulaiman, A. B.; Taylor, K. A.; Green, B. N., *J. Anal. At. Spectrom.*, **1997,** 12, 603-9.

117. Ikonomou, M. G.; Blades, A. T.; Kebarle, P., *Anal. Chem.*, **1990,** 62, 957-67.

118. Stewart, I. I.; Barnett, D. A.; Horlick, G., *J. Anal. At. Spectrom.*, **1996,** 11, 877-86.

Chapter 2

Instrumentation

2.1 Introduction

The purpose of this chapter is to provide a discussion of the instrumentation used throughout the work for this thesis. The chapter is composed of three sections: the first focuses on the electrospray source and interface region, the second briefly describes the mass spectrometer and the third describes the data acquisition procedure.

2.2 Electrospray

2.2.1 Source

The electrospray needle, shown in Figure 2.01, consists of an approximately 1 cm length of stainless steel capillary with dimensions of 200 μm outer diameter and 100 μm inner diameter. The tip was soldered into the end of a 10 cm length of factory cut, wide bore stainless steel capillary (1/16" o.d. x 250 μm i.d.) used for structural support. The length of ES capillary that protrudes from the end of the support capillary is between 1.5 to 2 mm. Longer capillary lengths are susceptible to microphonic vibrations induced by the MS vacuum pumps or atmospheric air currents.

The opposite end of the wide bore capillary was connected with a zero dead volume stainless steel fitting (Valco Instrument Co.) to a 30cm length of Teflon tubing (1/16" o.d. x 250 μm i.d.). The Teflon serves as a transfer line from a 250 μL syringe containing sample solution and isolates the high potential applied to the steel capillary from the syringe pump and the analyst. The tubing was in turn connected to either a glass or plastic disposable syringe with a stainless steel luer adapter. There are several disadvantages of this design that became increasingly apparent with its prolonged use. The outer diameter of the ES capillary (200 μm) is not well matched with the inner diameter of the larger support capillary (250 μm), creating a mixing chamber that requires high rinse volumes to flush out. Preparation of the ES needle is time

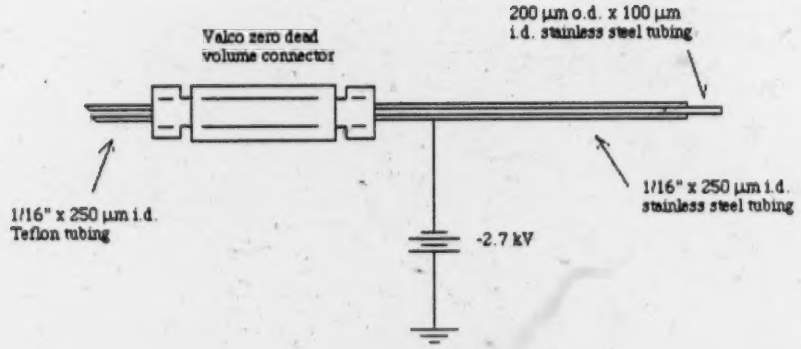

Figure 2.01 Electrospray needle design (not drawn to scale).

consuming owing to the difficulty in cutting a 1 cm length of 200 µm steel capillary evenly and without burrs. Subsequent polishing of the capillary with fine abrasive paper can also result in clogging and reproducibility in positioning of the capillary within the support tube is poor. An improved ES source, designed to generate charged spray from aqueous solution and reduce memory effects caused by mixing, is the subject of Chapter 6.

The stainless steel ES capillary was mounted on a three-dimensional translation stage and positioned on axis with the sampling orifice of the mass spectrometer. Electrical contact with the solution was accomplished by connecting a high voltage lead to the wide bore steel. The needle was electrically isolated from the translational stage by a cylindrical (10cm x 2.5cm diameter) Teflon mount. The bias voltage applied to the electrospray capillary was provided by an EH-series (0-10 kV) Glassman high-voltage power supply. Solution was delivered to the capillary at flow rates of 2.0 to 2.5 µL/min using a syringe pump (Harvard Apparatus, model 22).

2.2.2 Interface

A diagram of the electrospray interface used to transfer ions into the mass spectrometer (SCIEX/Perkin-Elmer ELAN Model 250) is shown in Figure 2.02. The interface consists of four main components: a front plate, spacer, sampling plate and skimmer cone, shown in Figure 2.03. The ES capillary was positioned along the central axis of the orifice in the front plate, at a separation distance of 5 mm. The front plate is a brass disk with a 3 mm diameter orifice at its center, mounted to a 4 mm thick brass spacer. A thin Teflon insulating plate separates the front plate from the spacer so that the two components can be differentially biased. The region immediately behind the front plate is used for introduction of dry nitrogen gas. The gas inlet is located at the top of the spacer such that nitrogen enters perpendicular to the capillary position and flows through the front plate orifice countercurrent to the ES capillary. The functions of the curtain gas and criteria for its selection are discussed in detail in section 2.2.3.

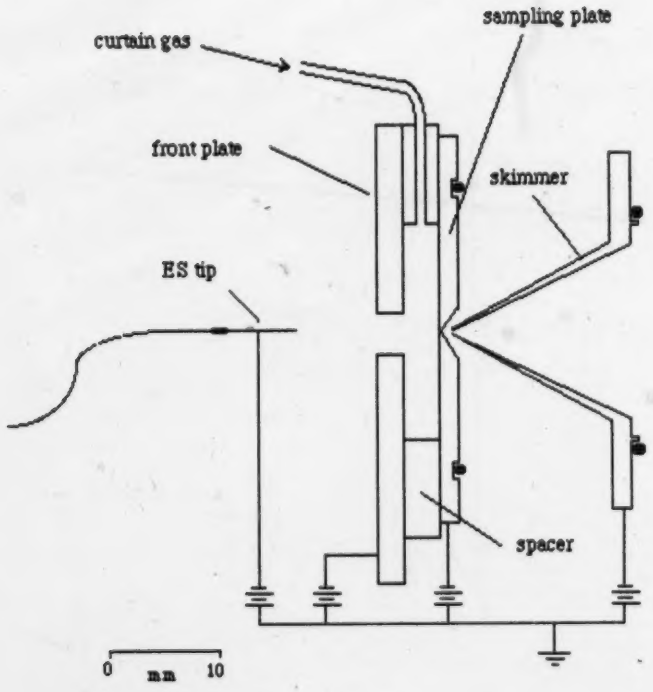

Figure 2.02 Schematic diagram of the electrospray interface to the mass spectrometer.

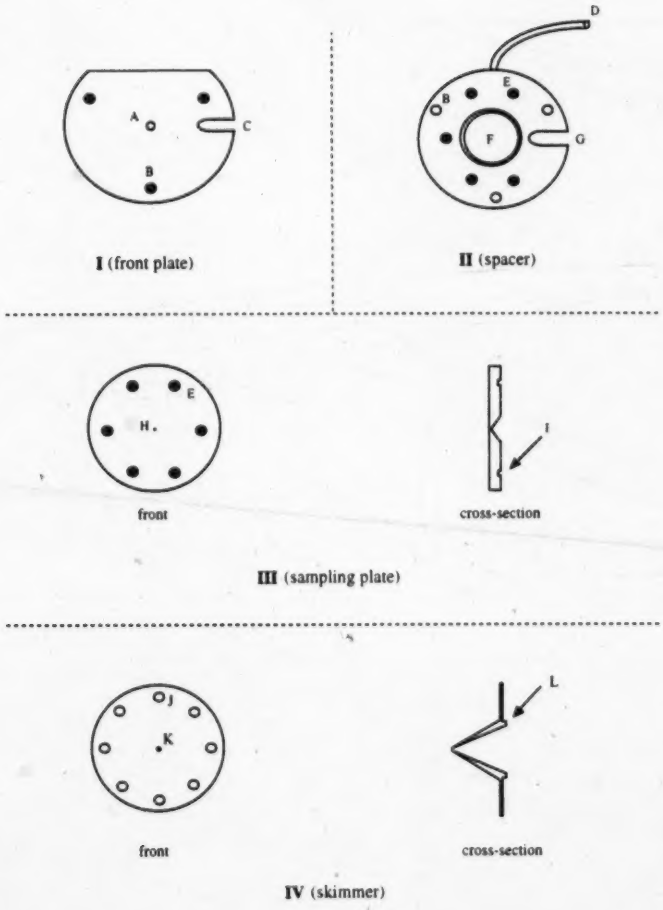

Figure 2.03 Electrospray interface components I) front plate, II) spacer, III) sampling plate and IV) skimmer cone.

At the rear of the curtain gas region is a flat copper sampling plate. The sampling plate has an orifice or "nozzle" diameter of 100 μm which replaces the sampling cone (0.75 to 1 mm orifice) originally used for ICP-MS measurements. The back of this plate is cut out in the shape of a cone with a half angle of 37°. The pressure to the right of the sampling plate is approximately 400 mTorr. This region is evacuated by an Edwards E2M18 double stage roughing pump at a pump speed of approximately 7 L/sec. Sample and atmospheric gases that pass through the sampling plate nozzle experience a jet expansion due to the drop in pressure across the plate. Details of the mechanics of free jet expansion are well documented in the literature [1, 2] and will not be repeated here. The final component of the source is the skimmer cone which is 1.9 cm high and has an orifice diameter of 1.2 mm. It is positioned to sample the jet expansion exiting the sampling plate. To the right of the skimmer is the main vacuum chamber of the mass spectrometer. The pressure in this region is maintained in the low μTorr range, typically 5 x 10^{-6} Torr, by a Cryo-Torr 8 cryopump using helium as a refrigerant.

During regular operation of electrospray in the negative ion mode the electrospray tip and front plate are biased at -2.7 kvolts and -600 volts, respectively. This establishes a potential difference of -2.1 kV, which is the potential responsible for electrostatic nebulization of sample. Potentials are also applied to the sampling plate and skimmer and variation of the potential difference, ΔV, between these components is used to effect collisional processes on analyte species, as discussed in Section 1.3.2 of the previous chapter. The absolute potential applied to the skimmer is used to optimize analyte ion kinetic energies to give optimal ion currents reaching the quadrupole analyzer rods and detector. A list of the various operating parameters used throughout this work for both negative and positive ion studies is given in Table 2.01.

2.2.3 Curtain Gas

Addition of the nitrogen curtain or "bath" gas into the interface region serves several

Table 2.01 Operating parameters for positive and negative ion electrospray mass spectrometry on the modified ELAN 250 ICP-MS.

Parameter	Negative-Ion Mode	Positive-Ion Mode
Voltage		
Capillary	-2.7 to –2.9 kilovolts	3.5 to 4.1 kilovolts
Front Plate	- 600 volts	600 volts
Sampling Plate	-6 to –200 volts	10 to 200 volts
Skimmer Cone	-4 to -6 volts	6 to 10 volts
Flow Rate		
Sample	1.0 to 2.5 µL/min	
Curtain Gas (N_2)	0.8 to 1.1 L/min	
Capillary		
Diameter (o.d. x i.d.)	200 µm x 100 µm	
Material	stainless steel	
Separation Distance	5 mm (on MS axis)	
Delivery Syringe		
Volume	250 µL or 1mL	
Inner Diameter	2.30 mm or 4.78 mm	

functions. The flow of dry nitrogen gas countercurrent to the electrospray needle not only aids in droplet desolvation, but also serves to prevent buildup of solvent vapour in the interface. Its function is particularly important since solvent evaporation results in adiabatic cooling of a droplet which dramatically decreases droplet evaporation rates. The degree of droplet cooling may be approximated by equation 2.01 [1].

$$T = T_o + \frac{\Delta H_v}{C_p} \ln X \qquad 2.01$$

where T is the temperature of the droplet when fraction 1-X has evaporated, T_o is the initial droplet temperature, ΔH_v is the enthalpy of vaporization of the solvent, and C_p is the heat capacity of the solvent. Collisions with nitrogen at atmospheric pressure are effective in compensating for this adiabatic cooling. Nitrogen may also be entrained through the sampling plate nozzle into the free jet expansion of the differentially pumped mass spectrometer, where it can be used as an effective collision gas for collision induced dissociation. Use of curtain gases other than nitrogen have been documented in the literature including carbon dioxide, oxygen and argon. Nitrogen is the most widely used owing to its high dielectric constant, reasonably large collisional cross-section, low cost and lack of a dipole moment.

2.3 Mass Spectrometer

A modified, first generation inductively coupled plasma quadrupole mass spectrometer, Perkin Elmer SCIEX Elan Model 250 ICP-MS, was used for the majority of experiments presented in this thesis. A schematic of the mass spectrometer is given in Figure 2.04. Several modifications were made to the mass spectrometer by Agnes and Horlick [3] in order to accommodate an electrospray source. Modifications to the mass spectrometer include removal of the ICP source, adaptation of the atmospheric pressure sampling interface and removal of both photon stops that were originally intended to block intense argon emission from reaching the detector. Removal of the photon stops improved ion transmission by at least two

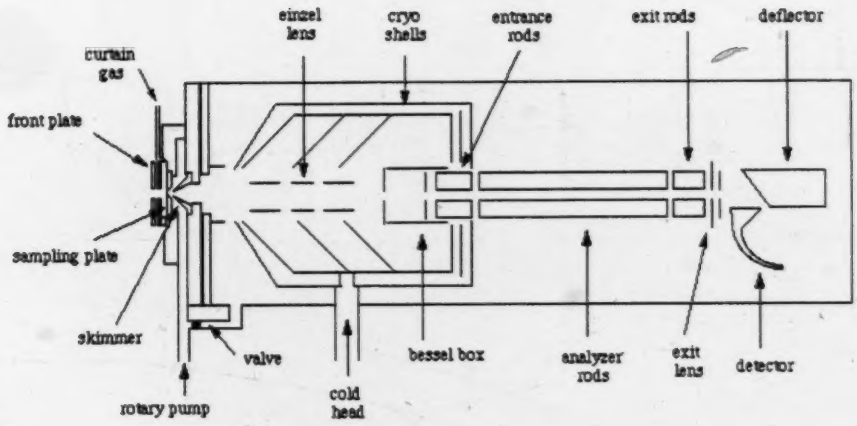

Figure 2.04 Schematic diagram of the modified SCIEX/Perkin Elmer ELAN Model 250 ICP-MS.

orders of magnitude. Changes to the interface were described in detail in section 2.2.2.

A set of three einzel lenses; E1, E2 and E3, are used to focus and guide the electrospray ion beam from the skimmer cone to a Bessel box. The majority of new mass spectrometers designed for atmospheric pressure sampling employ radio-frequency beam guides (quadrupoles, hexapoles and octapoles), rather than the simple electrostatic ion optics described here. The Bessel box consists of two plate electrodes at either end of a cylindrical ring electrode. The original function of the Bessel box was to manipulate ions around a photon stop; however, for ES applications its value is mostly nostalgic. This does not imply that its presence may be taken for granted since minimum threshold voltages must be applied to both the ring and plate electrodes, below which ion transmission at all values of *m/z* decays rapidly. Above these thresholds, ion transmission is essentially independent of voltage. However, if the plate voltage is set too high, defocusing collisions may be generated in the entrance optic region. The rest of the mass spectrometer was unchanged from its original factory specifications.

2.4 Spectrum and Data Acquisition

Mass spectra were collected by scanning with an integration time of either 100 or 300 ms per point (10 points per amu), while data used for quantitation were acquired in the peak-hopping mode with dwell times of 10 ms and total measurement times of 100 ms per point (1 point per amu). Average signal intensities were calculated for 10 measurements, resulting in typical relative standard deviations of 2-5%. In order to detect the presence of a corona discharge, which has negative effects on analyte intensities, background levels at *m/z* -32 (O_2^-) and 33 ($CH_3OH_2^+$) for negative and positive ion mode electrospray, respectively, were always monitored to alert the investigator to the presence of a discharge. The original ELAN software (version 11.0) is used to control data acquisition and routine instrument maintenance. Mass spectra may be viewed either on the screen or relayed through a printer port to a remote terminal where data are captured with a commercial data acquisition program,

Red Ryder (version 10.3). Data files generated by Red Ryder were filtered using an executable program written in Pascal, designed to remove extraneous text. The resultant files are then processed using Igor Pro 2.0.1 (Wavemetrics, Lake Oswego, OR, USA).

2.5 References

1. Hamdam, M.; Curcuruto, O., *Int. J. Mass. Spectrom. Ion. Proc.* **1991,** 108, 93-113.

2. Campargue, R., *J. Phys. Chem.* **1984,** 88, 4466-74.

3. Agnes, G. R. PhD Thesis, Unversity of Alberta, Edmonton, Alberta, 1994.

Chapter 3

Quantitative Electrospray Mass Spectrometry of Halides and Halogenic Anions[1]

[1] A version of this chapter has been published. David A. Barnett and Gary Horlick, J. Anal. At. Spectrom., **1997**, 12 (5), 497-501.

3.1 Introduction

Presently, the majority of analyses of the halides are performed by non-spectroscopic techniques including ion-exchange chromatography [1-4], capillary electrophoresis [5] and potentiometry [6]. The reason for the lack of spectroscopic methods is two-fold: firstly, halogen atoms are difficult to observe by atomic absorption because their atomic resonance states lie in the vacuum-ultraviolet spectral region. Secondly, their excitation and ionization potentials are high, resulting in poor sensitivity for both emission and mass spectrometry unless sources with high excitation temperatures are used, such as helium based plasmas. Despite these limitations, there have been several reports published on the determination of halides by atomic spectrometry using a variety of different sources and detection systems. Emission studies have commonly employed an argon inductively coupled plasma (Ar-ICP) [7], or a helium microwave induced plasma (He-MIP)[8-10]. Mass spectrometric studies include both negative and positive ion Ar-ICPMS [11-13], He-ICPMS [14, 15], and MIP-MS using both argon- [16] and helium-based plasmas [17-21].

In order to determine halide emission by argon-based plasmas a vacuum-ultraviolet detection system was developed by LaFreniere et al. [7] to monitor the atomic emission lines of chlorine, bromine, and iodine, resulting in limits of detection of 8, 15 and 6 ng/mL respectively. Vacuum-ultraviolet detection has also been used with a He-MIP source [8] but the reported detection limits were in the low µg/mL range. Limits of detection determined by positive ion Ar-ICPMS [11] for chlorine, bromine, and iodine are lower (5, 1, and 0.01 ng/mL, respectively) than for the corresponding emission studies. The only quantitative results reported for fluorine are by determination as negative ions using Ar-ICPMS with a reported detection limit of 110 ng/mL [11]. Halide analysis by He-MIPMS has been limited to the detection of volatile halo-organic compounds using gas-phase sample introduction. This is a result of the tendency for helium plasmas to become unstable and lose sensitivity upon the introduction of water. Typical absolute detection limits for halides detected in gas chromatographic eluates are in the low to sub-picogram range [20], although no results have yet been reported for fluorine.

In this study, an electrospray source is used to transfer anions present in a solution to the gas phase. Liberated ions are then sampled into a quadrupole mass spectrometer and subsequently detected. This combination of a low energy source with the very selective detection capabilities of the mass spectrometer offers several advantages over current analytical atomic- and chromatographic-based techniques. One very important advantage of this technique lies in the fact that electrospray can be a very mild source that may be used to sample solution ions directly without loss of speciation information. To date, inorganic electrospray mass spectrometry has been used primarily for qualitative studies. There have, however, been a few reports on attempts at quantitation with varying degrees of success in achieving linear calibration plots [22-26]. The lack of quantitative studies is not surprising as plenty of controversy surrounds the exact mechanism involved in conversion of ions from solution into the gas phase by the electrospray process. Nonetheless, Kebarle and Tang [26] presented an excellent discussion of some of the important features that must be considered in order to undertake quantitation by this technique. In addition, Agnes and Horlick [24] have shown that calibration plots, linear over four orders of magnitude, may be obtained for simple metal cations by employing an appropriate internal standard.

3.2 Experimental

All ESMS experiments were carried out on a modified Perkin-Elmer SCIEX ELAN Model 250 ICP-MS as described in Chapter 2. Mass spectra were collected by scanning with an integration time of 100ms per point (10 points per amu), while data used for quantitation were acquired in the peak-hopping mode with a dwell time of 10ms and total measurement time of 100ms per point (1 point per amu). Average signal intensities were calculated for 10 measurements resulting in typical relative standard deviations of 2-5%. The most abundant isotope was used for each of the species monitored. Typical background levels were 20-40 counts/s except for chloride, which was observed to be blank limited. In order to detect the presence of a corona discharge, which can have deleterious effects on analyte intensities, the

background level at *m/z* -32 (O_2^-) was always monitored to alert the investigator to the presence of a discharge.

3.2.1 Reagents

Stock solutions of the halides were prepared by dissolving the ACS-grade potassium salt in nanopure water to a concentration of 10 mM. The stock solution was then diluted 100-fold in distilled methanol for mass spectrometric analysis. Serial dilution of the aqueous stock solutions was used to prepare lower concentration methanolic standards used for the calibration curves in order to maintain the total water content at roughly 1-3%.

3.3 Results and Discussion

3.3.1 Halide Spectra

A sequence of mass spectra for an equimolar mixture of fluoride, chloride, bromide, and iodide is presented in Figure 3.01. The concentration of each component was roughly 0.1 mM. The first spectrum, Figure 3.01a, was acquired with the sampling plate and skimmer potentials set at -15 and –6 volts, respectively. These settings give a potential drop, ΔV, between the two plates of -9 volts. This results in a relatively low CID energy, hence an abundance of aqua-halide clusters, $X(H_2O)_n^-$, where X = F, Cl, Br, or I and n represents the number of water ligands, is observed in the spectrum. Fluoride exhibits the greatest degree of solvation or coordination to water ligands with an observed cluster distribution ranging from n = 1-5 with a maximum signal for $F(H_2O)_3^-$. At the same conditions, chloride exhibits a maximum signal for its doubly solvated anion, bromide favours coordination to one water ligand and the predominant peak for iodide corresponds to the bare singly charged anion at *m/z* -127.

The trend toward a lower degree of solvation with increasing ionic size correlates with the Gibb's free energy of solvation predicted by the Born equation in which solvation energy is proportional to $-z_i^2 / r$,

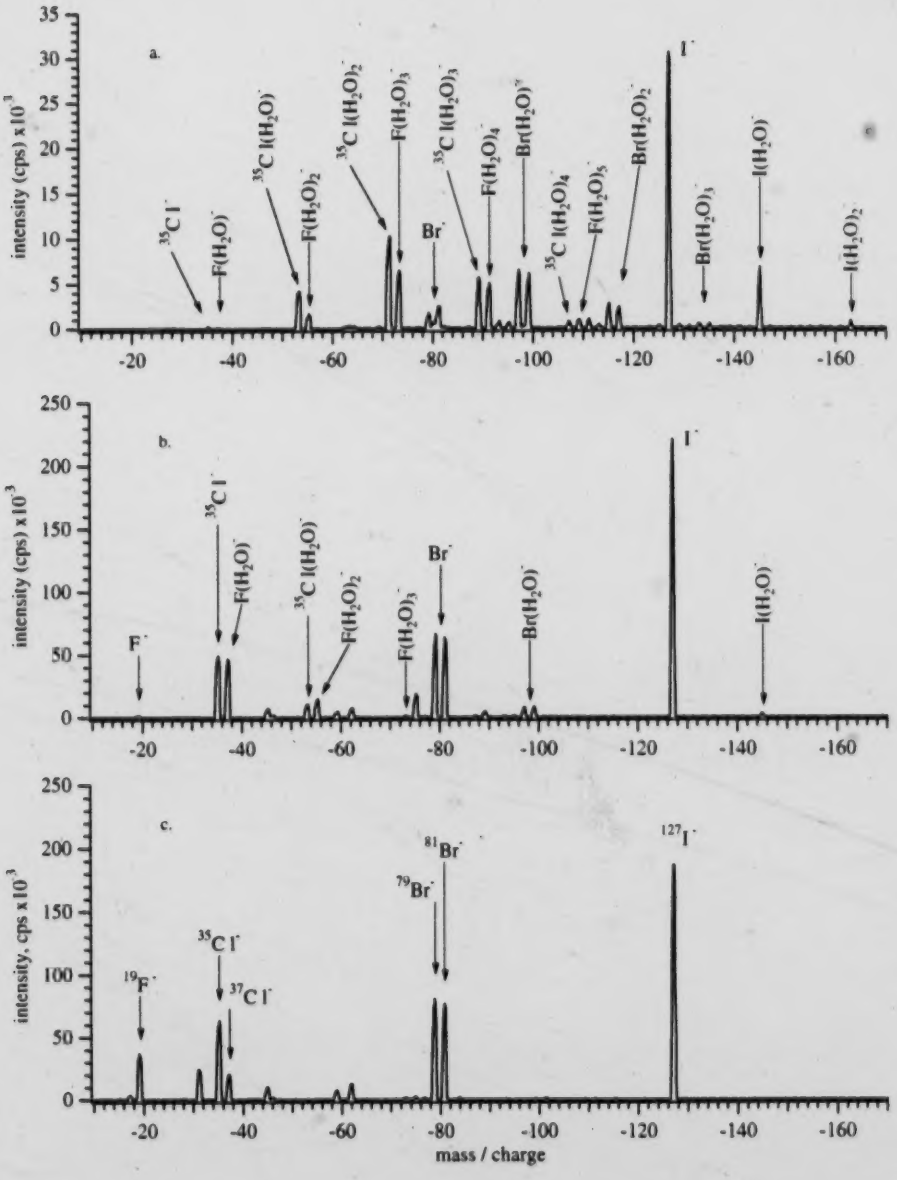

Figure 3.01 Electrospray mass spectra of a 0.1 mM methanolic solution of fluoride, chloride, bromide and iodide acquired with varying ΔV settings: (a) -9 V, (b) -14 V and (c) -34 V.

$$\Delta G^{o}_{sol} = -\frac{z_i^2 e^2 N_A}{8\pi\varepsilon_o r}\left(1-\frac{1}{\varepsilon_r}\right) \qquad 3.01$$

where z_i is the integral charge on the ion, e is the charge of an electron (1.6×10^{-19} C), N_A is Avogadro's number (6.02×10^{23} mole^{-1}), ε_o is the permittivity of vacuum, r is the ion radius, and ε_r is the dielectric constant of the solvent. The approximate relationship between ion radius and solvation sphere for both fluoride and iodide ions is illustrated in Figure 3.02. An increase in ΔV to −14 volts decreases the observed degree of solvation. This decrease in solvation in turn serves to decrease the complexity of the spectrum in Figure 3.01b. The mechanism of desolvation of a simple hydrated anion, $X(H_2O)_n$, by collisionally induced dissociation with nitrogen in the gas phase may be summarized by equation 3.02.

$$X(H_2O)_n^- + N_2 \rightarrow X(H_2O)_{n-1}^- + H_2O + N_2 \qquad 3.02$$

Despite the fact that the electrospray solvent is primarily methanolic, ion-solvent clusters with methanol in the coordination sphere are rarely observed in the electrospray mass spectra of simple inorganic ions. This may be attributed to both preferential solvation by water, and preferential evaporation of methanol from electrosprayed droplets.

It is important to notice in Figure 3.01b that there is considerable overlap of the ^{37}Cl species at *m/z* -37 and -55 with solvated ^{19}F species. It will be especially important when selecting operating conditions for quantitation to ensure that this type of interference is not present. Another potential spectral interference of this type that may cause considerable error in the determination of chloride is the solvated hydroxide ion, $OH(H_2O)^-$, at *m/z* -35. Fortunately, an increase in ΔV to -34 V, as shown in Fig. 3.01c, may be used to eliminate such possible interferences. At this potential, all of the halides are observed to exist as bare, singly charged anions. From these spectra, various prominent background species, which are always

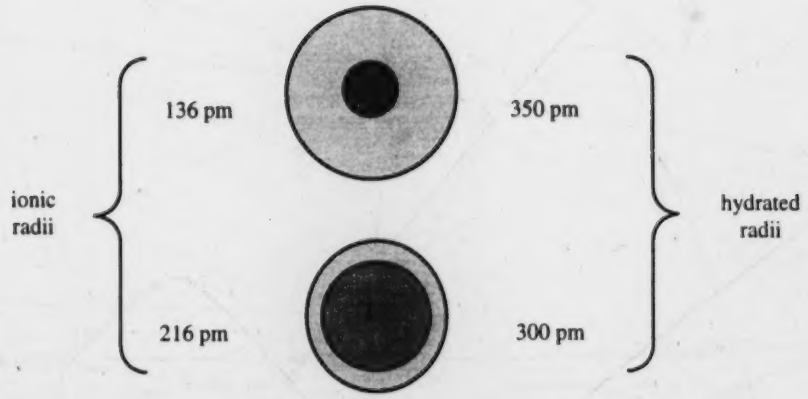

Figure 3.02 Cartoon showing relative ionic and hydrated radii of fluoride and iodide ions.

present when operating the electrospray in negative ion mode with a methanol/water solvent system, may be identified. A list of these background species, as observed in Figure 3.01c, is presented in Table 3.01.

3.3.2 Quantitation

It has been shown that stable electrospray operation is limited to a range of solution conductivity that is determined by the level of nonvolatile electrolyte present in the solvent [24, 26-28]. When the conductivity of the solution is too low, the electrospray current will fluctuate rapidly and produce mass spectra dominated by species indicative of corona discharge. High concentrations of ions at the interface also destabilize the Taylor cone, resulting in reduced spray efficiency. A conductivity or concentration window for stable electrospray may thus be defined. This operational window varies with electrospray operating parameters but typically results in stable signals for 10^{-5} – 10^{-3} M electrolyte in methanolic solvent. Figure 3.03 shows an attempt to establish a calibration curve for bromide over a concentration range of 1 x 10^{-7} to 3 x 10^{-3} M. The calibration curve is clearly non-linear. At low concentrations the observed ion intensity is low, unstable and independent of increasing concentration. This behavior is attributed to insufficient electrolyte that is required to establish the stable electrospray phenomenon. An abrupt increase in intensity is observed when the bromide concentration reaches 10^{-5} M, followed by a linear increase (log-log slope of ~1) in signal up to a concentration of 3 x 10^{-4} M, above which the signal levels off. The roll-off of the calibration curve at high concentration has been the focus of much research and debate in recent literature [26, 28, 29]. It may be explained in part by a practical limit in the number of ions that can reside on the surface of the Taylor cone and on the surface of charged droplets emanating from the apex of the cone. Fortunately, there are at least two ways to extend the linear range of the curve shown in Figure 3.03. To extend the curve to lower concentrations suitable for trace analysis, Agnes and Horlick [24] proposed the addition of a constant level of "supporting" or stabilizing electrolyte at the 0.1 mM level in the presence of the analyte of interest. In this study, it was observed that the addition of 0.1 mM potassium iodide to standard solutions of bromide resulted in the observation of stable

Table 3.01 Prominent background species observed for negative ion electrospray mass spectrometry using methanol/water solvent.

mass / charge	background species
-17	OH^-
-31	CH_3O^-
-32[a]	O_2^-
-45	HCO_2^-
-46	NO_2^-
-59	CH_3COO^-
-61	HCO_3^-
-62	NO_3^-
-75	$CH_3O(CO_2)^-$
-89	$HC_2O_4^-$

[a] indicative of corona discharge, not present during stable electrospray operation

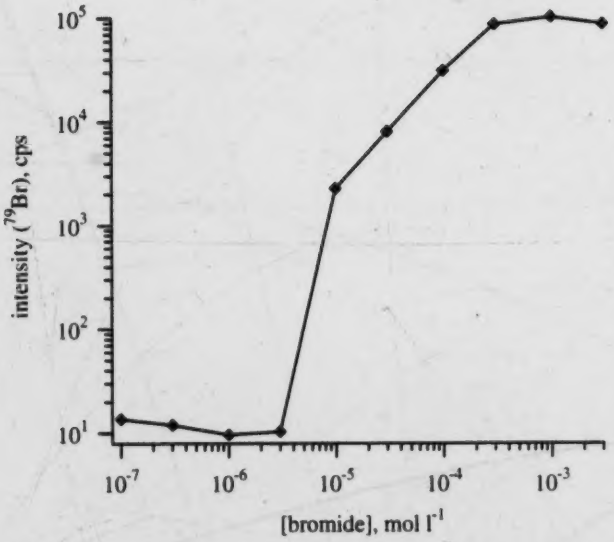

Figure 3.03 Attempted analytical curve for bromide in methanol using the ^{79}Br isotope, $\Delta V = -35$ volts.

bromide signals for concentrations as low as 10^{-8} M.

A plot of the absolute intensities of both bromide and iodide versus increasing bromide concentration is shown in Figure 3.04. From this plot it is seen that the addition of 0.1mM iodide may be used to effectively extend the calibration curve for bromide to lower concentrations. However, at high concentrations the roll-off of the bromide curve persists. It is observed that the iodide signal is relatively constant up to a bromide concentration of 3×10^{-6} M. Linearization of the analytical curve at higher concentrations may be accomplished by employing the electrospray stabilizer, iodide in this case, as an internal standard. The result of plotting the ratio of the bromide and iodide signal intensities is demonstrated in Figure 3.05a. In addition to effectively compensating for signal suppression at elevated concentrations, the use of an internal standard may also correct for instrument-related drift or moderate changes in electrospray operating parameters. The presence of iodide in this case is beneficial because of its multi-function role as an electrospray stabilizer and internal standard. Figure 3.05b illustrates a calibration curve for fluoride acquired in a similar manner to that for bromide. An intense investigation into the cause of signal suppression in electrospray mass spectrometry was not the focus this study. Nevertheless, it is seen in Figure 3.05 that regardless of the effect of suppression, the ratio of analyte to electrolyte signal is a linear function of analyte concentration.

3.3.3 Solvent Composition

Another benefit of employing an internal standard for quantitative electrospray studies results from the observation that analyte sensitivity is very dependent on solvent composition, in addition to the level of dissolved electrolyte. A demonstration of the effect of solvent composition is illustrated in Figure 3.06 for a binary solvent system of methanol and water. The plot consists of the observed intensities of 0.1mM bromide and 0.05mM iodide plotted on the left axis, and the ratio of the two signals plotted on the right axis, as a function of increasing water content. The signal for both

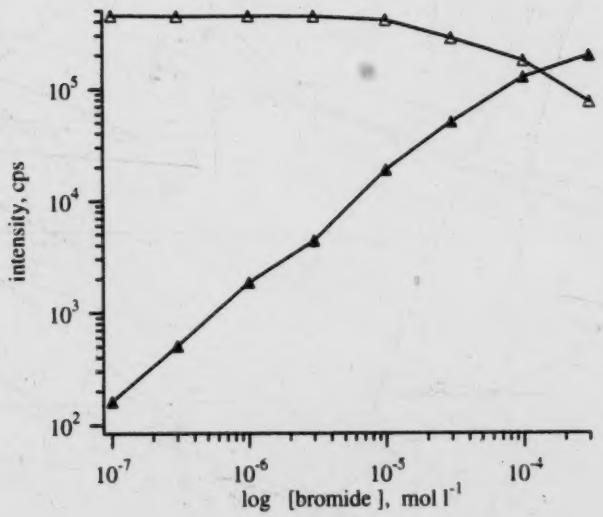

Figure 3.04 Signal intensities of bromide (▲ , ^{79}Br) and 0.1mM iodide (Δ, ^{127}I) plotted as a function of increasing bromide concentration, ΔV = -35 volts.

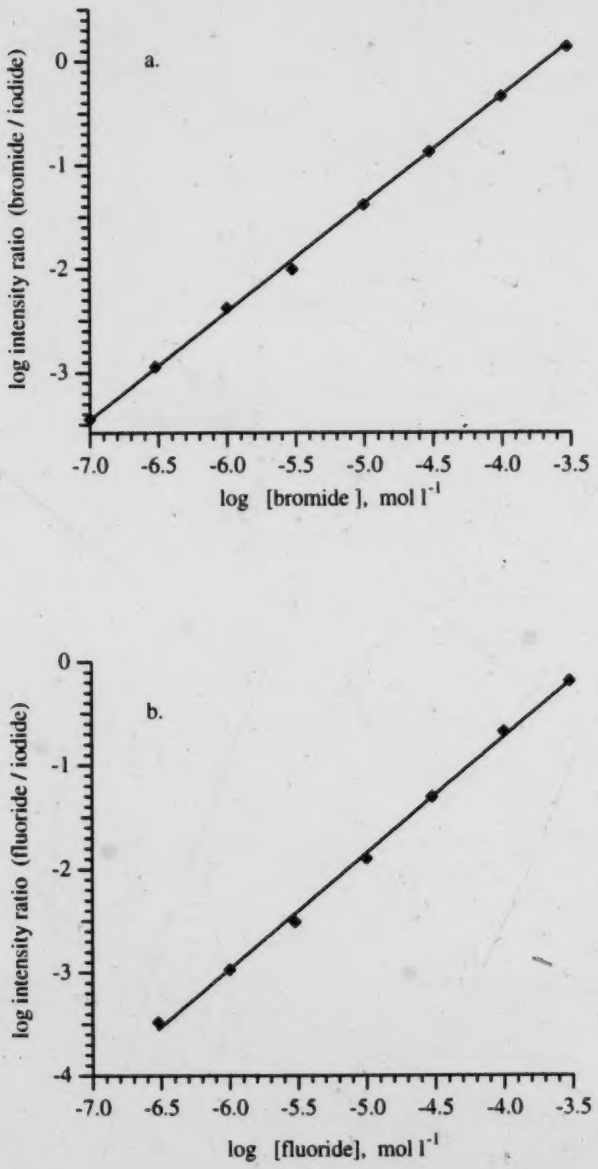

Figure 3.05 Analytical curves for (a) bromide and (b) fluoride employing 0.1mM iodide as an electrospray stabilizer and internal standard ΔV = -35 volts.

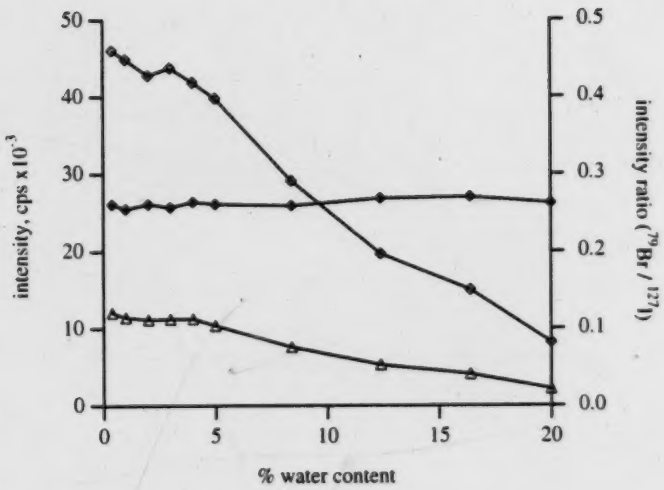

Figure 3.06 Effect of increasing water content on signal intensities of bromide (Δ), iodide (◇), and the signal ratio (◆) in methanolic solution, ΔV = -35 volts.

analytes is reduced by approximately 80% when the water content is raised to 20%. However, the relative signal intensities for the two analytes remain reasonably constant. The fact that both analytes are affected equally by changes in the solvent suggests that the decrease in sensitivity is the result of a change in the efficiency of ion liberation by the electrospray process. Increasing the aqueous content of the solution increases average droplet sizes and lowers the rate of droplet evaporation. These two factors are both important in the generation of gas-phase ion solvent clusters.

3.3.4 Effect of Multiply Charged Metal Ions

In consideration of possible matrix effects that may result in inaccurate quantitation of simple inorganic anions by electrospray mass spectrometry it is imperative to consider the effect of counterions, specifically metal ions in solution. Figure 3.07 shows mass spectra acquired at a sampling plate potential of –50 volts (ΔV = -45 volts) of three chloride salts. The observation of $CaCl_3^-$ in Figure 3.07a is rather surprising, although the presence of $FeCl_4^-$ and $ZnCl_3^-$ in concentrated (> 0.1 M) aqueous or methanolic solutions has been well documented [30, 31]. The samples used for the spectra in Figure 3.07 were much less concentrated (10^{-4} M) so it is likely that these species are not originally present in sample solutions but rather are formed during droplet desolvation. From these spectra it is clear that results for total free chloride ion concentration in samples containing calcium, iron, or zinc would appear artificially low in comparison to calibration with simple standard solutions of alkali metal salts. A recent report by Mollah et al. [32] discussed the occurrence of alkali metal "complexes" with halide and nitrate ions observed using an ionspray source. By employing gentle sampling conditions, the authors were able to observe such species as $CsCl_2^-$ and KNO_3^-, but only at electrolyte concentrations in excess of 0.1M. More stable complexes were observed for divalent metals such as zinc, but their studies were limited to samples with high acid matrices. Internal standardization may not be used to correct for metal ion interferences on halide determination, but it may be possible to employ a suitable masking or releasing agent to sample solutions that would preferentially bind interfering metal ions.

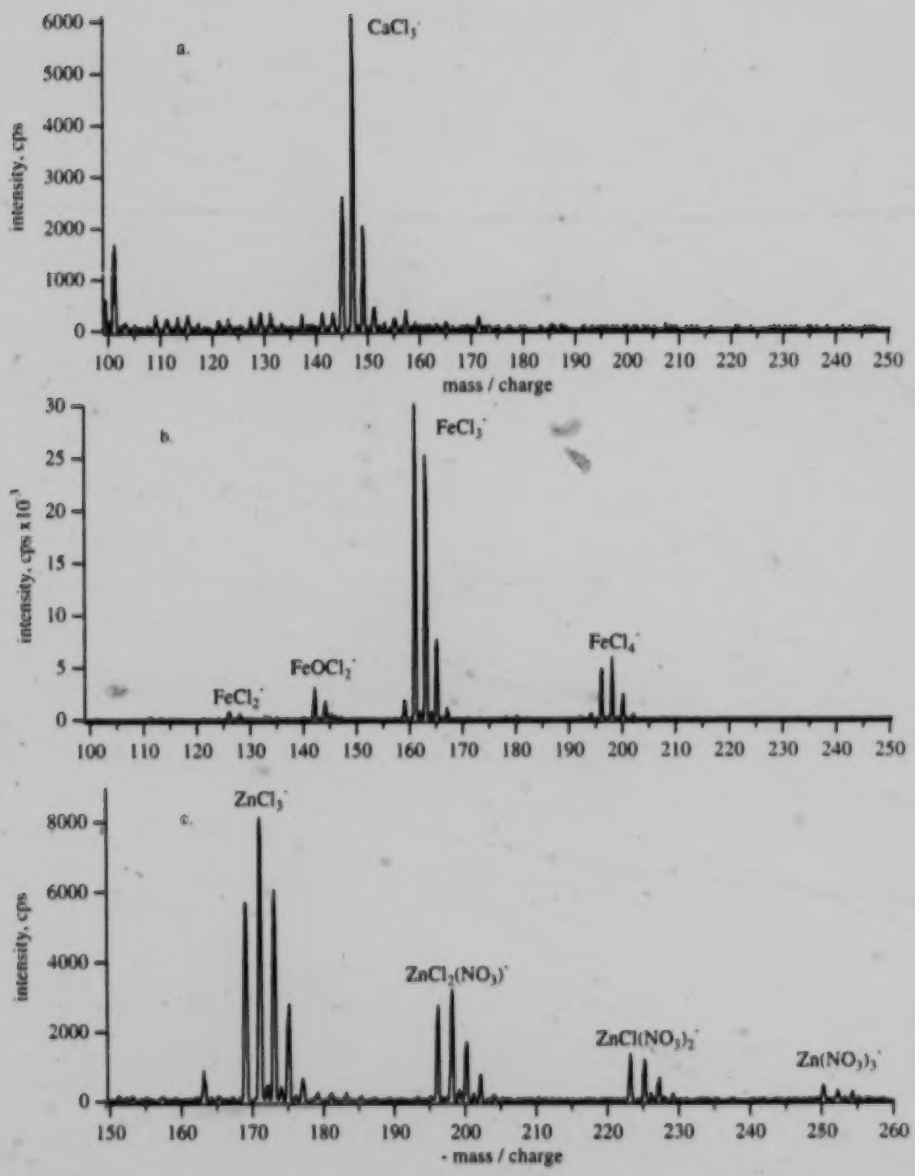

Figure 3.07 Effect of multiply charged metal ions on free gas-phase chloride ion concentrations: (a) 0.1mM calcium chloride, (b) 0.1mM ferric chloride and (c) 0.1mM potassium chloride in the presence of 0.1mM zinc nitrate, $\Delta V = -45$ volts.

3.3.5 Chlorine Speciation

One of the biggest concerns in speciation analysis is that the separation and/or detection mechanism does not alter the species originally present in solution. Figure 3.08 shows a series of spectra of an equimolar mixture of chloride, chlorate, and perchlorate. The first spectrum was acquired with ΔV = -34 V (the same potential used to efficiently desolvate the halides); the result is a relatively clean spectrum containing the usual background peaks and the characteristic chlorine isotope profile for the three chlorine containing species. The second spectrum was acquired at a potential difference of -54 volts. It is observed that the increased collisional energy results in the observation of the decomposition product, ClO_2^-. The potential gradient in the third spectrum was increased to -74 V, resulting in a very significant decrease in the observed intensity for the ClO_4^-, ion coupled with the appearance of a ClO^- species and an increase in the ClO_2^- intensity.

Similar decomposition products have been observed when only ClO_3^- is present in solution, therefore even though the chlorate signal appears to remain constant in these three spectra, it is likely that some chlorate is being dissociated while more is being formed by the decomposition of the larger perchlorate ions.

A plot of the relative observed intensities for the various decomposition products of perchlorate as a function of increasing CID potential is shown in Figure 3.09. At low potentials, the intensity of perchlorate is low due to incomplete desolvation and poor ion focusing into the mass spectrometer. From this diagram, it is clear that the window available for sensitive and accurate speciation of perchlorate is quite narrow since less than 5 volts separate the maximum intensity from the point at which chlorate is evident in the mass spectrum. In addition, it is seen that as decomposition occurs, the signal corresponding to oxygen radical ion at *m/z* -16 rises dramatically. Based on the appearance of the oxygen radical, the following cumulative decomposition reaction for perchlorate to bare chloride is suggested.

$$ClO_4^- + 4N_2 \rightarrow Cl^- + 4O^- + 4N_2^+ \qquad 3.03$$

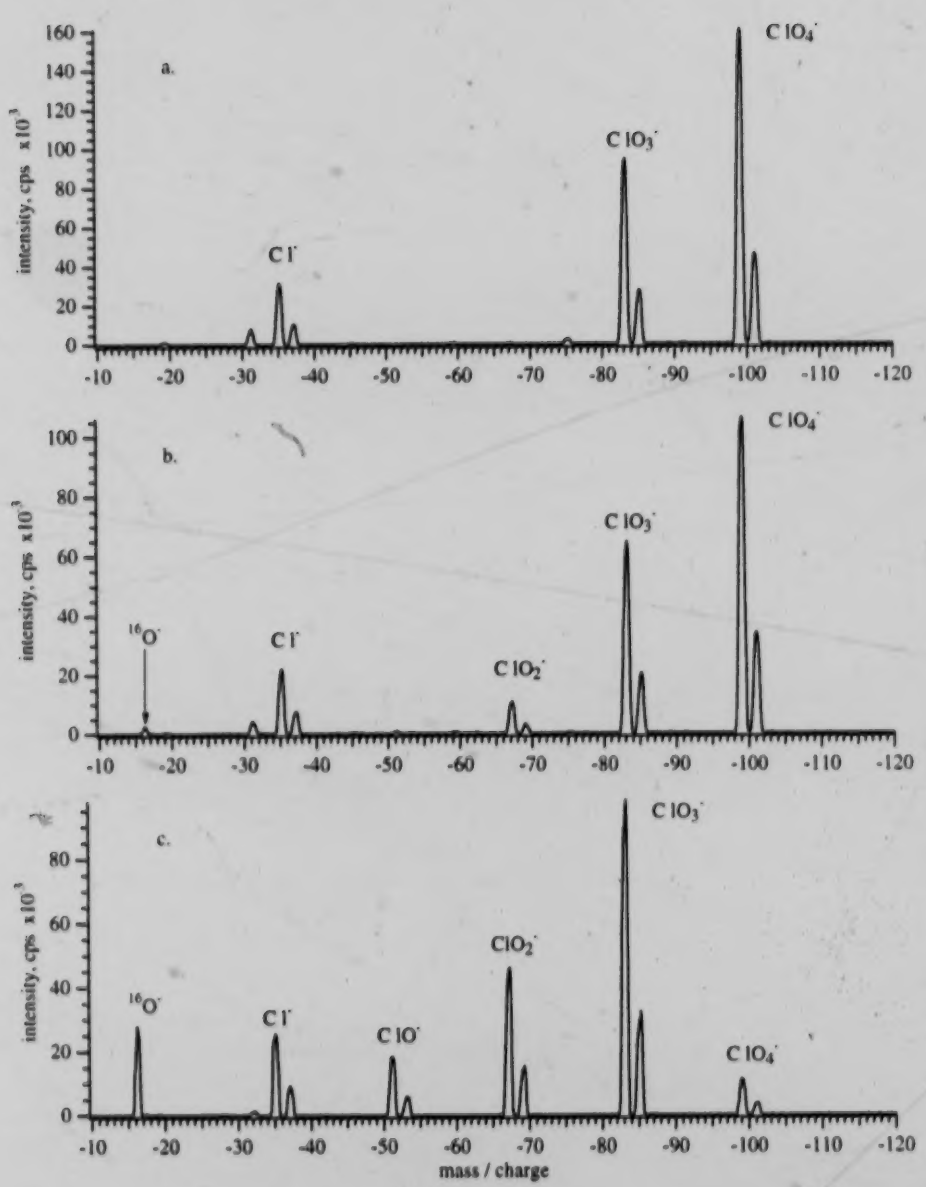

Figure 3.08 Electrospray mass spectra of a 0.1 mM methanolic solution of chloride, chlorate, and perchlorate acquired at varying values of ΔV: (a) -34V, (b) -54 V and (c) -74 V.

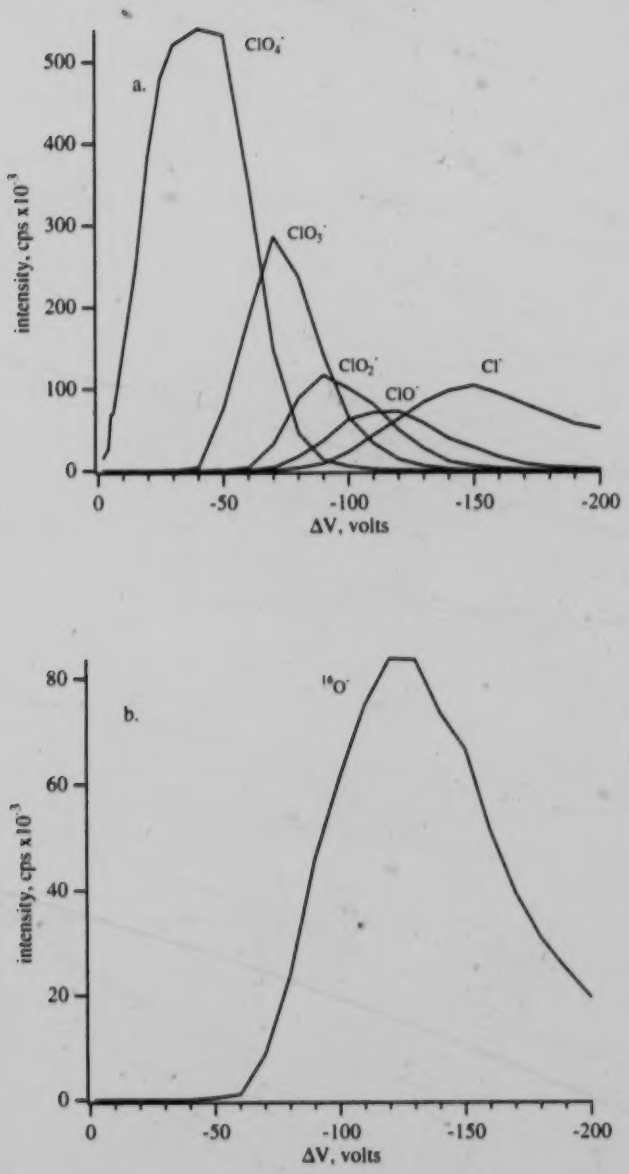

Figure 3.09 Effect of increasing sampling plate to skimmer potential difference, ΔV, (skimmer cone voltage = -5 volts) on (a) perchlorate ion speciation and (b) oxygen radical ion signal intensity.

It is important to carefully choose CID conditions for quantitation that will effectively desolvate the analytes of interest without resulting in their decomposition. Fortunately, for these three particular species, this CID energy "window" is reasonably large, allowing for the determination of calibration curves for all three species simultaneously. Figure 3.10 shows calibration curves, plotted on logarithmic axis, achieved for the three chlorine species present in the same 0.1mM methanolic solution of potassium iodide. The curves for chlorate and perchlorate are both linear over three orders of magnitude, while the chloride signal levels off just below a concentration of 1×10^{-6} M. Chloride has a much shorter linear range owing to impurities present in the potassium iodide supporting electrolyte and the solvent. One of the more subtle, yet most significant, features of this calibration is that despite the fact that the three species were present in the same solution, their individual signal ratios to the iodide signal increase linearly with concentration. This implies that the suppression of the ion signal intensities is dependent on the total ion concentration rather than the individual properties of the ions present in solution. This is an important observation in consideration of the number of possible concomitant ions present in real samples. Given that the signals of various analytes are affected equally by changing electrolyte concentrations it should be possible to obtain meaningful analyte concentrations in samples by establishing analytical curves with appropriate internal standards.

3.3.5 Bromate Analysis

The accurate determination of bromate in municipal water supplies has become of particular concern in recent years, following its classification as a Group 2B carcinogen [33]. In several instances, natural bromate levels are elevated as a result of chlorination or ozonation, both of which are popular water purification processes. A recent study [34] has investigated the use of ion-exchange chromatography coupled with ESMS detection for sub-ppb analysis of bromate in French drinking water supplies. In view of the observed decomposition of perchlorate ion by collisional

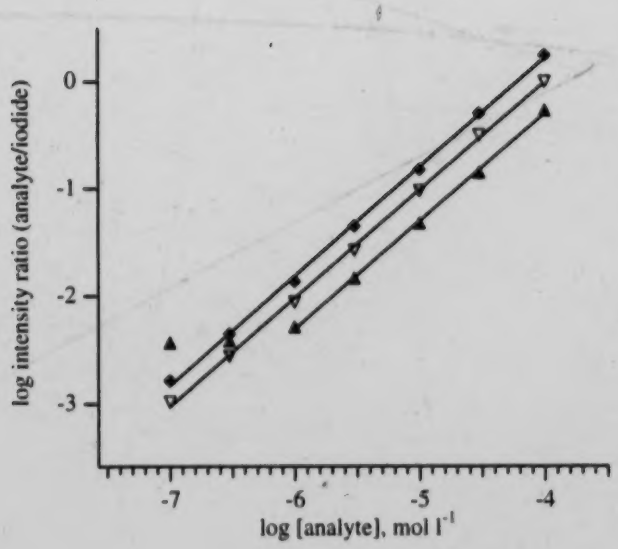

Figure 3.10 Multiple component analytical curves for chloride (▲), chlorate (▽) and perchlorate (◆). A 0.1mM level of iodide was employed as the electrospray stabilizer and internal standard, $\Delta V = -34$ volts.

induced dissociation, a similar investigation was performed on bromate in order to select a proper interface voltage setting. The result of this experiment is presented in Figure 3.11 as a fractional composition plot for bromate as a function of CID potential. Figure 3.12 shows calibration results for bromate (BrO_3^-) using formate ion as the electrospray stabilizer and internal standard. Iodide was not used for this analysis due to isobaric overlap of ^{127}I with $^{79}BrO_3^-$. The results of the calibration curve are similar to those observed in Figure 3.05 with the exception that the electrospray was stable to an overall higher total electrolyte concentration. The slight improvement in dynamic range may be due to the lower molar conductivity of formic acid.

3.3.7 Detection Limits

Calibration curves were established for fluoride, chloride, chlorate, perchlorate, bromide, bromate, iodide and iodate. Detection limits were estimated based on three times the standard deviation of the blank signal and are listed in Table 3.02, along with the slopes and the linear dynamic ranges of the logarithmic calibration curves. In the case of iodide, 0.1 mM bromide was used as the stabilizer and internal standard. Similarly, 0.1 mM formate ion was used as the internal standard for bromate. The high detection limit for chloride was the consequence of a high blank response.

3.3.6 Fluoride Analysis

A calibration curve for fluoride, linear over 2.5 orders of magnitude with a slope of 1.00, was shown in Figure 3.05b. In order to determine fluoride in a more complex matrix, another calibration curve was established over a much narrower range that spanned the concentration of samples to be analyzed. This calibration curve is shown in Figure 3.13 and is seen to be linear with a near-zero intercept. Volumes of 100 µl of two synthetic mouthwash samples used in an undergraduate teaching lab (M1169 and M1259) as well as two commercial samples (Cepacol® and Oral-B®) were diluted to 50 ml with methanol, which had been spiked to give 1×10^{-4} M potassium iodide in solution, and analyzed for fluoride content. The synthetic samples contained sodium fluoride, methyl salicylate and 4-chloro-1-butanol. The same samples were also

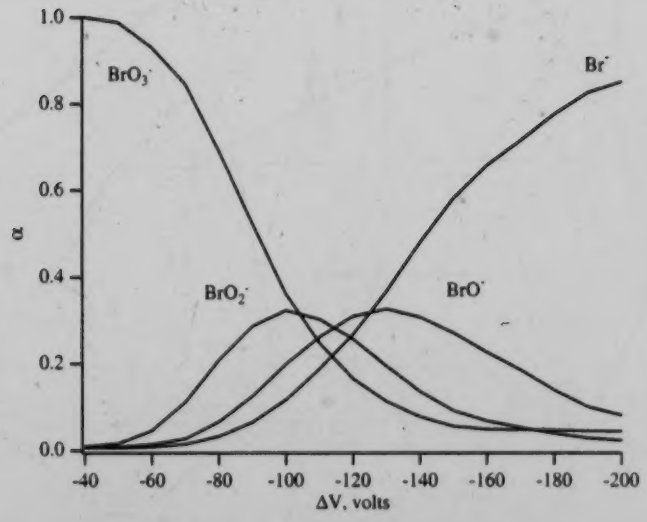

Figure 3.11 Fractional composition diagram for 0.1mM bromate (BrO_3^-) as a function of increasing sampling plate to skimmer potential (skimmer = -6 volts).

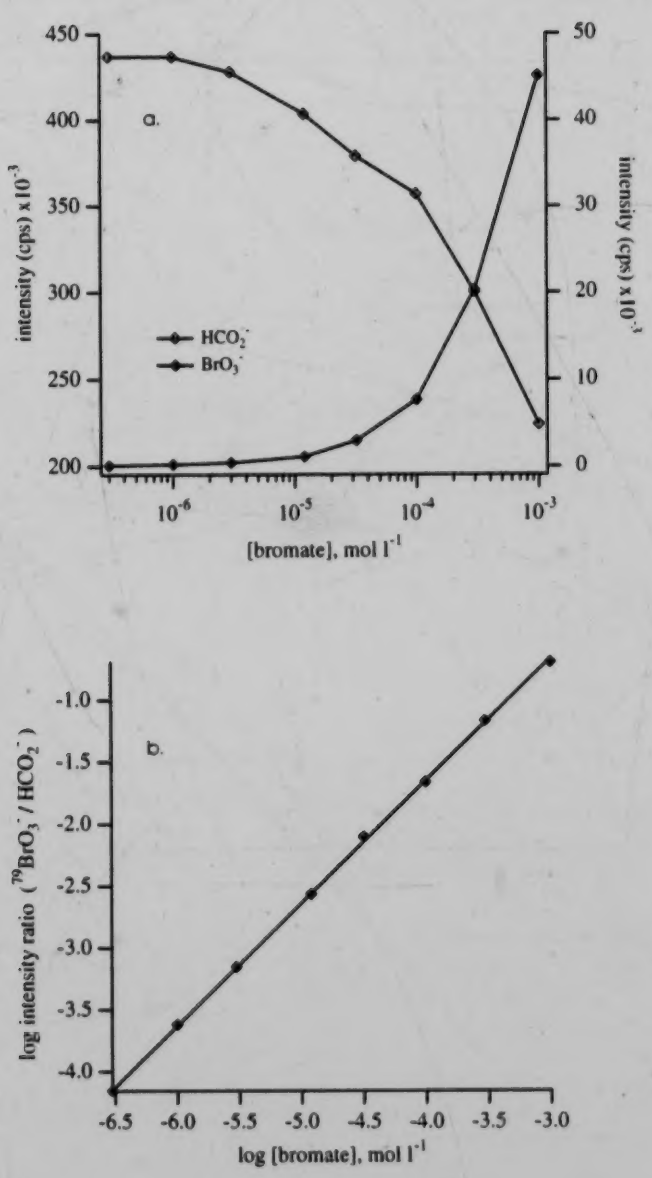

Figure 3.12 (a) Signal intensities of bromate (◆, $^{79}BrO_3^-$) and 0.1 mM formate (◇, HCO_2^-) ions as a function of increasing bromate concentration and (b) Analytical curve for bromate employing formate as the electrospray stabilizer and internal standard.

Table 3.02 Detection limits and analytical figures of merit for several anionic species by electrospray mass spectrometry.

Analyte	Log-log slope	Dynamic Range (μM)	Detection Limit (ng/mL)
^{19}F	1.00	0.3 – 300	0.8
^{35}Cl	1.00	1.0 – 300	35
$^{35}ClO_3$	1.03	0.1 – 300	0.7
$^{35}ClO_4$	1.03	0.1 – 300	0.5
^{79}Br	1.00	0.1 – 300	0.9
$^{79}BrO_3$	0.99	0.3 –1000	1.2
^{127}I	1.00	0.1 – 300	0.8
$^{127}IO_3$	1.01	0.1 - 300	1.0

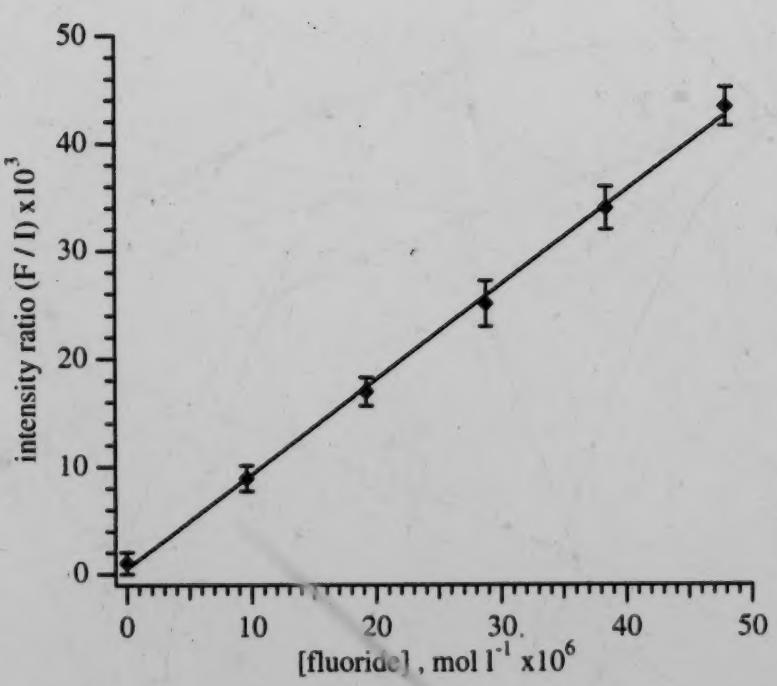

Figure 3.13 Analytical curve for fluoride with 0.1 mM iodide as the internal standard and electrospray stabilizer.

analyzed using a fluoride ISE as a check on the ESMS results. The results of the two methods are summarized in Table 3.03. It is seen that the fluoride concentration for the two synthetic samples determined by ESMS and using the fluoride electrode are in good agreement. The results for the two commercial samples, however, were much lower than expected (0.021%NaF and 0.009%NaF for Cepacol^{R} and Oral-B^{R} respectively) when determined using the calibration curve in Figure 3.13.

A second attempt to determine the fluoride content in the commercial samples using the method of standard additions was employed. The resulting curves for the two samples are shown in Figure 3.14. The sensitivity for the fluoride ion was much lower than for the standards used for the previous calibration as may be expected, however extrapolation of the sample fluoride levels from the standard addition plots correlate well with those determined by F-ISE. The fact that the fluoride concentrations determined in the commercial mouthwash samples from the calibration curve did not agree with the results obtained by standard addition, indicates that there may be an additional matrix effect occurring in electrospray that is not accounted for in simple electrolytic solutions. To determine if cetylpyridinium chloride, a component present at the same level as fluoride in both commercial mouthwashes for its anti-bacterial properties, was the cause of the matrix or suppression effect in the commercial samples, calibration standards were prepared with addition of 0.05% cetylpyridinium chloride. Determination of fluoride by matrix matching in this manner produced excellent agreement with the results of the F-ISE, indicating that the cetylpyridinium ion was responsible for the lower analyte sensitivity in the commercial samples. The cetylpyridinium ion is a large solvophobic cation with a relatively high surface activity and is shown in Figure 3.15a. The high surface activity of this cation may have a pronounced effect on both droplet formation and evaporation, which are crucial phenomena in the electrospray process. Figure 3.15b is a simple cartoon illustrating the expected orientation of a surfactant ion in a gas-phase aqueous or methanolic droplet.. In addition to its surface properties, there may also be a tendency for this large cation to form ion-pairs with fluoride, especially in a low dielectric solvent such as methanol. Rundlett and Armstrong [35] have recently published a

Table 3.03 Determination of fluoride in various synthetic and commercial mouthwash samples.

Sample	Concentration (% NaF) ESMS	ESMS (std. add.)[a]	Fluoride ISE[b]
M1169	0.050 ± 0.003[a]		0.051 ± 0.001
M1259	0.026 ± 0.002[a]		0.026 ± 0.001
Cepacol	0.021 ± 0.002[a]	0.062 ± 0.003	0.063 ± 0.001
	0.063 ± 0.002[c]		
Oral-B[R]	0.009 ± 0.001[a]	0.054 ± 0.001	0.056 ± 0.001
	0.057 ± 0.001[c]		

[a]error based on least squares analysis of curves shown in Figure 3.13 and 3.14. [b]error based on least squares analysis of ISE calibration curve. [c]determined using calibration standards containing 0.05% cetylpyridinium chloride.

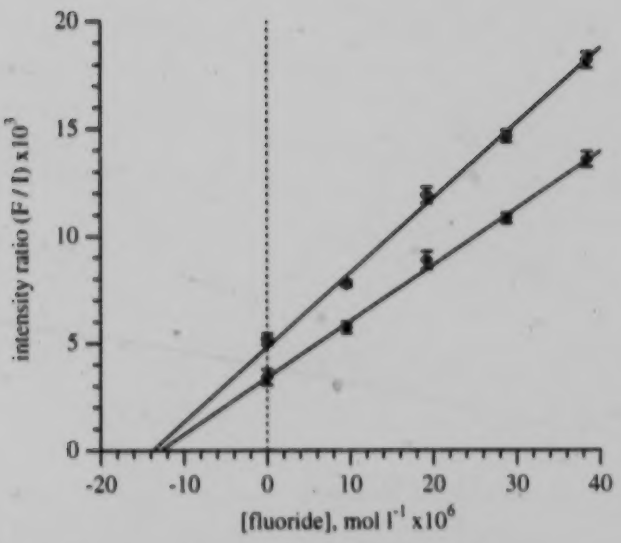

Figure 3.14 Standard addition calibration plots for the two commercial mouthwash samples (◆, Oral-B®) and (◇, Cepacol®) employing iodide as the internal standard and electrospray stabilizer.

report detailing a modified aerosol ionic redistribution model (mod-AIR) as a proposed mechanism for signal suppression in electrospray caused by surfactants. their experimental observations and subsequent proposal are consistent with the observations reported in this study.

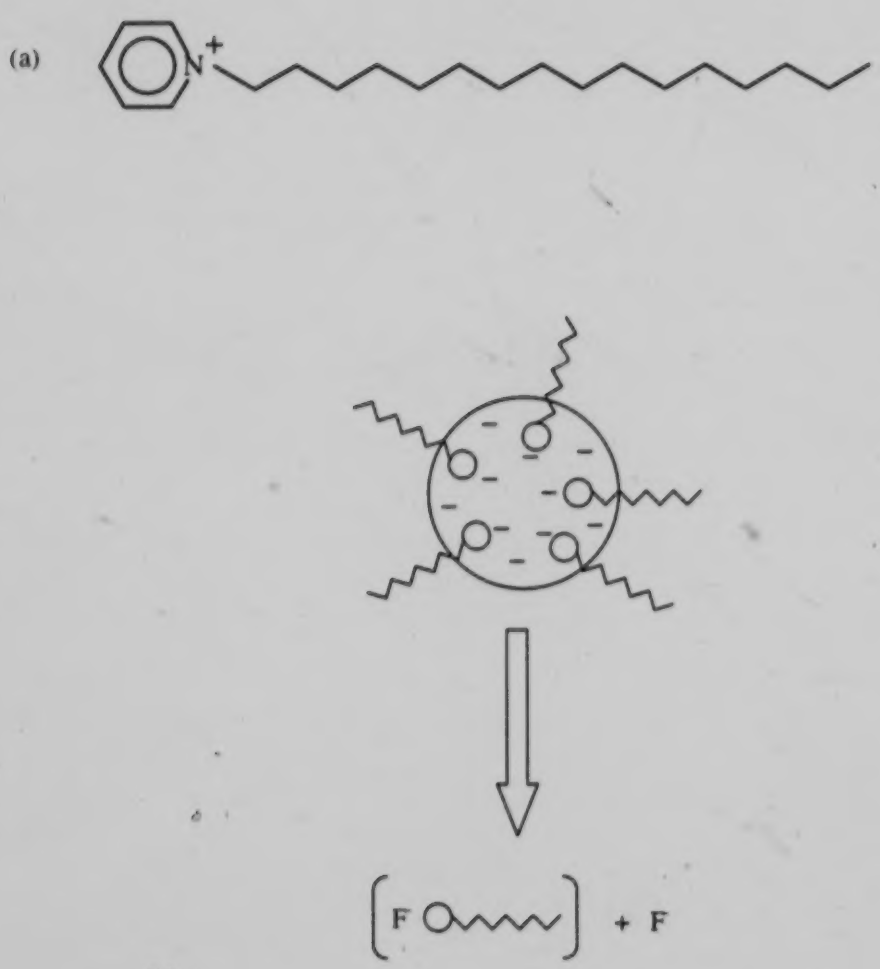

Figure 3.15 (a) Structure of cetylpyridinium chloride and (b) the predicted droplet structure and liberated fluoride ion species in the presence of a cationic surfactant.

3.4 Conclusions

The analytical utility of negative ion ESMS for quantitation and speciation of several halogenic anions has been presented. For these simple inorganic systems, it was found that despite the fact that analyte signal intensities are suppressed when the total electrolyte concentration exceeds 0.1 mM, the relative intensities of these simple inorganic ions present at constant levels in solution remain constant. It was also observed that analyte signals are independent of the identity of foreign electrolyte present in solution provided they do not introduce a chemical interference. Detection limits for most of the halogenic anions were found to be on the order of ~1 ng/mL which is comparable to current atomic techniques for bromide and iodide. However, the most significant advantage of this method is in its ability to speciate different forms of the halides directly and especially its sensitivity in the determination of fluoride.

Reliable determination of fluoride present in two real mouthwash samples was not achieved by a determination utilizing a simple calibration curve. However the methods of standard addition and matrix matching both resulted in a measured fluoride content in agreement with that determined by a fluoride ISE. This implies that additional matrix effects not accounted for in the simple inorganic systems studied thus far may be present in real samples. It is concluded that reliable quantitation by electrospray mass spectrometry may require the method of standard addition coupled with the addition of an appropriate internal standard and electrospray stabilizer.

3.5 References

1. Maki, S. A.; Danielson, N. D., *Anal. Chem.*, **1991,** 63, 699-703.

2. Dasgupta, P. K., *Anal. Chem.*, **1992,** 64, 775A-83A.

3. Shotyk, W., *J. Chromatogr.*, **1993,** 640, 309-16.

4. Umile, C.; Huber, J. F. K., *J. Chromatogr.*, **1993,** 640, 27-31.

5. Rhemrev-Boom, M. M., *J. Chromatogr. A*, **1994,** 680, 675-84.

6. vandenHoop, M. A. G. T.; Cleven, R. F. M. J.; Staden, J. J. v.; Neele, J., *J. Chromatogr. A*, **1996,** 739, 241-8.

7. LaFreniere, B. R.; Houk, R. S.; Fassel, V. A., *Anal. Chem.*, **1987,** 59, 2276-82.

8. Alvarado, J.; Carnahan, J. W., *Appl. Spectrosc.*, **1993,** 47, 2036 - 43.

9. Camuna, F.; Uria, J. E. S.; Medel, A. S., *Spectrochim. Acta*, **1993,** 48B, 1115-25.

10. Jin, Q.; Zhang, H.; Ye, D.; Zhang, J., *Microchem. J.*, **1993,** 47, 278.

11. Fulford, J. E.; Quan, E. S. K., *Appl. Spectrosc.*, **1988,** 42, 425-8.

12. Chong, N. S.; Houk, R. S., *Appl. Spectrosc.*, **1987,** 41, 66-74.

13. Vickers, G. H.; Wilson, D. A.; Hieftje, G. M., *Anal. Chem.*, **1988,** 60, 1808 - 12.

14. Montaser, A.; Chan, S.-K.; Koppenaal, D. W., *Anal. Chem.*, **1987,** 59, 1240-2.

15. Mohamad, A. H.; Creed, J. T.; Davidson, T. M.; Caruso, J. A., *Appl. Spectrosc.*, **1989,** 43, 1127-31.

16. Douglas, D. J.; French, J. B., *Anal. Chem.*, **1981,** 53, 37-41.

17. Creed, J. T.; Mohammed, A. H.; Davidson, T. M.; Ataman, G.; Caruso, J. A., *J. Anal. At. Spectrom.*, **1988,** 3, 923-6.

18. Creed, J. T.; Davidson, T. M.; Shen, W.-L.; Caruso, J. A., *J. Anal. At. Spectrom.*, **1990,** 5, 109-13.

19. Brown, P. G.; Davidson, T. M.; Caruso, J. A., *J. Anal. At. Spectrom.*, **1988,** 3, 763-9.

20. Story, W. C.; Caruso, J. A., *J. Anal. At. Spectrom.*, **1993,** 8, 571-5.

21. Satzger, R. D.; Fricke, F. L.; Brown, P. G.; Caruso, J. A., *Spectrochimica Acta.*, **1987,** 42B, 705-12.

22. Rafaelli, A.; Bruins, A. P., *Rapid Commun. Mass Spectrom.*, **1991,** 5, 269-75.

23. Ikonomou, M. G.; Blades, A. T.; Kebarle, P., *Anal. Chem.*, **1990,** 62, 957-67.

24. Agnes, G. R.; Horlick, G., *Appl. Spectrosc.*, **1994,** 48, 649-54.

25. Mann, M., *Org. Mass Spectrom.*, **1990,** 25, 575 - 87.

26. Tang, L.; Kebarle, P., *Anal. Chem.*, **1993,** 65, 3654-68.

27. Kebarle, P.; Tang, L., *Anal. Chem.*, **1993,** 65, 972A.

28. Tang, L.; Kebarle, P., *Anal. Chem.*, **1991,** 63, 2709-15.

29. Enke, C. G., *Anal. Chem.*, **1997,** 69, 4885-93.

30. Giubileo, G.; Magini, M.; Licheri, G.; Paschina, G.; Piccaluga, G.; Pinna, G., *Inorg. Chem.*, **1983,** 22, 1001-2.

31. Wertz, D. L.; Kruh, R. F., *J. Chem. Phys.*, **1969,** 50, 4013-8.

32. Mollah, S.; Fowler, K.; Houk, R. S., "Identification of inorganic ions in complex by electrospray mass spectrometry in counter-ion mode." in *A Kaleidoscope of Chemistry,* Pittconn (New Orlean, Louisiana, 1998).

33. Diemer, J.; Heumann, K. G., *Fres. J. Anal. Chem.*, **1997,** 357, 74-9.

34. Charles, L.; Pepin, D.; Casetta, B., *Anal. Chem.*, **1996,** 68, 2554-8.

35. Rundlett, K. L.; Armstrong, D. W., *Anal. Chem.*, **1996,** 68, 3493-7.

Chapter 4

Determination of Metals as EDTA Complexes

4.1 Introduction

An ideal elemental analysis technique for solution samples must be able to provide both qualitative and quantitative information about all solution components. Solution components include both anions and cations in elemental, molecular and complexed forms. Atomic spectroscopy has become the preferred method for measuring trace elements because of its sensitivity, selectivity and wide dynamic range. Currently, the most successful and widely used atomic techniques for elemental analysis are atomic absorption spectrometry (AAS), ICP-AES and ICP-MS. Unfortunately, these techniques are limited primarily to metallic cations and are incapable of discerning valence state, anionic composition, molecular form or complexation. In order to overcome these limitations, several researchers have successfully coupled separation techniques with atomic methods [1-7]. However, there are still many instances where speciation is ambiguous [4].

Numerous investigators have reported the utility of electrospray as a source for elemental speciation of a variety of doubly and triply charged metal cations in solution [8-18]. In particular, Agnes and Horlick [13] have demonstrated that electrospray mass spectrometry may be used to successfully differentiate valence states of several metals using what they refer to as three modes of positive ion electrospray: the ion- solvent cluster mode, the ion-counter ion mode and the bare metal ion mode. The ion-cluster mode employs gentle ESMS interface conditions to preserve and detect ion-solvent clusters produced by the ES source. Under these conditions, both cobalt and manganese were observed as doubly charged solvated ions $M(CH_3OH)_n^{2+}$ with n ranging from 4-13. This mode is useful for determining valence state, although quantitation is complicated by the fact that the metal ion intensity is distributed over many peaks, and the degree of solvation (value of n) is highly dependent on interface parameters as well as solvent composition.

The ion-counter ion mode employs slightly harsher conditions than the ion-cluster mode. This mode provides information on both valence state and the anionic composition of the solution. In the case of cobalt, several charge reduced species are

observed in the mass spectrum including $CoOH^+$, $CoCl^+$, $CoBr^+$ and $CoNO_3^+$. Quantitation remains difficult owing to the complexity of the spectrum and the variety of anionic compositions found in real samples. The affinities of metal cations for different anions are also expected to vary with solvent composition.

The bare metal ion mode is the harshest of the three modes. It strips all of the solvent and anions from the metal, producing spectra similar to those observed in ICP-MS. Lanthanide speciation by Stewart and Horlick [16] demonstrated that this mode also produces stable metal-oxides resulting in similar spectral interferences as observed in ICP-MS. The extent of persistence of metal oxides is more severe with the ES source owing to its lower energy characteristic. This mode essentially provides no speciation information and appears to have little or no advantage over ICP-MS.

In the aforementioned work by Agnes and Horlick [13], the potential strengths of electrospray operated in negative ion mode were also demonstrated. In this mode, it is possible to observe anionic composition directly, including species such as metallic oxo-anions, CrO_3^-, MnO_4^- and VO_3^-, and metal-ligand complexes, $Ag(CN)_2^-$ and FeF_3^-. Recent work [19-22] has examined speciation of sulfur, chromium, several halogenic anions and arsenic by negative ion electrospray or ionspray mass spectrometry, further demonstrating the strength of electrospray in elemental speciation analysis.

In order to overcome the limitations outlined above in metal ion speciation by electrospray, it is proposed that the virtues of negative-ion electrospray mass spectrometry be explored further. It has been well known for several decades that the complexing agent, ethylenediaminetetraacetic acid (EDTA) forms very stable negatively charged metal-ion complexes in solution. A singly charged metal ion such as sodium, forms a relatively weak $Na(EDTA)^{3-}$ complex, while doubly and triply charged metal cations form much stronger complexes with charges of –2 and –1, respectively. All of these complexes could potentially be transferred to the gas phase by electrospray and detected by mass spectrometry.

4.2 Ethylenediaminetetraacetic Acid (EDTA)

EDTA is a hexaprotic acid, with the fully deprotonated form designated as Y^{4-} and shown in Figure 4.01a. The pK_a values for the highlighted acidic hydrogen ions are as follows: $pK_{a1} = 0.0$, $pK_{a2} = 1.5$, $pK_{a3} = 2.0$, $pK_{a4} = 2.66$, $pK_{a5} = 6.16$, $pK_{a6} = 10.24$. Under sufficiently basic conditions EDTA will exist predominantly in the fully deprotonated Y^{4-} state. A fractional composition diagram of EDTA over the pH range of 0 to 14 is shown in Figure 4.01b.

The formation constant K_f of a metal-EDTA complex is the equilibrium constant for the reaction of free metal ion with Y^{4-}. Although Y^{4-} is not the only form of EDTA that reacts with metal ions, the equilibrium constant is expressed here in terms of the concentration of Y^{4-} for simplicity.

$$M^{n+} + Y^{4-} \Leftrightarrow MY^{n-4} \qquad 4.01$$

$$K_f = \frac{[MY^{n-4}]}{[M^{n+}][Y^{4-}]} \qquad 4.02$$

The formation constants of several metal-EDTA complexes studied in this work are listed in Table 4.01. To account for differences between the formal concentration of EDTA and the concentration of Y^{4-}, the conditional formation constant, K_f', is used.

$$[Y^{4-}] = \alpha_{Y^{4-}} F_{EDTA} \qquad 4.03$$

$$K_f' = \alpha_{Y^{4-}} K_f = \frac{[MY^{n-4}]}{[M^{n+}]F_{EDTA}} \qquad 4.04$$

Equation 4.04 may be used to describe the formation of MY^{n-4} at any particular pH, where α is the fraction of EDTA in the Y^{4-} form as shown in Figure 4.01b and listed in Table 4.02. It may also be necessary to consider the effect of auxiliary complexing

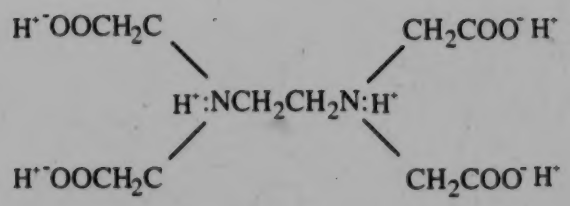

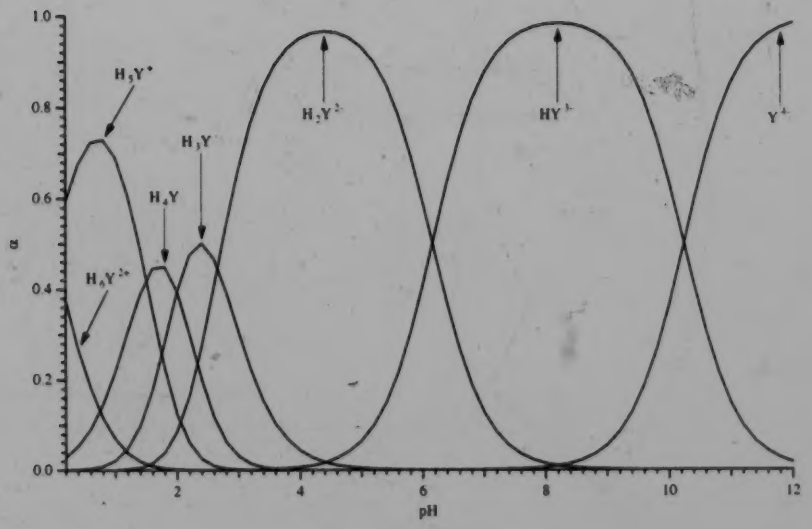

Figure 4.01 a) Structure of ethylenediaminetetraacetic acid, EDTA, and b) fractional composition diagrams for EDTA species as a function of aqueous pH.

Table 4.01 Formation constants, K_f, for several metal-EDTA complexes [28].

Ion	log K_f	Ion	log K_f
Na^+	1.66	Fe^{3+}	25.1
K^+	0.8	VO^{2+}	18.8
Be^{2+}	9.2	VO_2^+	15.55
Mg^{2+}	8.79	Zn^{2+}	16.50
Ca^{2+}	10.69	Al^{3+}	16.3
Sr^{2+}	8.73	Ga^{3+}	20.3
Ba^{2+}	7.86	In^{3+}	25.0
Fe^{2+}	14.32	Pr^{3+}	16.40
Hg^{2+}	21.7	Lu^{3+}	19.83
Sm^{3+}	17.14	Dy^{3+}	18.30
Cu^{2+}	18.80	Gd^{3+}	17.37

Table 4.02 Fraction of EDTA in the Y^{4-} form at various pH values [28].

pH	α_{Y4-}
0	1.3×10^{-23}
1	1.9×10^{-18}
2	3.3×10^{-14}
3	2.6×10^{-11}
4	3.8×10^{-9}
5	3.7×10^{-7}
6	2.3×10^{-5}
7	5.0×10^{-4}
8	5.6×10^{-3}
9	5.4×10^{-2}
10	0.36
11	0.85
12	0.98
13	1.00
14	1.00

ligands that reduce the concentration of free metal ion in solution. Consider a metal ion, M, that may form two complexes with a ligand, L, governed by the formation constants, β_1 and β_2.

$$M + L \Leftrightarrow ML \qquad \beta_1 = \frac{[ML]}{[M][L]} \qquad 4.05$$

$$ML + L \Leftrightarrow ML_2 \qquad \beta_2 = \frac{[ML_2]}{[ML][L]} \qquad 4.06$$

The fraction of free metal ion may be expressed as α_M:

$$\alpha_M = \frac{[M]}{C_M} \qquad 4.07$$

where

$$C_M = [M] + [ML] + [ML_2] \qquad 4.08$$

$$C_M = [M] + \beta_1[M][L] + \beta_2[M][L]^2 \qquad 4.09$$

therefore

$$\alpha_M = \frac{1}{1 + \beta_1[L] + \beta_2[L]^2} \qquad 4.10$$

Substitution of Equation 4.07 into Equation 4.04 leads to the following effective formation constant, K_f'', of metal-EDTA complexes.

$$K_f'' = \alpha_M \alpha_{Y^{4-}} K_f = \frac{[MY^{n-4}]}{C_M F_{EDTA}} \qquad 4.11$$

This equation may be used to describe the formation of metal-EDTA complexes in the presence of auxiliary complexing agents over a wide range of pH.

4.3 Experimental

4.3.1 Mass Spectrometry

Electrospray mass spectrometric (ESMS) experiments were performed on either the previously described SCIEX ELAN Model 250 or a commercially available SCIEX API-100 LCMS. The second mass spectrometer has a similar atmospheric pressure interface as the ELAN and a mass range of 30-1200 amu, which enabled the detection of complexes with mass-to-charge ratios, *m/z*, in excess of –285. Electrospray source and interface parameters for the two systems are summarized in Table 4.03.

4.3.2 Quantitation

In this study, it was observed that the presence of 0.1mM EDTA effectively meets the "supporting" electrolyte requirement for stable electrospray operation. The optimum level of nitric acid or sodium hydroxide that results in complete (>99.9%) metal complexation while keeping signal suppression to a minimum and avoiding precipitation of insoluble metal hydroxides in methanolic solution must be determined experimentally.

4.3.3 Atomic Emission Spectrometry

Flame atomic emission spectrometry was used to analyze for calcium in real samples for comparison with ESMS results. The instrument used was a Varian SpectrAA-200. Calcium emission in nitrous oxide-acetylene was monitored at 422.7 nm. Quantitation was performed using standard additions methodology. Addition of 3000 ppm potassium chloride to both sample and standard solutions was used to suppress ionization of calcium in the high temperature flame.

Table 4.03 Electrospray interface operating conditions for the modified ELAN 250 ICP-MS and the API 100 LCMS.

Component	ELAN 250	API 100 LCMS
needle	-2.7 kV	-3.2 kV
front plate	-600 V	-1100 V
sampling plate	-40 to -50 V	0 to -100 V
skimmer	-5 V	0 V

4.3.4 Reagents

Stock solutions of metal ions (10 mM) were prepared from either ACS-grade chloride or nitrate salts in nanopure water or by dilution of 1000 ppm ICP standard solutions containing 2% nitric acid. A 10 mM stock solution of ethylenediaminetetraacetic acid (EDTA) was prepared from the disodium salt. Distilled reagent grade methanol was used to dilute stock solutions by 100-fold for mass spectrometric analysis.

4.3.5 Sample Preparation

(i) Calcium supplement (Calais®): 50µL of the degassed supplement was diluted in 25mL distilled methanol containing 0.1mM EDTA and 0.05mM $Ba(NO_3)_2$

(ii) Tap Water: 250 µL was diluted in the same solvent and matrix described in (i)

4.4 Results and Discussion

4.4.1 EDTA Spectra

Two mass spectra of the disodium salt of EDTA acquired on the ELAN 250 with a ΔV of –40 volts are shown in Figure 4.02. The first spectrum exhibits three distinct peaks at *m/z* ratios of –123, -145 and –156. The latter two peaks correspond to the doubly charged EDTA species, H_2Y^{2-} and $NaHY^{2-}$. If it is assumed that the sensitivity for both species observed in the spectrum is similar, and that $NaHY^{2-}$ is formed in stoichiometric proportions from HY^{3-}, it is reasonable to attempt to correlate observed intensities with the fractional composition diagram in Figure 4.01b. Upon doing so, the relative intensities lead to an extrapolated pH of approximately 5.4 in methanolic solution. A 0.1 mM aqueous solution of the disodium salt of EDTA has a measured pH of 5.6. It is reasonable to assume that the observed $NaHY^{2-}$ is formed stoichiometrically from HY^{3-} since the formation constant of the sodium complex is

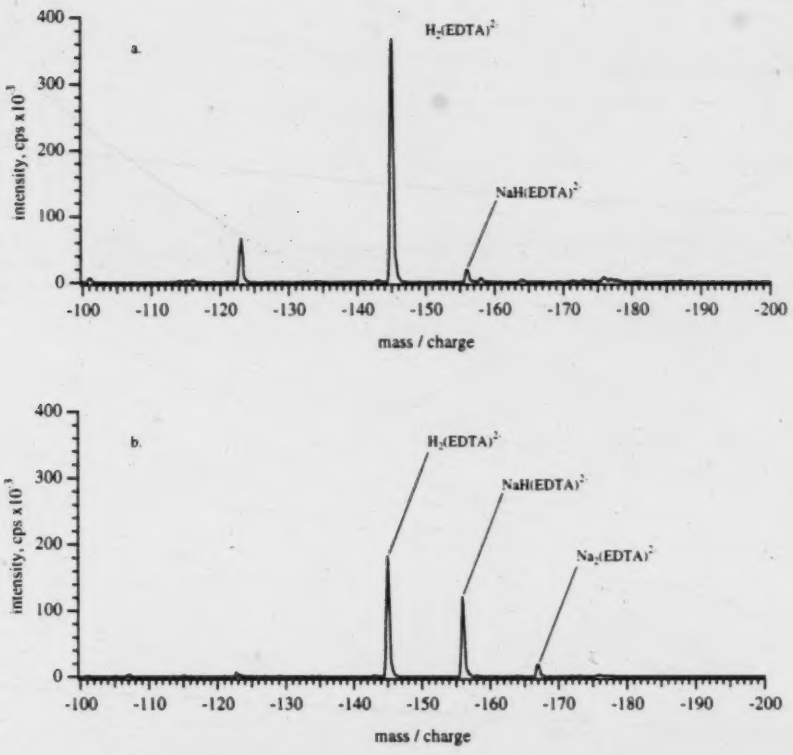

Figure 4.02 Mass spectra of 0.1 mM of the disodium salt of EDTA acquired on the ELAN 250 with a) no sodium hydroxide added and b) 0.1mM sodium hydroxide added, $\Delta V = -40$ volts.

small, $pK_1 = 1.66$. Hence, sodium is unlikely to displace a proton from H_2Y^{2-} via the following reaction.

$$Na^+ + H_2Y^{2-} \Leftrightarrow NaHY^{2-} + H^+ \qquad 4.12$$

The peak at *m/z* –123 is a doubly charged fragment of EDTA corresponding to the loss of $-CO_2$ *via* gas phase collision induced dissociation with nitrogen.

$$C_6H_{12}N_2(COO)_4^{2-} + N_2 \rightarrow C_6H_{12}N_2(COO)_3^{2-} + CO_2 + N_2 \qquad 4.13$$

where $C_6H_{12}N_2(COO)_4^{2-} = H_2Y^{2-}$. Lowering the magnitude of the sampling plate voltage by as little as 5 volts eliminated the observation of this fragment ion.

Figure 4.02b is a mass spectrum of 0.1mM disodium EDTA with a 0.1mM level of sodium hydroxide present. As expected with an increase in pH, there is a shift in the relative intensities of H_2Y^{2-} and $NaHY^{2-}$ to favour the latter. In addition a new unexpected species appears at *m/z* –168 corresponding to Na_2Y^{2-}. The strength of EDTA in titrimetric analysis is the fact that it forms strong complexes with metals in solution with 1:1 stoichiometry, which initially makes the observation of this species a bit puzzling. The observation of Na_2Y^{2-} may be the result of the formation of sodium adducts in the gas phase. The formation of sodium and potassium adducts from electrosprayed droplets has often produced limitations in both resolution and the maximum achievable charge state for several biological applications that rely predominantly on protonation or deprotonation for analyte charging. Further increases in the concentration of sodium hydroxide did not result in improved sensitivity for any of the three species, nor did it result in the observation of HY^{3-} or Y^{4-}. It is also likely that several singly charged EDTA species also exist in solution or are produced in the gas phase but owing to the limited mass range of the ELAN 250 they could not be detected.

Figure 4.03 shows a mass spectrum of a similar solution with the exception that

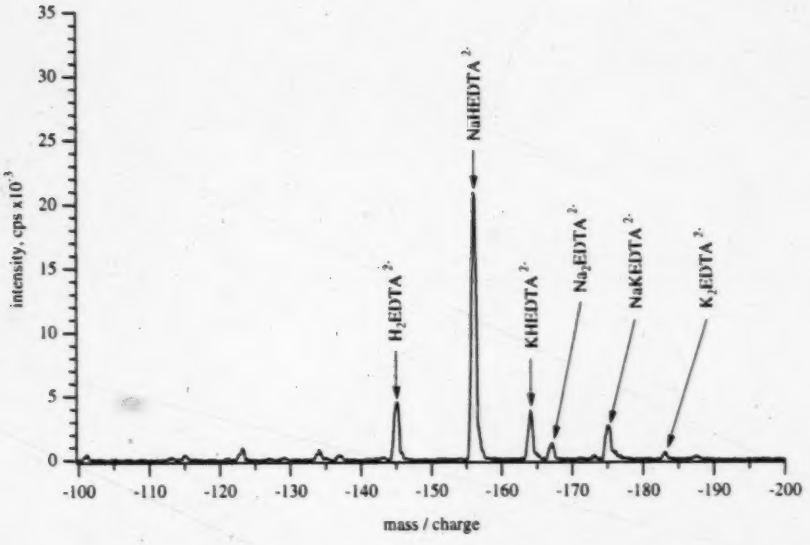

Figure 4.03 Mass spectrum of 0.1 mM of the disodium salt of EDTA acquired on the ELAN 250 with 0.1 mM potassium hydroxide added, $\Delta V = -35$ volts.

0.1 mM potassium hydroxide has been added instead of sodium hydroxide. The sodium complex exhibits much higher intensity than the potassium complex. This is consistent with its higher concentration and larger pK_f. The mixed complex, $KNaY^{2-}$, at *m/z* –174.5 is therefore a gas phase potassium adduct of the sodium EDTA complex.

In order to evaluate the full range of EDTA species observed in the gas phase, subsequent spectra of the disodium salt were acquired on a SCIEX API-100 LCMS. The first set of spectra is shown in Figure 4.04. These spectra were acquired with a ΔV of –50 volts for solutions containing 0.1 mM disodium EDTA with a decreasing level of sodium hydroxide from panel a through c in the figure. In panel c, no NaOH was added and the only species observed was H_3Y^-. Although the lower mass region is not shown, there were no doubly charged species present. This spectrum demonstrates that sodium is unable to displace a proton from the H_3Y^- form of EDTA to form a complex. Addition of 0.02 mM NaOH, as shown in panel b, results in the observation of several sodium complexes and subsequent sodium adducts of these complexes. Finally the addition of 0.2 mM NaOH, shown in panel a, results in conversion of all observed EDTA into the Na_3Y^- form. It is important to stress, that in all three of the spectra, no doubly charged species were observed, regardless of changes to solution pH. The reason for this observation becomes clear from the next spectrum in which the potential gradient is varied from 0 to –50 volts for a solution of 0.1mM disodium EDTA.

In Figure 4.05a, it is observed that a low ΔV setting results in several uncomplexed EDTA species, including doubly charged H_2Y^{2-} and $NaHY^{2-}$, as well as singly charged H_3Y^-, NaH_2Y^-, and Na_2HY^-. An increase in ΔV to –20 volts, shown in Figure 4.05b, almost eliminates the doubly charged species, while the only species to survive a further increase to –50 volts is H_3Y^-, as was observed in Figure 4.04. These results suggest that gas-phase collisions in the sampling region are responsible for the differences in observed spectra between the ELAN 250 and the API-100. Doubly charged ions are the first to be lost since they are accelerated to a greater degree under the electric field than singly charged ions. It is possible that these ions collide with

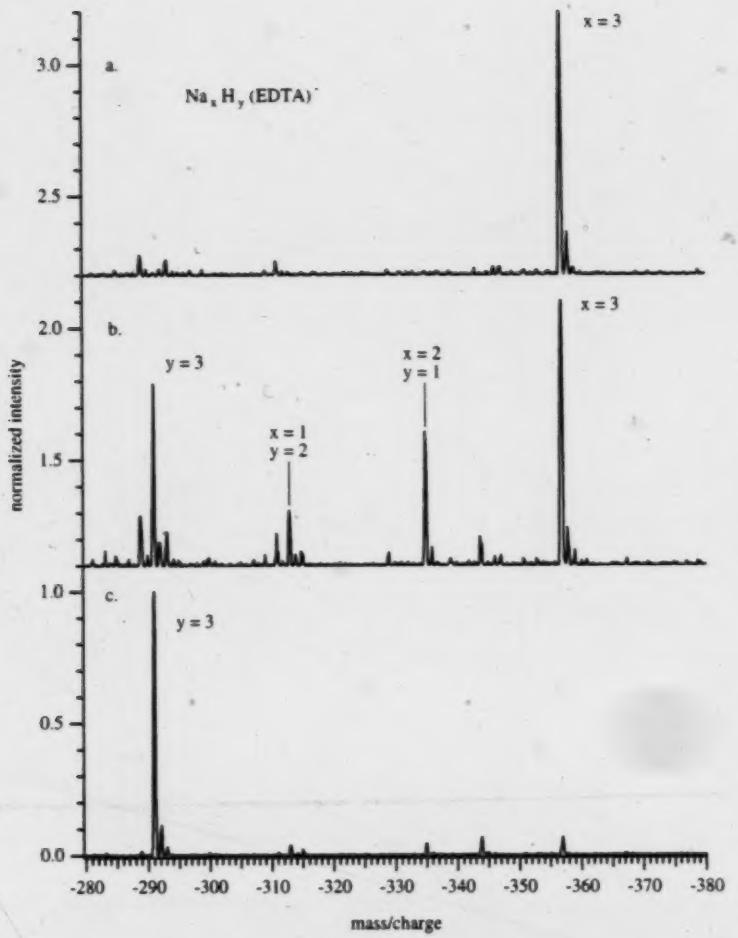

Figure 4.04 Series of mass spectra of the disodium salt of EDTA (0.1mM) with varying levels of sodium hydroxide added (a) 0.2 mM, (b) 0.02 mM and (c) 0.0 mM in methanol. Spectra were acquired on the SCIEX API-100 LCMS with $\Delta V = -50$ volts.

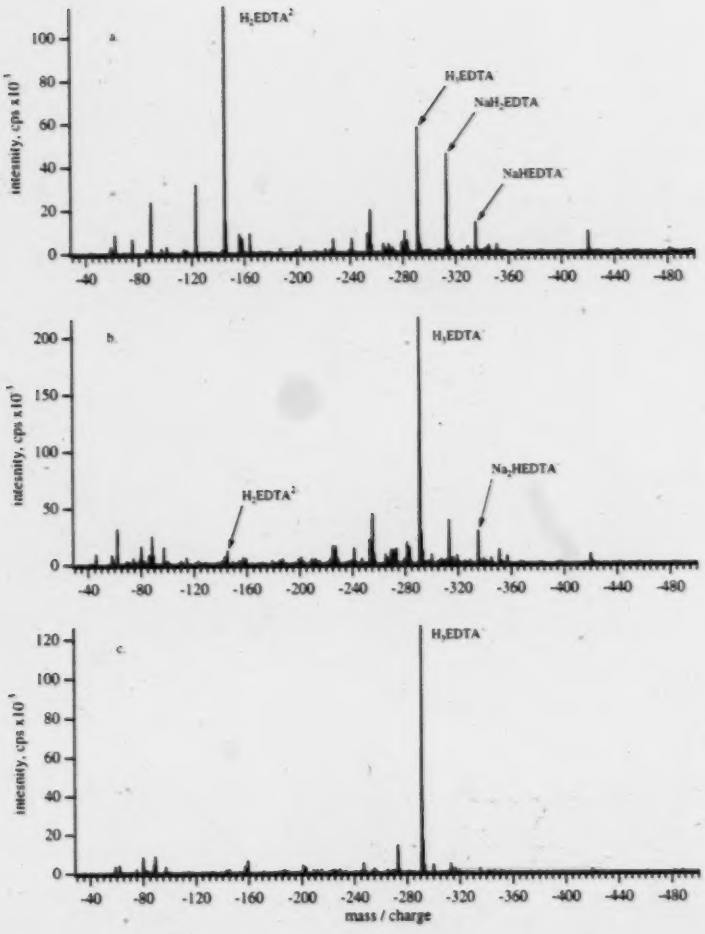

Figure 4.05 Series of mass spectra of the disodium salt of EDTA acquired on the SCIEX API-100 LCMS at ΔV settings of: (a) 0 volts, (b) -20 volts and (c) -50 volts.

nitrogen or water resulting in fragmentation or conversion to singly charged species *via* charge separation or proton transfer. Fragmentation may be expected to result in the observation of *m/z* –123. This ion is observed in the first spectrum but not in subsequent spectra when ΔV is increased. Collision with water may give the following reaction, resulting in an increase in the peak intensity at *m/z* -291.

$$H_2Y^{2-} + H_2O \Leftrightarrow H_3Y^- + OH^- \qquad 4.14$$

Another consideration arising from this experiment is that the desolvation or CID region in the API-100 mass spectrometer is apparently more efficient than that in the ELAN system, even though the design of the first stage vacuum interface is similar. This difference may be due to small differences in spacing between interface plates, differences in curtain gas flow rate and profile, or because of a significant difference in entrance ion optical arrangements. The entrance ion optics of the ELAN are located in the main vacuum chamber of the mass spectrometer (5×10^{-6} Torr) and consist of an Einzel lens configuration, while the API employs an rf-quadrupole focusing lens operating at mTorr pressure.

4.4.2 Divalent Metal Complexes

The complexation of divalent metals by EDTA is governed by the following equilibrium, which results in an overall formal charge on the complexes of 2–.

$$M^{2+} + Y^{4-} \Leftrightarrow MY^{2-} \qquad 4.15$$

The molecular mass of the Y^{4-} species is 288 amu, while the upper mass to charge limit of the ELAN 250 mass spectrometer is 285 units. For this reason, the only metal-EDTA complexes that are detectable with this mass spectrometer must be at least doubly charged. It is therefore important in the analysis of divalent metal ions to minimize charge reduction processes such as adduct formation and gas phase proton transfer.

4.4.2.1 Alkaline Earth Metals

The mass spectrum of a mixture of alkaline earth metal-EDTA complexes, in which each of the metals is present at 0.02 mM is given in Figure 4.06. A 0.1mM level of sodium hydroxide is added to the solution to increase α_{Y4-}, since the K_1 values for these metals are relatively low. Despite the high level of sodium, no sodium EDTA complexes are detected, since sodium has a much lower formation constant than the alkaline earth metals, see Table 4.01. It is not possible to resolve the isotopic distribution for these doubly charged complexes on a low-resolution quadrupole instrument since the isotopes are only separated by 0.5 amu and EDTA also contributes a significant group of ^{13}C satellite peaks. This spectrum is similar to an ICP-MS spectrum of the alkaline earth elements with a few exceptions. The most obvious exception is the difference in the mass scale, but in addition there is no argon, ^{40}Ar, interference on the calcium signal, and it is clear that the metals are doubly charged. Valence state speciation is of course more important for metals that commonly exist in more than one charge state, but the alkaline earth metals pose another problem for ICP-MS and positive mode ESMS owing to their low second ionization potentials. This is particularly true for barium, which is often observed in the gas phase as both Ba^{2+} and Ba^{+}. A testimonial to this fact is the inclusion of the Ba^{2+}/Ba^{+} ratio as a figure of merit in new ICP instrumentation.

4.4.2.2 Copper Sulfate and Cobalt Bromide

The simultaneous examination of both cationic and anionic solution compositions is a unique advantage of detecting positively charged metals as anionic metal-EDTA complexes. Figure 4.07 illustrates simultaneous detection of copper sulfate and cobalt (II) bromide. Note that both solutions have an aqueous solution pH of approximately 8. At this pH the sulfate anion would not be expected to occur as bisulfate, HSO_4^-, although the observation of bisulfate is a consequence of gas-phase equilibria and has been documented previously [19, 23].

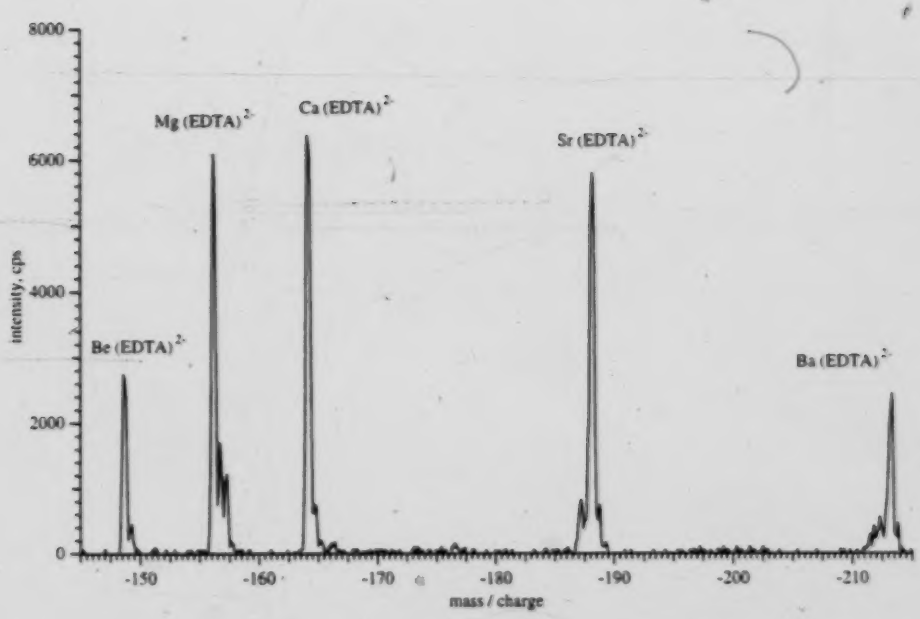

Figure 4.06 Mass spectrum of the alkaline earth metals (0.02mM Be, Ca, Mg, Sr and Ba) in 0.12mM Na_2EDTA and 0.1mM NaOH in methanol ($\Delta V = -35$ volts).

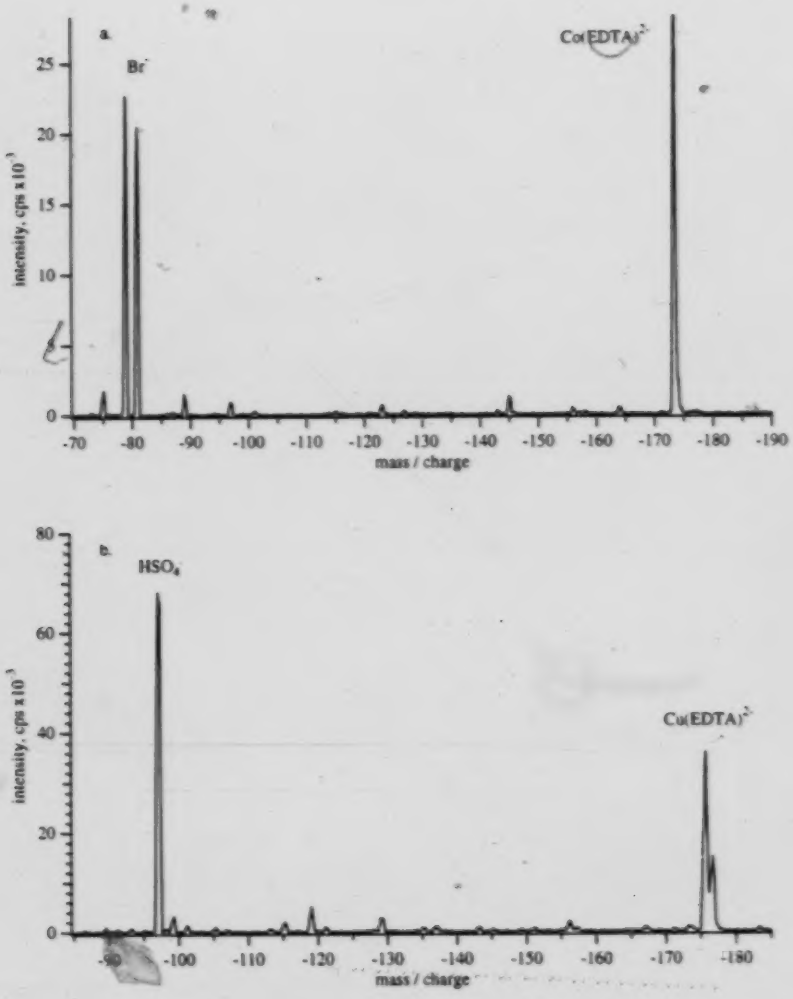

Figure 4.07 Mass spectra of a) 0.08 mM cobalt bromide and b) 0.08 mM copper sulfate with 0.1 mM Na_2EDTA at approximately pH 9.5 in methanol.

It is interesting to note that there have been reports in recent literature of attempts to use EDTA complexation to accomplish simultaneous separation and detection of metals and inorganic anions by ion chromatography employing either conductivity or indirect UV-detection [24-26]. The main limitation of these studies for sample analysis was the use of detection methods that were not species specific. Multitudes of poorly resolved peaks were observed in sample chromatograms upon the addition of EDTA. Attempts to identify the majority of the observed peaks were unsuccessful. Electrospray mass spectrometric detection coupled with these chromatographic separations could result in a powerful analytical combination.

4.4.2.3 Zinc Nitrate

Zinc is an element of significant biological activity, known to incorporate into several bioorganic complexes and fill an essential role in mammalian life processes. There have been numerous electrospray investigations involving the interaction of the divalent metal ion with amino acid residues and other biological molecules. A major concern of these studies has been to distinguish between solution phase interactions and those spawned in the gas-phase, in particular the observation of ion adducts [27]. EDTA is a strong chelator that is capable of stripping metals from weak non-covalent interactions. However, several complexing agents that may be used to establish a scale of binding strengths are available in order to address this concern.

A simple example of relative binding strengths for zinc with inorganic ions is demonstrated in Figure 4.08a, in which a 10-fold excess of zinc nitrate over EDTA (0.01mM) is diluted in methanol and analyzed on the ELAN 250 with a ΔV of –35 volts. In addition to the doubly charged ZnY^{2-} species, there are several other singly charged zinc related species. The isotope distribution of the EDTA complex is compressed by half compared to that of the $Zn(NO_3)_3^-$ species since it's mass is now divided in half. In Figure 4.08b, an excess of EDTA is present, which effectively eliminates $Zn(NO_3)Cl_2^-$, $Zn(NO_3)_2Cl^-$, and $Zn(NO_3)_3^-$ from the spectrum. Addition of 1mM ammonium hydroxide to a solution of 0.1mM ZnY^{2-} resulted in the

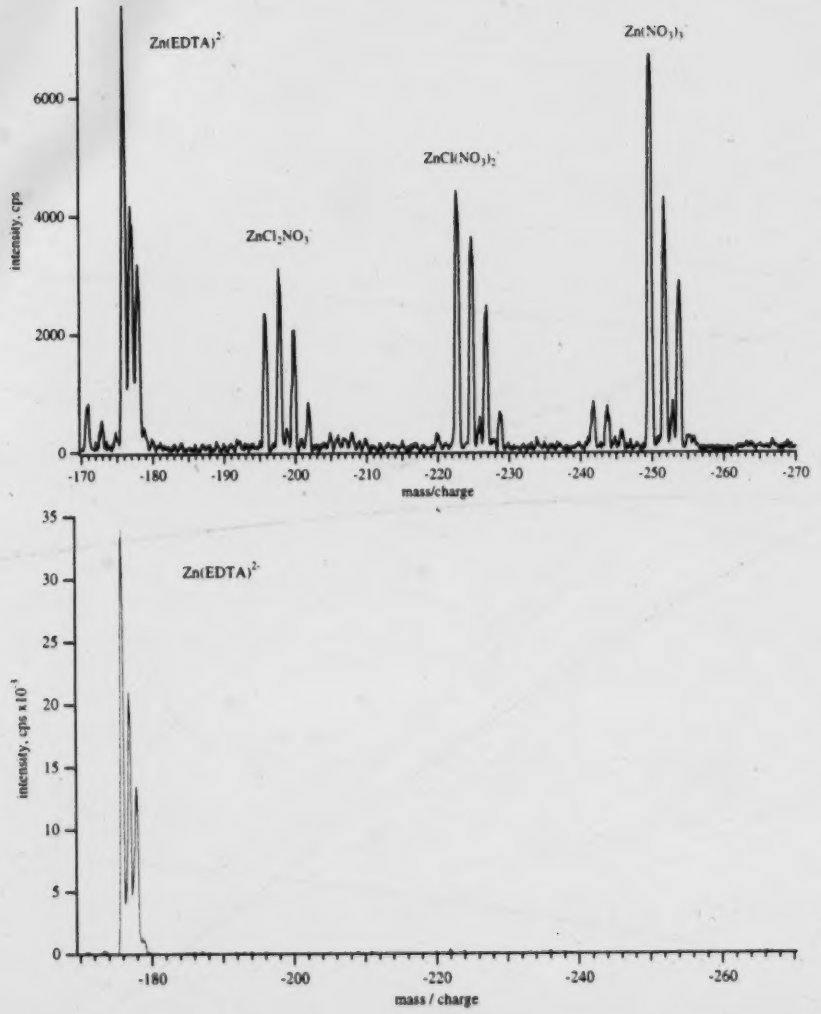

Figure 4.08 Mass spectrum of (a) 0.1 mM zinc nitrate and 0.01 mM Na_2EDTA and (b) 0.1mM zinc nitrate and 0.12 mM Na_2EDTA in methanol, ΔV =–35 volts.

disappearance of all zinc containing species in the negative ion mass spectrum, presumably due to the formation of $Zn(NH_3)_4^{2+}$ and/or $Zn(NH_3)_6^{2+}$. However, attempts to detect these species by positive mode electrospray were unsuccessful. It is also possible that a zinc hydroxide, $Zn(OH)_2$, may have been formed and gone undetected.

4.4.2.4 Mercury (II) Nitrate

Mercury is considered a "problem element" for atomic spectroscopists because of its relatively high volatility and its affinity for glass and quartz. These two factors lead to long equilibration times and memory effects in nebulizers. Because of low recoveries (< 80%) of this element, analytical chemists tend to prefer cold vapour or hydride generation analysis techniques. In addition to the volatility of mercury, it also has a high ionization potential and several abundant isotopes, which compromises ICP-MS detection. Fortunately, monomeric mercury forms stable, doubly charged complexes of low volatility with EDTA. Unfortunately, the complex isotope distribution of mercury combined with the double charge results in a broad unresolved peak on a low-resolution mass spectrometer so it was necessary to use the API-100. An electrospray mass spectrum of 0.2 mM monomeric mercury complexed to EDTA is shown in Figure 4.09. The potential difference ΔV was –20 volts, and as a result there are two isotope packets resembling the isotopic distribution of mercury, separated by 22 mass units. The two distributions are identified as $HgHY^-$ centered at *m/z* –495 and $NaHgY^-$ centered at *m/z* –517. Addition of EDTA could potentially be used to differentiate between the two common forms of ionic inorganic mercury, Hg^{2+} and Hg_2^{2+}, based on the stability of the Hg(II)-EDTA complex and the inability of dimeric mercury to react with EDTA. Unfortunately, this would require two separate measurements since the ions are of opposite polarity.

4.4.2.5 Vanadium (VO^{2+} *versus* VO_2^+)

Vanadium exists in several oxidation states ranging from 2 to 5 and as a result has relatively complex redox chemistry. Chromatographic separation of the various vanadium species is complicated owing to rapid, pH dependent equilibria between

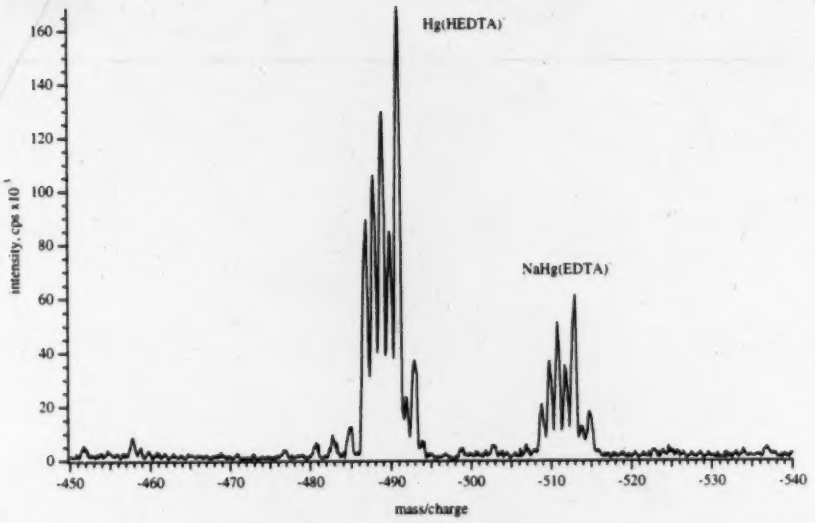

Figure 4.09 Mass spectrum of 0.08mM $Hg(NO_3)_2$ and 0.1mM Na_2EDTA acquired on the SCIEX API-100 LCMS, $\Delta V = -20$ volts.

oxidation states. The two most common oxidation states in nature are the +5 and +4 states, namely vanadate (VO_2^+) and vanadyl (VO^{2+}) respectively. Both of these species are known to form stable EDTA complexes; see Table 4.01 for relative formation constants. It was proposed that it may be possible to "freeze" these ions in solution by complexation with EDTA and speciate them simultaneously by electrospray. Sodium vanadate, $NaVO_3$, was used as the source of VO_2^+ ion. The equilibrium expression for inter-conversion of VO_3^- to VO^{2+} is given by equation 4.16:

$$VO_3^- + 2H_2O \rightarrow VO^{2+} + 4OH^- \qquad 4.16$$

Vanadyl sulfate, $VOSO_4$, was used as the source of vanadyl ions. The complexation equilibria for these two complexes are given as Equations 4.17 and 4.18.

$$VO_2^+ + EDTA \rightarrow VO_2EDTA^{3-} \qquad 4.17$$

$$VO^{2+} + EDTA \rightarrow VOEDTA^{2-} \qquad 4.18$$

It is clear from these expressions that vanadate reacts to form a triply charged anion and it was therefore expected to have a relatively complex spectrum composed of various doubly and singly charged vanadate-EDTA species. Vanadyl was expected to produce a cleaner spectrum owing to one less original charge on the complex. Figure 4.10a shows a mass spectrum of 0.08mM vanadate and 0.1mM EDTA. The spectrum is complex owing to the presence of several species associated with the excess EDTA as well as three vanadate containing complexes, namely HVO_2Y^{2-} at *m/z* –186, $NaVO_2Y^{2-}$ at *m/z* –197 and KVO_2Y^{2-} at *m/z* –205. Unfortunately this spectrum was not acquired on the API-100 so the presence and relative intensities of the singly charged vanadate complex species is unknown.

The vanadyl spectrum is much cleaner with only one major peak at *m/z* –177.5 corresponding to VOY^{2-}, shown in Figure 4.10b. The absence of peaks corresponding to excess EDTA may be due to a lower solution pH, which favours singly charged complex species. The difference in pH could be explained by equation 4.16.

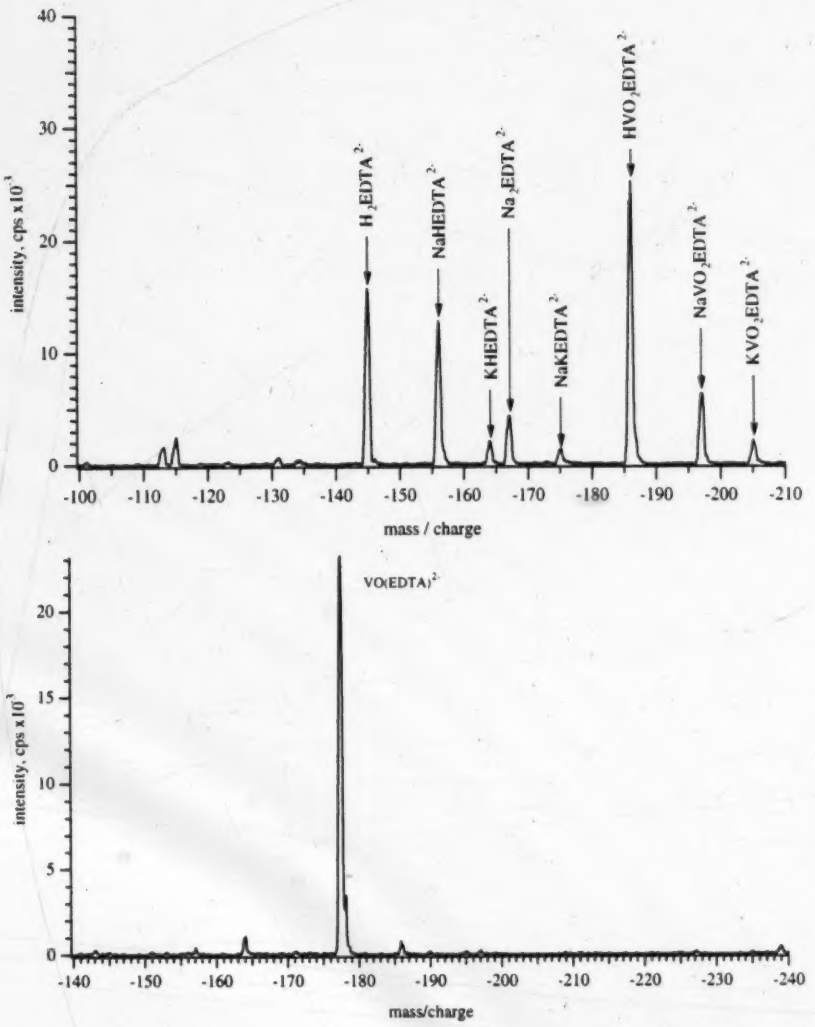

Figure 4.10 Mass spectra of a) 0.08 mM sodium vanadate and b) 0.08mM vanadyl sulfate in 0.1mM Na_2EDTA, $\Delta V = -35$ volts.

Otherwise, the difference may be attributed in part or in whole to the difference in the effect of sampling potential on complexes of different charge.

4.4.3 Trivalent Metal Complexes

The complexation of trivalent metals by EDTA is governed by the following equilibrium expression, resulting in an overall formal charge on the complex of –1.

$$M^{3+} + Y^{4-} \Leftrightarrow MY^{-} \qquad 4.19$$

Since the complexation constants for most trivalent metal ions are in excess of 10^{15}, complete complexation may be achieved in solutions that are more acidic than for divalent ions. This is fortunate since many solvated transition metals are subject to hydrolysis in neutral or slightly basic solution.

4.4.3.1 Aluminum Nitrate

A spectrum of a mixture of 0.08mM aluminum nitrate, $Al(NO_3)_3$, and 0.1mM EDTA acquired with a ΔV of 0 volts, is shown in Figure 4.11. At these gentle sampling conditions, several peaks appear in the mass spectrum in addition to the expected AlY^- ion at *m/z* –315. Through close inspection of the spectra, it is possible to distinguish two separate distributions of EDTA related ions having regularly spaced mass intervals. This behavior closely resembles solvated distributions observed in Chapter 3 for the halide ions; however, the peaks are not closely spaced enough to be solvent clusters involving methanol or water. The first distribution appears to involve the AlY^- ion with peaks at *m/z* values of –315, -400, -485 and –570. The regular separation of 85 mass units suggests that the "solvent" or adduct species is the neutral ion pair, $NaNO_3$. The second distribution begins at *m/z* –653, corresponding to an AlY^- dimer forming an adduct with one sodium ion. The next three peaks, designated y = 1, 2 and 3 occur at *m/z* values of –738, -823 and –908, all separated by 85 mass units; therefore these species are also assigned to sodium nitrate adducts.

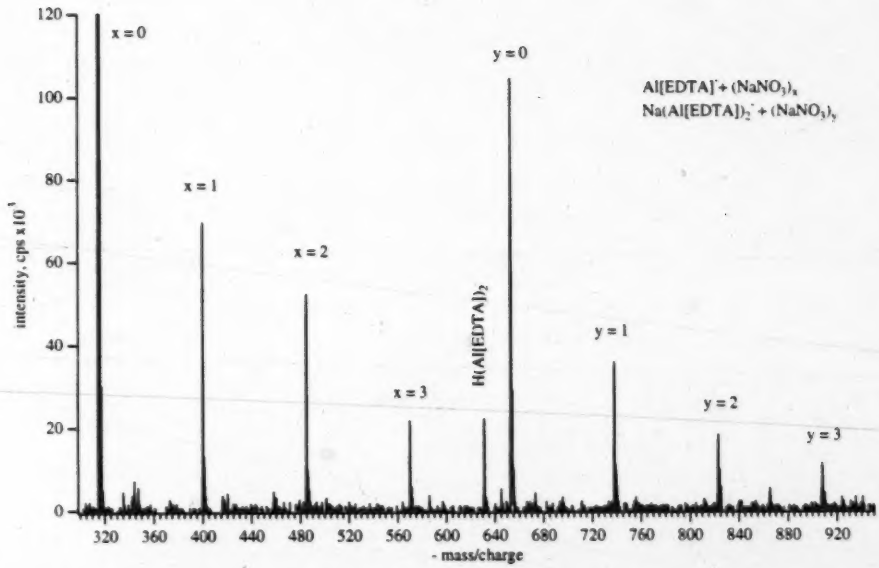

Figure 4.11 Mass spectrum of 0.08 mM aluminum nitrate and 0.1 mM Na_2EDTA acquired on the SCIEX API-100 LCMS, $\Delta V = 0$ volts.

One last peak, at *m/z* –631, does not appear to fit either distribution and is identified as $H(AlY)_2^-$. This mass spectrum is remarkably different from that observed for free EDTA with a ΔV of 0 volts in Figure 4.05a. This may be due to differences in charge on the originally sampled ions, H_2Y^{2-} *versus* AlY^-, which would result in greater apparent collisional energies for doubly charged ions, observed in the first case. Note that although the sampling and skimmer potential on the API are listed as 0 volts, there is still an accelerating potential in this region due to a 400 volt potential on a ring electrode positioned around the skimmer cone. Another factor that must be considered is that the ionic strength is much higher in the aluminum nitrate solution meaning that ions will not be as well separated in solution and the concentration of ions in charged droplets will be greater. This promotes electrostatic interactions between ions in both solution and the gas phase.

The results of increasing ΔV for the preceding solution to –20, -50 and –100 volts are illustrated in Figure 4.12. At –20 volts, nitrate is the dominant ion in the mass spectrum, as expected because of the 3:1 stoichiometry in the aluminum nitrate salt. There are still minor contributions from sodium nitrate adducts at *m/z* –400 and –485, and the observation of $Na(NO_3)_2^-$ due to high concentrations of both ions in the sample solution. The spectrum acquired at –50 volts contains a fragment ion peak at *m/z* –271 produced by the loss of $-CO_2$ from EDTA. A further increase in ΔV to –100 volts results in more extensive fragmentation. A second CO_2 "tooth" of EDTA may be lost to form a product at mass 227, or losses of one and two $-CH_2COO$ "arms" and $-N(CH_2COO)_2$ to produce peaks at *m/z* –257, -199 and –185 respectively. Figure 4.13 shows a clean mass spectrum for an equimolar mixture of aluminum, gallium and indium. It is important to understand that the sampling dependent results presented for the Al-EDTA complex are characteristic of EDTA complexes of trivalent metal ions and not a special case for aluminum. This spectrum illustrates that under the proper sampling conditions a clean mass spectrum can be generated. The ^{13}C satellite peaks can be observed clearly for each of these three species along with contributions from NaH_2Y^- and unknown peaks at *m/z* –313 and –340, respectively.

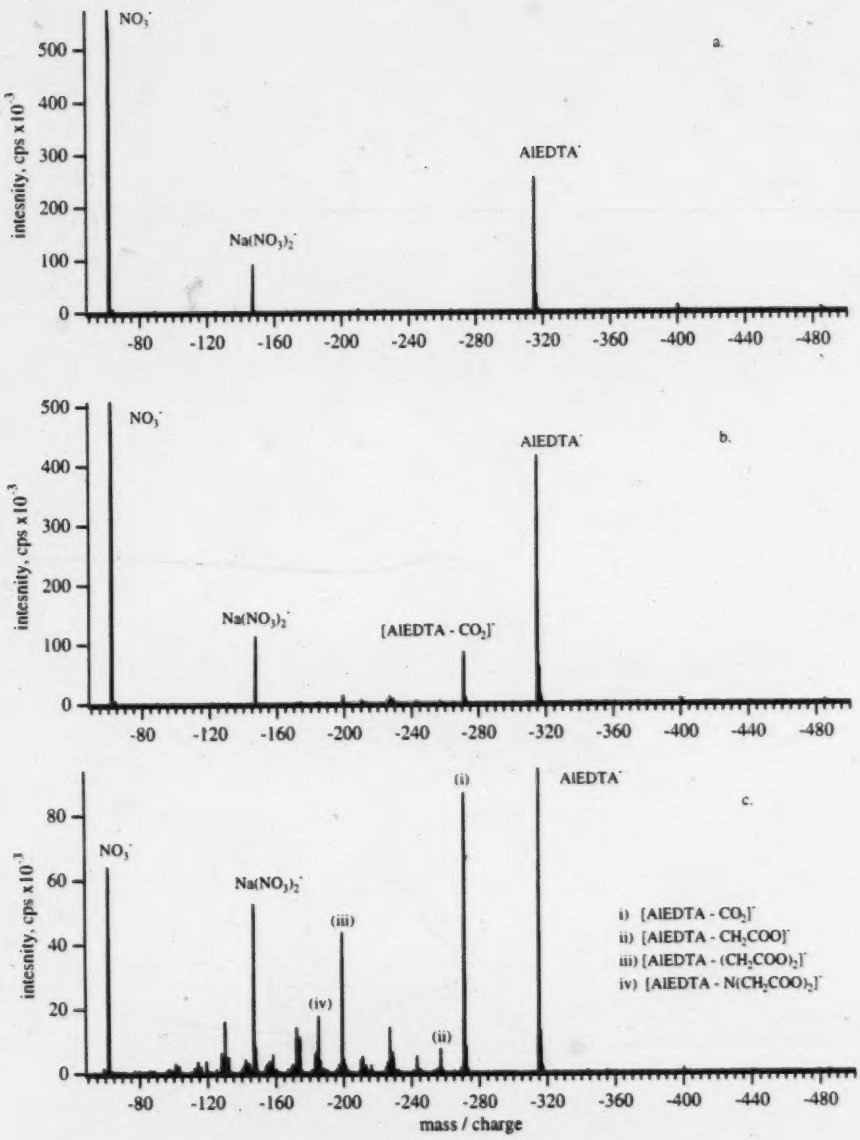

Figure 4.12 Series of mass spectra of 0.08 mM aluminum nitrate and 0.1 mM Na_2EDTA acquired on the SCIEX API-100 LCMS at varying ΔV settings: a) -20 volts, b) -50 volts and c) -100 volts

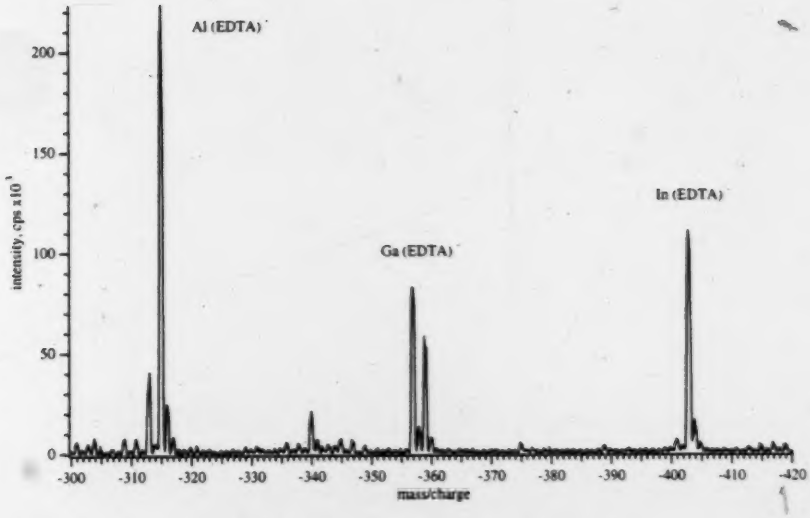

Figure 4.13 Mass spectrum of an equimolar mixture (0.03 mM) of aluminum, gallium and indium in 0.1 mM Na_2EDTA acquired on the SCIEX API-100 LCMS, ΔV = -20 volts.

4.4.3.2 Praseodymium, Gadolinium and Lutetium

As mentioned previously, mass spectra of multiply charged cations using bare-metal ion conditions are very similar to those obtained by ICP-MS, and in certain cases spectra exhibit similar or worse degrees of oxides, poly-atomics and multiply charged ions. Figure 4.14 shows mass spectra of a mixture of praseodymium, gadolinium and lutetium, prepared from their nitrate salts, acquired under bare metal ion conditions (panel a) and as singly charged EDTA complexes (panel b). In the first spectrum there are several oxides and poly-atomics that cause significant isobaric overlap. In addition, the energy or CID potential used to produce the species present in this spectrum results in poor ion extraction into the mass spectrometer and subsequently low sensitivity.

The second spectrum is completely free of these interferences and exhibits higher sensitivity. In order to produce this spectrum, the addition of 0.01 mM nitric acid, in addition to EDTA, was necessary to prevent metal hydrolysis. In the absence of acid, the only species present were indicative of free EDTA.

4.4.3.3 Samarium and Dysprosium

Mass spectra of samarium and dysprosium are illustrated in Figure 4.15. Both metals have high K_f values as listed in Table 4.01; however, the dominant metal containing species in both spectra is not the EDTA complex, but the metal ion coordinated to four nitrate ligands. In order to understand this observation, it is instructive to consider the case of samarium. The source of samarium in this solution is a 1000ppm ICP standard in a 2% nitric acid matrix. Dilution of the standard by a factor of 70 produced a methanolic solution containing 0.1 mM samarium and approximately 4.5mM nitric acid. Under these conditions, the effect of pH and auxiliary complexing ligands on the formation constant of equation 4.20 can be very important.

$$Sm^{3+} + Y^{4-} \Leftrightarrow SmY^{-} \qquad 4.20$$

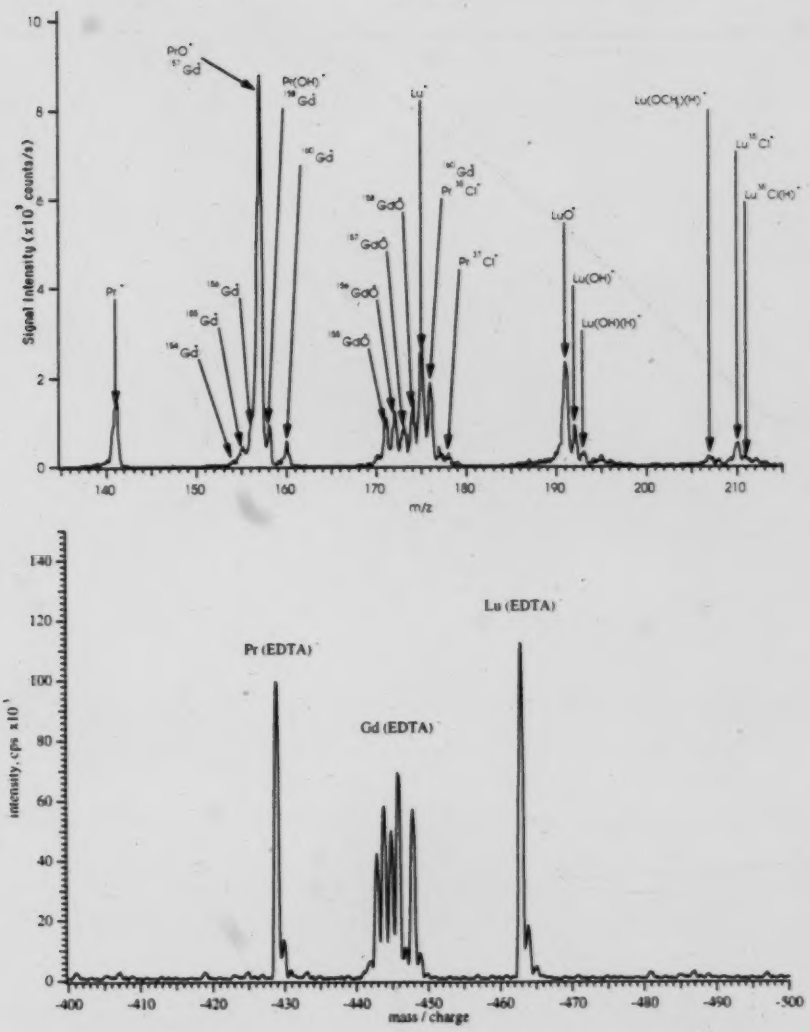

Figure 4.14 Mass spectra of (a) 0.2 mM of each of the three metals acquired under bare metal ion conditions on the Elan 250 (adapted with permission from Anal. Chem. 66 (22) **1996**, 3983-3993) and (b) 0.02mM praseodymium, 0.04mM gadolinium and 0.02 mM lutetium with 0.1mM Na_2EDTA acquired on the SCIEX API-100 LCMS.

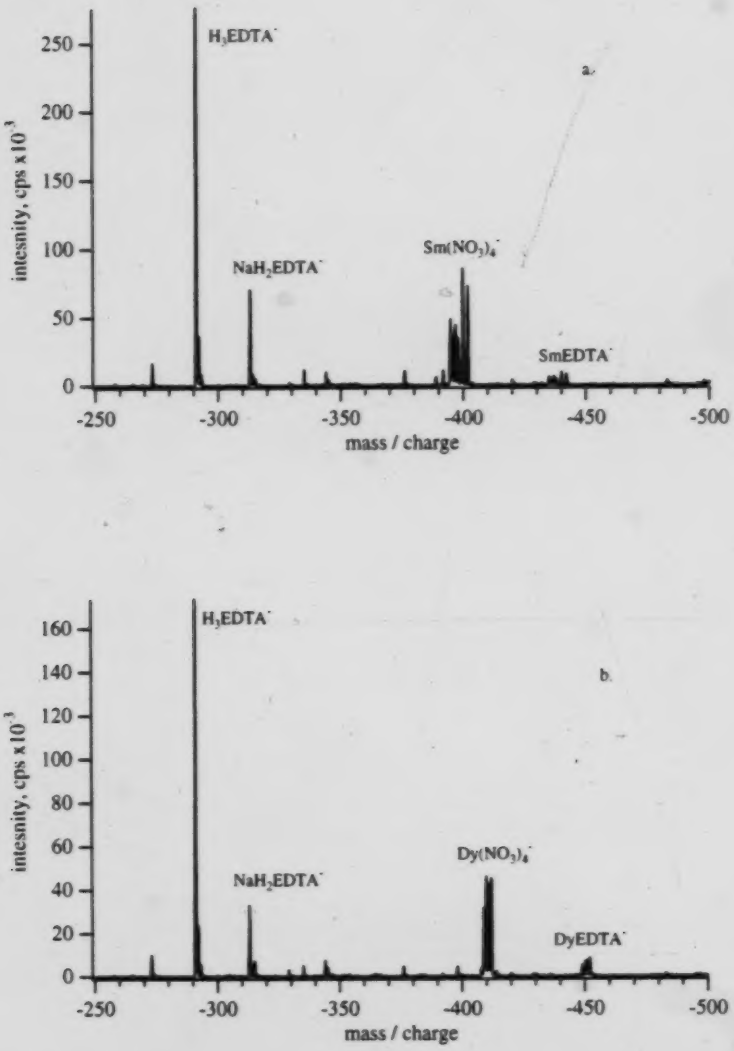

Figure 4.15 Mass spectra of a) 0.1 mM samarium and b) 0.1 mM dysprosium prepared by 1000-fold dilution of ICP standards containing 2% nitric acid into methanol with 0.1 mM Na_2EDTA present. Spectra acquired on SCIEX API-100 LCMS, $\Delta V = -20$ volts.

The lower fraction of EDTA present as Y^{4-} at low pH serves to decrease the magnitude of the conditional formation constant, K_f', of the samarium-EDTA complex.

$$K_f' = \alpha_{Y^{4-}} K_f = \frac{[SmY^-]}{[Sm^{3+}]F_{EDTA}} \qquad 4.26$$

In Table 4.01, the formation constant, K_f, of the SmY^- is 1.38×10^{17}. The pH of the test solution is 2.3 due to the nitric acid in the original ICP standard, which gives an approximate fraction of EDTA in the Y^{4-} form of 4×10^{-13}. The formal concentrations of samarium and EDTA are both 0.1mM. The conditional formation constant is then calculated using equation 4.26:

$$K_f' = 4x10^{-13}(1.38x10^{17}) = 5.5x10^4$$

In order to achieve 99.9% complexation in the absence of auxiliary complexing agents it can be shown that a conditional formation constant of 10^6 is required [28]. Hence, in this example complete complexation is not expected. The relative amounts of free and complexed samarium can also be calculated by rearranging equation 4.26.

$$\frac{[SmY^-]}{[Sm^{3+}]} = K_f' F_{EDTA}$$

$$\frac{[SmY^-]}{[Sm^{3+}]} = 5.5x10^4(0.0001M) = 5.5$$

If complexation equilibria are not disturbed in the electrospray process and the intensities of the nitrate and EDTA complexes linearly reflect the relative concentrations of free and complexed metal ion, then the degree of complexation may be estimated from the observed spectral intensities in Figure 4.15a. The logic behind using the $Sm(NO_3)_4^-$ ion as an indicator of free samarium concentration is based on the expectation that this ion is not originally present in methanolic solution, but this may

not be entirely valid. The intensities of the $^{152}Sm(NO_3)_4^-$ at *m/z* –400 and $^{152}SmY^-$ at *m/z* –440 are 85350 and 7050 cps, respectively. These values result in a complexed to free metal ion ratio of 0.0826 (7.6% complexation) which is almost two orders of magnitude lower than that calculated using the rearranged equation 4.26.

This discrepancy is not surprising since several important assumptions were made in determining this value. It is important to remember that mass spectrometrically observed ion currents can not be directly related to concentration without proper calibration and that the $Sm(NO_3)^-$ complex likely does not reflect the concentration of free samarium ion. Additionally, the transfer of $Sm(NO_3)_4^-$ and SmY^- ions from solution to the gas phase by the electrospray process may have a large impact on their observed ion intensities. Perhaps most important is the fact that SmY^- is a reasonably strong conjugate base in solution, that is to say that the extent to which the neutral weak acid, HSmY, is dissociated at ~pH 2.3 in methanol may explain the low SmY^- intensity in the mass spectrum.

4.4.3.4 Iron (Fe^{2+} *versus* Fe^{3+})

The simultaneous determination of iron (II) and iron (III) is important for understanding the environmental redox processes in biological systems. Iron activity affects several chemical processes in natural waters and its speciation is a significant factor in the evaluation of water quality. $Fe(H_2O)_6^{2+}$ is easily oxidized to $Fe(H_2O)_6^{3+}$ by air except in acidic solution. However, FeY^{2-} is easily oxidized by air regardless of sample pH; therefore, an attempt to speciate the two valence states of iron using EDTA complexation was unsuccessful.

$$Fe(H_2O)_6^{3+} + e^- \Leftrightarrow Fe(H_2O)_6^{2+} \qquad E^\circ = 0.77 \text{ (SHE)} \qquad 4.23$$

$$Fe^{III}EDTA^- + e^- \Leftrightarrow Fe^{II}EDTA^{2-} \qquad E^\circ = -0.12 \text{ (SHE)} \qquad 4.24$$

A mass spectrum of an equimolar mixture of ferrous and ferric ions with disodium EDTA is shown in Figure 4.16. The major peak in the spectrum occurs at mass 344

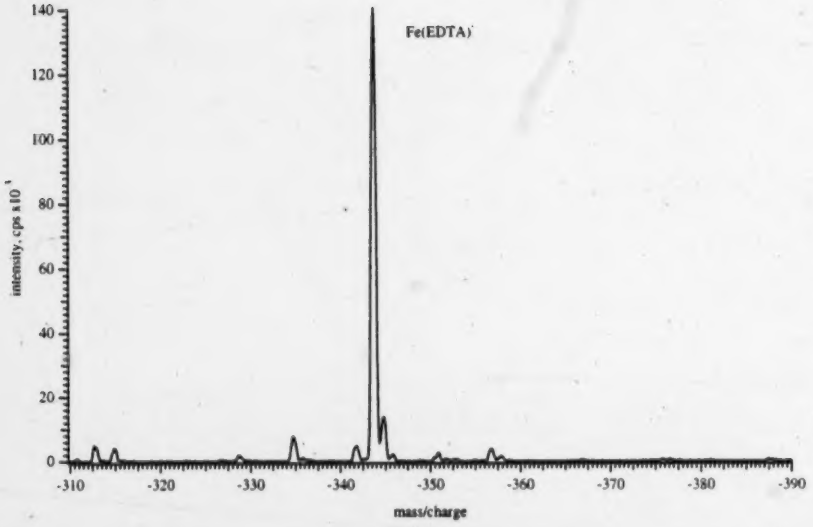

Figure 4.16 Mass spectrum of 0.04 mM ferric chloride, 0.04 mM ferrous ammonium sulfate and 0.1mM Na_2EDTA acquired on the SCIEX API-100 LCMS, ΔV = -20 volts.

and is identified as Fe(III)Y^-. There were no ferrous ion complexes observed in the spectrum.

4.4.5 Quantitation of Calcium

Calcium levels were determined following complexation with EDTA in tap water and a commercial calcium supplement, Calais®. For comparison, the samples were also analyzed for calcium by flame atomic emission spectrometry. A mass spectrum acquired on the SCIEX API-100 for 0.08mM calcium standard with 0.1mM EDTA and 0.1mM NaOH added is given in Figure 4.17. Owing to limitations in the availability of the API instrument, quantitative results were obtained on the ELAN 250 using CaY^{2-} at *m/z* –164.

The first step in performing the calcium assay involved optimization of the sample basicity to ensure 99.9% complexation, to avoid precipitation of insoluble $Ca(OH)_2$ and to obtain the highest sensitivity for the analyte peak accounting for opposing effects of signal suppression at high ionic strength and shifts toward $HCaY^-$ at low pH. Figure 4.18a shows the results of increasing the concentration of NaOH in a sample of 0.05mM $CaCl_2$ from 0 to 1.2mM. The upper trace is the observed intensity of ^{35}Cl, while the lower curve is the observed CaY^{2-} intensity. Figure 4.18b shows the ratio of the intensity of the metal complex to that of chloride. There are four distinct regions in this plot labeled as A, B, C, and D. In region A (0 – 0.1mM OH^- added) the abundance of the complex is increased as its formation is favoured, while that of chloride decreases due to analyte suppression. In region B the chloride and EDTA complex signals decrease proportionately, suggesting that they are affected equally by the suppression effect which is physical rather than chemical in nature. In region C, the complex is affected more drastically than chloride, which implies a chemical deviation or shift in complex equilibria. A plausible gas-phase equilibrium expression used to explain the loss in sensitivity is given by equation 4.25.

$$CaY^{2-} + Na^+ \Leftrightarrow NaCaY^- \qquad 4.25$$

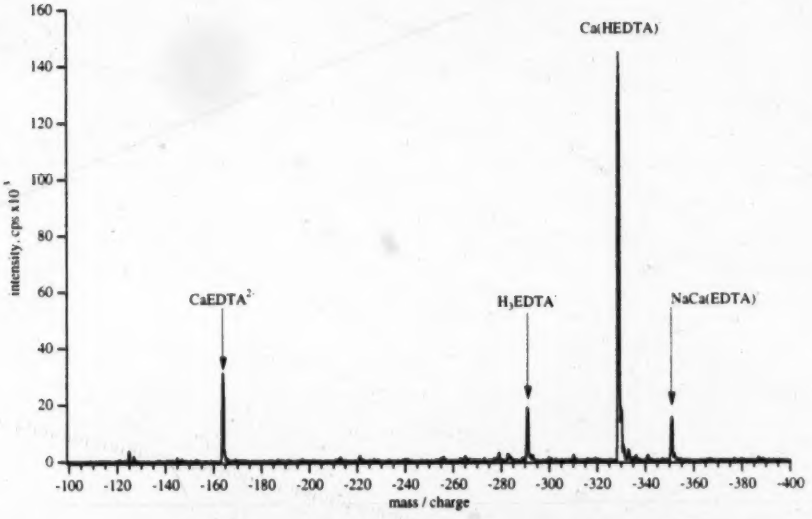

Figure 4.17 Mass spectrum of 0.08 mM calcium chloride, 0.1 mM sodium hydroxide and 0.1 mM Na_2EDTA acquired on the SCIEX API-100 LCMS, ΔV = -50 volts.

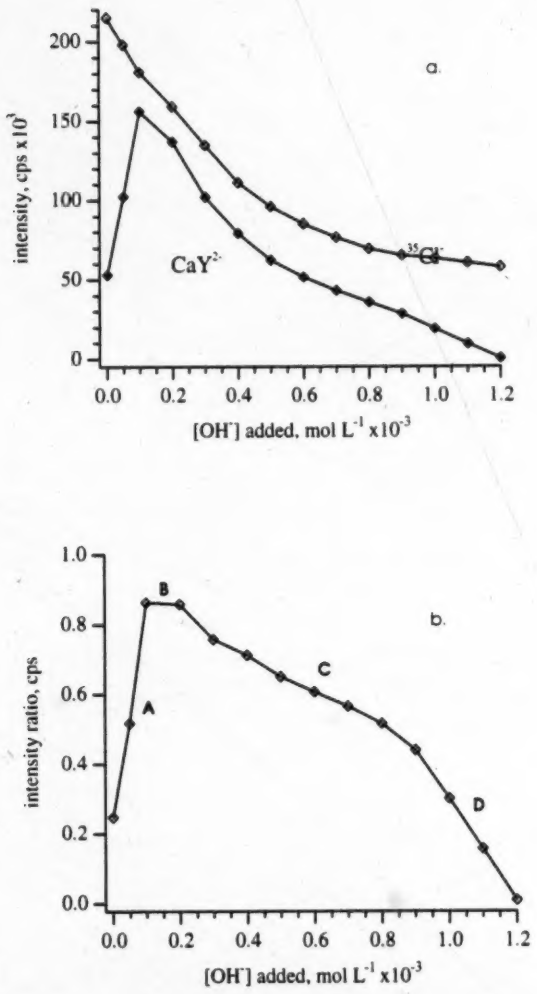

Figure 4.18 (a) Observed signal intensities of chloride and CaY^{2-} as a function of increasing sodium hydroxide concentration and (b) signal intensity ratio of CaY^{2-} to chloride for a mixture of 0.05 mM $CaCl_2$ and 0.1 mM Na_2EDTA (A,B,C and D refer to specific regions of the calibration plot).

The final region exhibits a dramatic decrease in the abundance of the complex however the chloride level eventually reaches a plateau. The different behavioral trends in region D for these two ions suggests that the increasing level of hydroxide is causing precipitation of $Ca(OH)_2$, such that the total electrolyte concentration is no longer increasing. This explains why the relative suppression of chloride appears to reach a limiting value. Based on these results, quantitation of calcium at levels below 0.05mM was attempted using 0.1mM disodium EDTA and 0.15 mM sodium hydroxide, these concentrations correspond to region B of Figure 4.18.

The determination of calcium in water by EDTA titration is well known to most analytical chemists as a water hardness titration. One of the most widely used indicators for this titration is commonly known as calmagite, shown in Figure 4.19. Calmagite has three acidic protons and exists predominantly in the HIn^{2-} form at ~pH10. At this pH free calmagite is blue while the calcium complex is red. The mass spectrum of 5 µM calmagite in the presence of 0.1 mM disodium EDTA and 0.15mM sodium hydroxide is shown in Figure 4.20. The doubly charged ion results in an intense peak at *m/z* –178 under these conditions. Prior to the analysis of real samples for calcium content, a simulated water hardness titration was performed in which increasing levels of EDTA were added to solutions containing 0.05 mM calcium chloride and 0.15 mM NaOH. The intensities of the calcium complex measured at *m/z* –164 and of free calmagite at *m/z* –178, were monitored with increasing EDTA concentration. The CaY^{2-} and free indicator, HIn^{2-}, signals were then normalized to the highest observed CaY^{2-} intensity and plotted along with the theoretical calculated concentration of the complex. This plot is shown in Figure 4.21. The results of this simulated titration demonstrate that the complex formation is rapid and quantitative. The observation of a sharp increase in free indicator intensity, detected mass spectrometrically, corresponding to the liberation of calcium by EDTA binding is a good demonstration of the ability of electrospray to accurately reflect solution composition.

In addition to the concerns discussed above, accurate quantitation of calcium in the two water samples required the addition of 0.05mM barium nitrate to all standard and

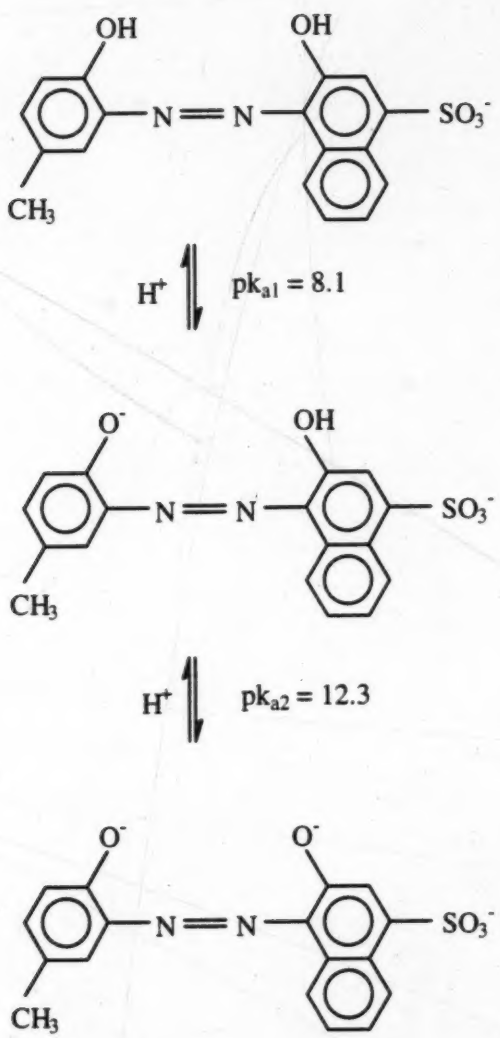

Figure 4.19 Structure and acid equilibria of calmagite indicator

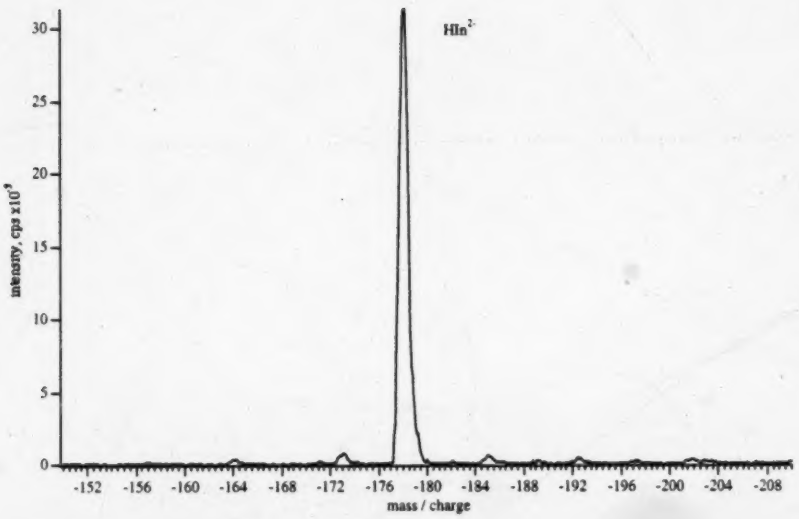

Figure 4.20 Electrospray mass spectrum of 0.01mM calmagite indicator in the HIn^{2-} form acquired on the ELAN 250 with 0.15mM sodium hydroxide and 0.1mM Na_2EDTA.

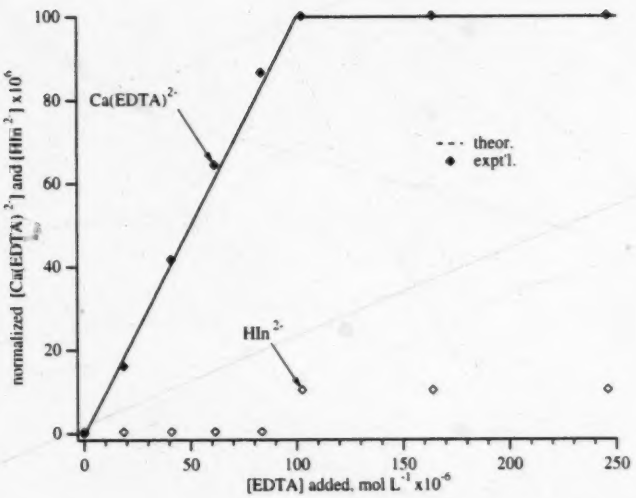

Figure 4.21 Simulated titration of 0.1mM calcium chloride with EDTA in the presence of calmagite indicator with ESMS detection.

sample solutions. The reason for this addition is to eliminate an interference at *m/z* – 164 caused by potassium. The ^{39}K isotope forms a complex with excess EDTA in solution, namely KHY^{2-}, which overlaps $^{40}CaY^{2-}$. Because barium has a much higher complexation constant than potassium it may be used to complex the excess EDTA, thereby eliminating the potassium interference. Barium does not, however, interfere with calcium complex formation since calcium can easily displace the weaker bound barium. The BaY^{2-} complex has a *m/z* of –213. A similar potassium interference, KH_2Y^- may be predicted for the $CaHY^-$ species observed at *m/z* –329 in Figure 4.17.

Determination of calcium by atomic emission spectrometry was accomplished using the method of standard additions. Since calcium experiences a high degree of ionization in a nitrous-oxide acetylene flame, 3000 ppm of potassium was added to the samples to suppress ionization. The results in Table 4.03 show excellent agreement between the two methods of calcium determination, showing that electrospray gives accurate results with practical limits of quantitation.

4.5 Conclusions

The analytical utility of negative ion ESMS for determination of several metallic cations was the focus of this study. The use of ethylenediaminetetraacetic acid, EDTA, as a complexing agent to convert multiply charged metals to singly and doubled charged anionic metal-EDTA complexes was shown to offer several advantages over positive mode ESMS of metal ions. Among the advantages are the simplification of mass spectra *via* elimination of solvation effects, prevention of oxide and polyatomic species formation, improved sensitivity, and valence state speciation.

Table 4.03 Determination of calcium by EDTA complexation coupled with electrospray mass spectrometric detection and by flame atomic emission spectrometry in tap water and a commercial calcium supplement.

	Concentration of Calcium, ppm	
Sample	ESMS	Flame-AES
Tap Water	110.1 ± 0.6	110.5 ± 0.9
Calais®	1090 ± 10	1050 ± 10

4.6 References

1. Vela, N. P.; Caruso, J. A., *J. Anal. At. Spectrom.*, **1993,** 8, 787-94.

2. VanLoon, J. C.; Barefoot, R. R., *Analyst*, **1992,** 117, 563-70.

3. Chau, Y. K., *Analyst*, **1992,** 117, 571-5.

4. Salov, V. V.; Yoshinaga, J.; Shibata, Y.; Morita, M., *Anal. Chem.*, **1992,** 64, 2425-8.

5. Shum, S. C. K.; Houk, R. S., *Anal. Chem.*, **1993,** 65, 2972-6.

6. Ebdon, L.; Fisher, A. S.; Worsfold, P. J., *J. Anal. Atom. Spec.*, **1994,** 9, 611-4.

7. Brown, A. A.; Ebdon, L.; Hill, S. J., *Anal. Chim. Acta.*, **1994,** 286, 391-9.

8. Blades, A. T.; Jayaweera, P.; Ikonomou, M. G.; Kebarle, P., *Int. J. Mass. Spectrom. Ion. Proc.*, **1990,** 102, 251-67.

9. Blades, A. T.; Jayaweera, P.; Ikonomou, M. G.; Kebarle, P., *J. Chem. Phys.*, **1990,** 92, 5900-6.

10. Blades, A. T.; Jayaweera, P.; Ikonomou, M. G.; Kebarle, P., *Int. J. Mass. Spectrom. Ion Proc.*, **1990,** 101, 325-36.

11. Jayaweera, P.; Blades, A. T.; Ikonomou, M. G.; Kebarle, P., *J. Am. Chem. Soc.*, **1990,** 112, 2452-4.

12. Agnes, G. R.; Horlick, G., *Appl. Spectrosc.*, **1992,** 46, 401-6.

13. Agnes, G. R.; Stewart, I. I.; Horlick, G., *Appl. Spectrosc.*, **1994,** 48, 1347 - 59.

14. Agnes, G. R.; Horlick, G., *Appl. Spec.*, **1994,** 48, 655-61.

15. Agnes, G. R.; Horlick, G., *Appl. Spectrosc.*, **1994,** 48, 649-54.

16. Stewart, I. I.; Horlick, G., *Anal. Chem.*, **1994,** 66, 3983 - 93.

17. Cheng, Z. L.; Siu, K. W. M.; Geuvremont, R.; Berman, S. S., *Org. Mass. Spectrom.*, **1992,** 27, 1370-6.

18. Cheng, Z. L.; Siu, K. W. M.; Geuvremont, R.; Berman, S. S., *J. Am. Soc. Mass. Spectrom.*, **1992,** 3, 281-8.

19. Stewart, I. I.; Barnett, D. A.; Horlick, G., *J. Anal. At. Spectrom.*, **1996,** 11, 877-86.

20. Stewart, I. I.; Horlick, G., *J. Anal. At. Spectrom.*, **1996,** 11, 1203-14.

21. Barnett, D. A.; Horlick, G., *J. Anal. At. Spectrom.*, **1997,** 12, 497-501.

22. Corr, J. J., *J. Anal. At. Spectrom.*, **1997,** 12, 537-46.

23. Blades, A. T.; Kebarle, P., *J. Am. Chem. Soc.*, **1994,** 116, 10761-6.

24. Yamamoto, M.; Yamamoto, H.; Yamamoto, Y.; Matsushita, S.; Baba, N.; Ikushige, T., *Anal. Chem.*, **1984,** 56, 832-4.

25. Hajos, P.; Revesv, G.; Sarzanini, C.; Sacchero, G.; Mentasti, E., *J. Chromatogr.*, **1993,** 640, 15-25.

26. Hajos, P.; Revesv, G.; Horvath, O.; Peear, J.; Sarzanini, C., *J. Chromatogr. Sci.*, **1996,** 34, 291-9.

27. Hu, P.; Ye, Q.-Z.; Loo, J. A., *Anal. Chem.*, **1994,** 66, 4190-4.

28. Harris, D. C. *Quantitative Chemical Analysis*, 2nd ed.; W. H. Freeman and Company: New York, 1987.

Chapter 5

Direct Speciation of Selenium

5.1 Introduction

In the last decade there has been an increasing recognition that selenium is an important metalloid with industrial, environmental, biological and toxicological significance [1, 2]. Elevated selenium levels may be found in the environment as a result of volcanic activity, fossil fuel combustion, widespread use in the glass and electronic industries, manufacture of insecticides and metallurgical operations. The main interest in selenium speciation arises from its ambiguous behaviour in biological systems [3-6]. With the exception of narrow, species dependent concentration ranges, several conditions or diseases caused by selenium deficiency or poisoning are known to occur. Selenium has been identified as an essential element in many mammalian species, in which it is incorporated into glutathione peroxidase, an enzyme responsible for removal of harmful peroxides from living cells. It is also known to alleviate toxic effects associated with high levels of arsenic and mercury [7]. On the other hand, excess selenium intake has been correlated to various types of skin infections, heart disease and cancer.

Selenium, like sulphur, may exist in the environment in several oxidation states in a variety of organic and inorganic forms. In natural water, inorganic selenium can be found as selenide Se(-II), colloidal elemental selenium Se(0), selenite anions $HSeO_3^-$ and SeO_3^{2-} i.e. Se(IV), and as selenate anions $HSeO_4^-$ and SeO_4^{2-} i.e. Se(VI). In an aqueous environment, the two prevalent inorganic forms are selenite and selenate, while biological samples may contain both inorganic and organic forms of selenium. The majority of selenium recovered from plant and animal tissue is present in various amino acid derivatives, with the most common forms being selenomethionine, selenocysteine, selenocystine and methyl-selenocysteine.

The principal source of selenium for most individuals is diet. Since the uptake of selenium from food depends largely on its chemical form, it is necessary to develop methods that enable species selective quantification of selenium compounds. The separation of inorganic selenium species has been described extensively in the literature [2, 3, 5, 8-11]. Although some authors have suggested the use of ion-pairing

HPLC, the most common separation method is ion exchange chromatography. Detection methods vary from non-specific conductimetric and indirect UV detection to atomic absorption with hydride generation (HG-AAS), neutron activation, fluorimetry, ICP-AES and ICP-MS. Selective determination of selenite may also be accomplished by hydride generation [12] or formation of piazselenols [13]. A selection of prior oxidation-reduction reactions may be used to convert the other oxidation states of selenium to Se (IV) in order to elucidate total selenium content and levels of the other oxidation states by difference. These methods are specific to oxidation state but not to individual chemical species.

Reversed-phase ion-pairing liquid chromatography [8, 14], ion exchange chromatography [9, 15], gas chromatography after formation of silylated derivatives [16] or capillary zone electrophoresis [17] have been applied to the separation of both inorganic and organic selenium species. ICP-MS has become a powerful instrumental technique for the determination of many trace elements because of its sensitivity and ability to handle difficult matrices. However, prevalent polyatomic interferences encountered around the mass-to-charge ratio (m/z) of 80 with quadrupole instruments [18, 19] pose a particular problem in the determination of selenium by ICP-MS. The presence of argon dimers at m/z 78 ($^{38}Ar^{40}Ar$) and 80 ($^{40}Ar^{40}Ar$) cause the most severe interference while samples rich in chlorine result in the $^{40}Ar^{37}Cl$ overlap with ^{77}Se. Both sample preparation and ICP-MS system parameter control may be used to minimize these interferences. Addition of gases such as nitrogen, methane or trifluoromethane [20-22] to the argon plasma gas flow or of solutes such as carbonate, ethanol, glycerol or propanol to the sample solution [23-25] may also result in reduced polyatomic interferences and improved detection capabilities for selenium.

Other limitations of using the argon based ICP for the determination of selenium arise from poor ionization efficiency owing to the high ionization potential of selenium. Improved efficiency has been reported using nitrogen- or helium-based microwave induced plasmas [26, 27]. However, neither source is well suited for aqueous sample introduction. Granted, the direct coupling of high performance liquid chromatography with ICP-MS is a successful combination, but species identification depends on

retention behavior of the analyte in the column and the availability of matching standards.

The objective of this study is to investigate electrospray as an alternative source for the mass spectrometric determination of selenium species in solution. The intention is to lay the groundwork necessary for accurate identification and quantitation of unknown selenium species in environmental and biological samples. Concerns regarding the preservation of speciation for selenite, selenate, selenomethionine and selenocysteine in the electrospray process and the mass spectrometer sampling process are addressed. Preliminary work using methionine and cysteine, the sulfur analogues of the aforementioned seleno-amino acids is shown to correlate well with the behavior of the seleno acids which makes further method development more straightforward. Use of the sulfur analogues for method development and as internal standards is an advantage not realized for HPLC-ICPMS due to inherent difficulties in the sensitive detection of sulfur by ICP-MS.

A major difference of ESMS of inorganic and bio-inorganic compared to organic compounds is the occurrence of several abundant isotopes for most inorganic elements. The observation of the molecular weight of a biological compound only provides limited information about its identity. Consequently, collision-induced dissociation experiments are required to characterize the compound. In contrast, the molecular ion of an inorganic compound can have a complex isotopic distribution, which may be used to characterize elemental composition. The profile of naturally occurring selenium isotopes is depicted in Figure 5.01. This characteristic isotope distribution will be used to identify various selenium reaction products and fragments in this work.

5.2 Experimental

5.2.1 Reagents

Stock solutions of sodium selenite and sodium selenate (10mM) were prepared from ACS-grade salts in nanopure water. Standard DL-methionine and DL-cysteine

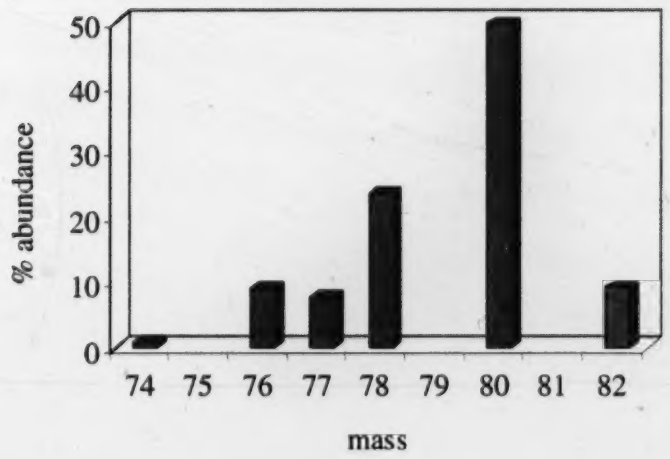

Figure 5.01 Natural isotope distribution of elemental selenium.

hydrochloride were obtained from Aldrich while 99% DL-selenomethionine and DL-selenocysteine were purchased from Sigma Chemical Company (St. Louis, MO). Stock solutions of amino and seleno-amino acids were prepared in distilled deionized water and stored in the dark at approximately 10°C. Distilled reagent grade methanol was used to dilute stock solutions for ESMS analysis. The structures of the four selenium compounds are given in Figure 5.02.

5.3 Results and Discussion

Determination of selenium is generally divided into two broad classes: organic and inorganic speciation. This section will begin with speciation results of inorganic selenium with formal oxidation states of IV and VI, followed by studies of cysteine, cystine and methionine, which are sulfur analogs of relatively common organic selenium compounds. Results of the study of the more readily available sulfur compounds will then be extended to selenomethionine and selenocysteine.

5.3.1 Inorganic Selenium

5.3.1.1 Selenate

An electrospray mass spectrum of 0.1 mM sodium selenate in methanol is shown in Figure 5.03a. The sampling potential gradient, ΔV, was –29 volts. The spectrum consists of the characteristic isotope pattern of selenium, see Figure 5.01, with the major isotope at *m/z* –145, corresponding to $H^{80}SeO_4^-$. There was no doubly charged selenate ion, SeO_4^{2-}, observed in this spectrum. The sole observation of biselenate, $HSeO_4^-$, in the spectrum contradicts the expected composition of this sample based on simple acid/base equilibria. The pH of the solution was not measured but it should be slightly basic since the selenate anion is a weak conjugate base of selenic acid. A fractional composition plot for selenic acid is shown in Figure 5.03b. From this plot it is clear that at pH values in excess of 5, all selenium in solution is in the form of divalent selenate. A position on the composition plot in which biselenate is the only form present does not exist, even at pH 0.

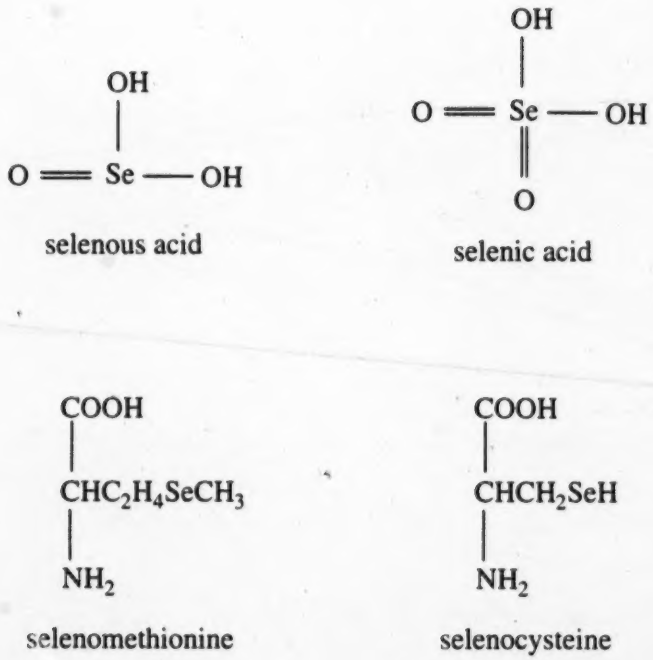

Figure 5.02 Chemical structures of the selenium compounds of interest in this study.

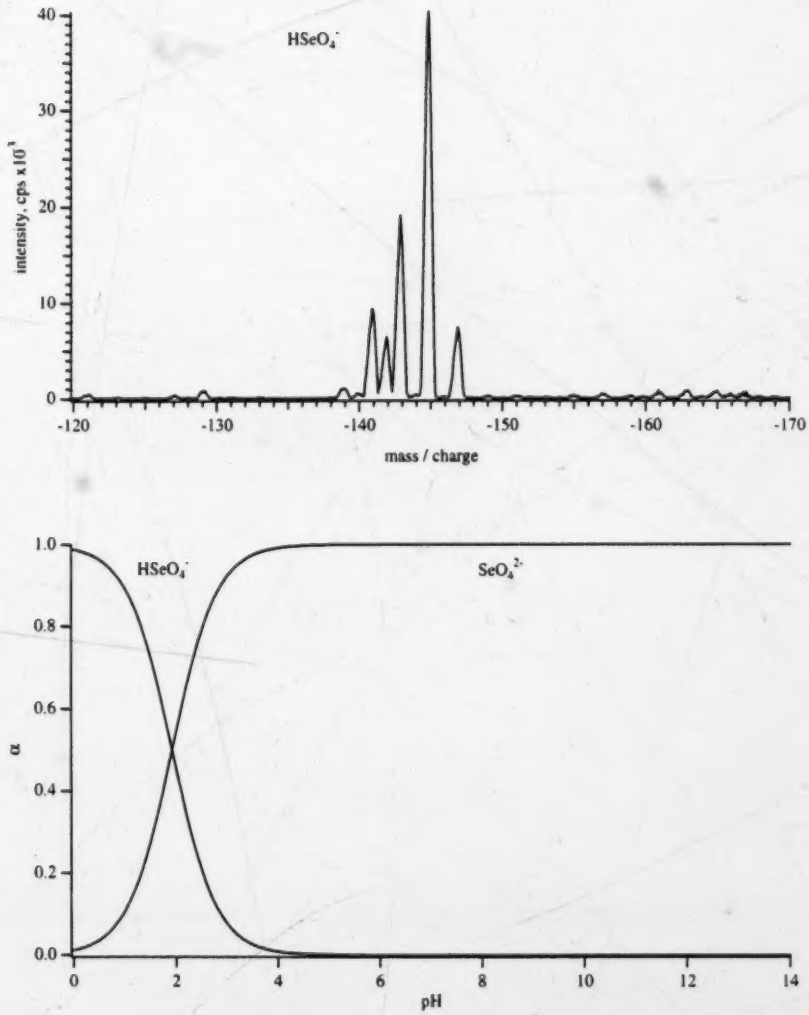

Figure 5.03 (a) Mass spectrum of 0.1 mM sodium selenate in methanol, ΔV = -29 volts (b) pH dependent fractional composition plot for selenate.

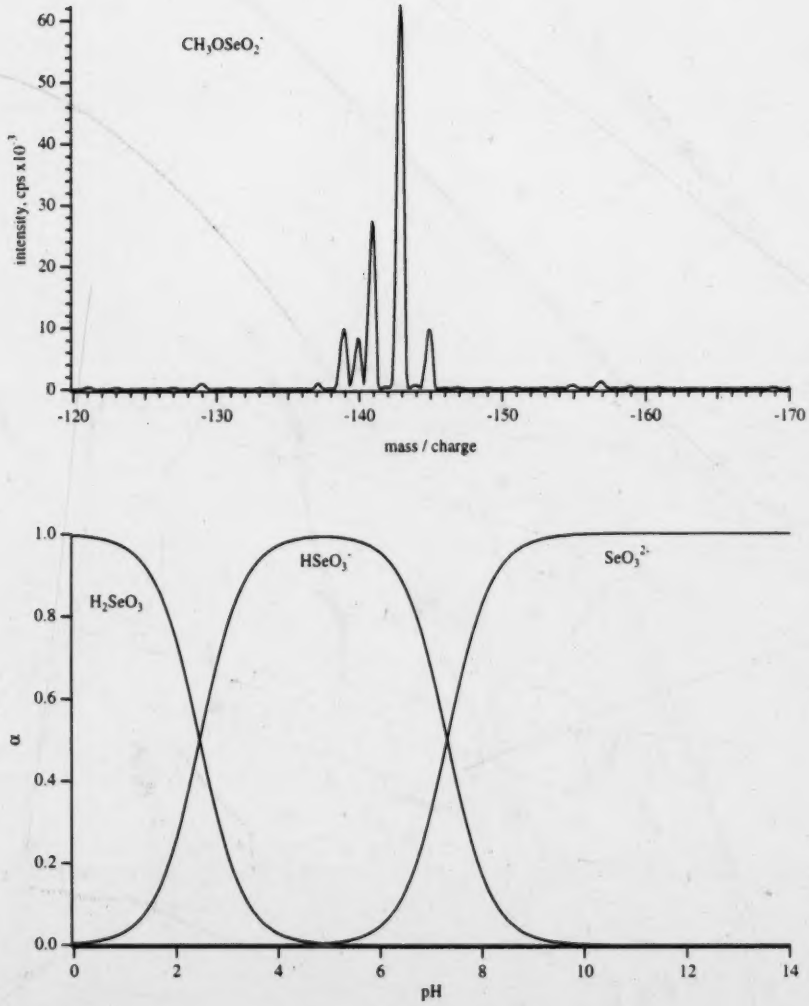

Figure 5.04 (a) Mass spectrum of 0.1 mM sodium selenite in methanol, ΔV = -29 volts (b) pH dependent fractional composition plot for selenite.

5.3.1.2 Selenite

An electrospray mass spectrum of 0.1 mM sodium selenite in methanol is shown in Figure 5.04a. The ΔV used for this spectrum was also –29 volts. As expected, the spectrum is similar to the one presented for selenate since both species contain one selenium atom. Surprisingly, the major isotope in this species is observed only two units lower than biselenate, at *m/z* –143 rather than 16 units lower at *m/z* –129. A 14 mass unit discrepancy in this mass spectrum is not easily assigned to charge adduction, oxide formation or proton transfer gas-phase processes similar to those discussed in chapter 4. Organic mass spectometrists routinely observe losses of 14 mass units (loss of $-CH_2$) due to fragmentation in an electron impact source, but the gain of $-CH_2$ is uncommon. The formation of a selenium ester, $CH_3OSeO_2^-$, by the reaction of selenite and methanol as shown in equation 5.01 is given as a tentative assignment of this species.

$$HOSeO_2^- + CH_3OH \rightarrow CH_3OSeO_2^- + H_2O \qquad 5.01$$

This reaction essentially results in the addition of $-CH_2$, a mass of 14 units, to selenite. A fractional composition plot for selenous acid is shown in Figure 5.04b, if the assignment of the seleno-ester is correct then the possibility that this species may be formed from any of the three selenite species precludes correlation of the composition plot with the mass spectrum.

5.3.1.2 Solvent Study: Confirmation of the Seleno-Ester Formation

In order to confirm the identity of the ester described in the previous section, a solution of selenite was prepared in deuterated methanol, CD_3OD. This resulted in the observation of a shift in the selenium isotope profile of three mass units to *m/z* –146, shown in Figure 5.05a. Dilution of selenite in ethanol and isopropyl alcohol, Figures 5.05b and 5.05c, also resulted in mass spectrometrically observed products of a reaction between selenite and the simple alcohols in which –OH group is effectively replaced by –OR of the alcohol.

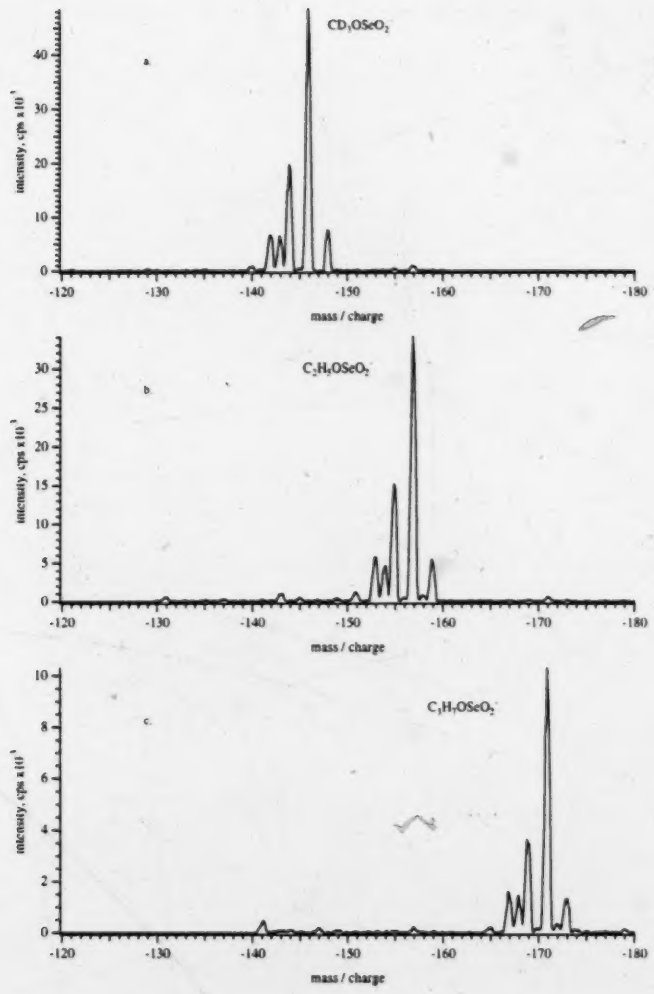

Figure 5.05 Electrospray mass spectra of 0.1 mM sodium selenite in (a) deuterated methanol, (b) ethanol and (c) isopropanol.

A study of the relative affinity of selenite for each of the three alcohols, involved comparison of mass spectra acquired for six binary mixtures containing 95:5 v/v ratios of the two solvents to spectra acquired in each of the three pure solvents containing 0.1 mM selenite ion. In all cases, the seleno-ester formed from the lower molecular weight alcohol was the only one observed in the mass spectrum regardless of the relative percentage (i.e. 95% or 5%) of the alcohol in the mixture. Hence the affinity of the alcohols for selenite is concluded to increase in the order of isopropanol < ethanol < methanol. An increase of the aqueous content of methanolic standards from 1 to 10 % v/v produced a slight but negligible peak at *m/z* –129 corresponding to direct observation of $HSeO_3^-$.

A similar reaction is also observed for the sulfur analogue of selenite in methanol, as shown in the electrospray spectrum of the sulfite-derived ester and sulfate shown in Figure 5.06. A previously published study of sulfur speciation also reported the presence of $CH_3OSO_2^-$, formed by the reaction of sulfite and methanol [28]:

$$HSO_3^- + CH_3OH \rightarrow CH_3OSO_2^- + H_2O \qquad 5.02$$

The conversion of selenite to seleno-ester in methanol turns out to be detrimental to speciation analysis of selenite and selenate due to rather severe overlap of the isotopes of the two species. Consider an equimolar mixture of the two species in which the conversion of selenite to the ester is quantitative and the mass spectrometric observed sensitivity of both species is equal. A plot of the calculated overlap for this situation is given in Figure 5.07. The degree of isobaric overlap is extensive. The use of solvents other than methanol to alleviate this isobaric overlap may be possible in lieu of the observation of esters formed with isopropyl and ethyl alcohol. However, attempts to achieve sensitive detection of selenate in either of these solvents have proven unsuccessful. A spectrum acquired using a mixture of 0.1 mM selenite and 0.3 mM selenate in ethanol is shown in Figure 5.08. It is unclear what becomes of the majority of selenate in solution, as only a small signal at *m/z* –145, indicative of selenate, is present in the spectrum. Mass spectra of pure selenate in either ethanol or isopropyl alcohol are observed to consist solely of solvent and

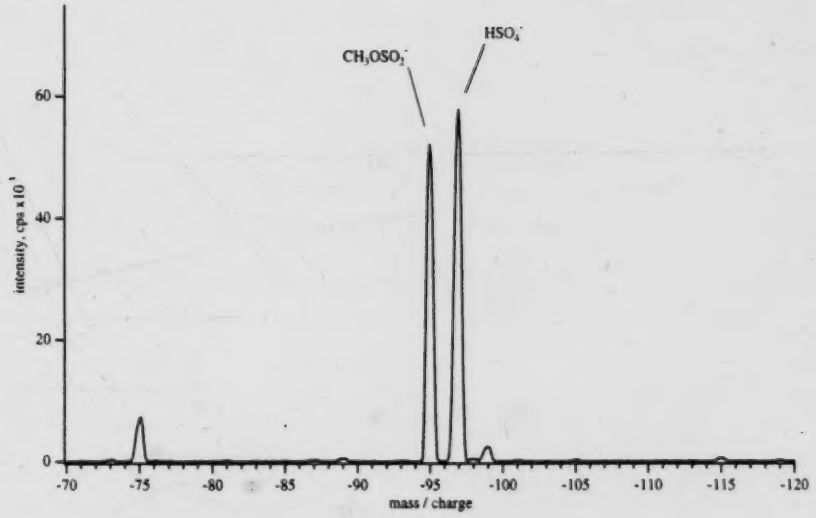

Figure 5.06 Mass spectrum of 0.1 mM sodium sulfite and sodium sulfate in methanolic solution, $\Delta V = -29$ volts.

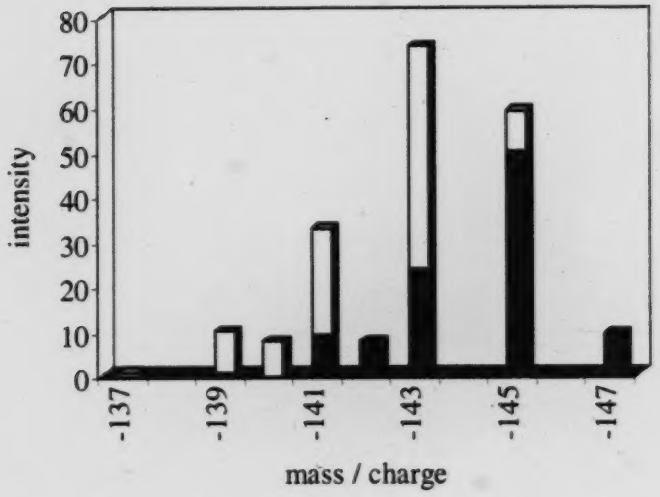

Figure 5.07 Calculated isotopic overlap between selenate ($HSeO_4^-$) and the methyl seleno-ester ($CH_3OSeO_2^-$).

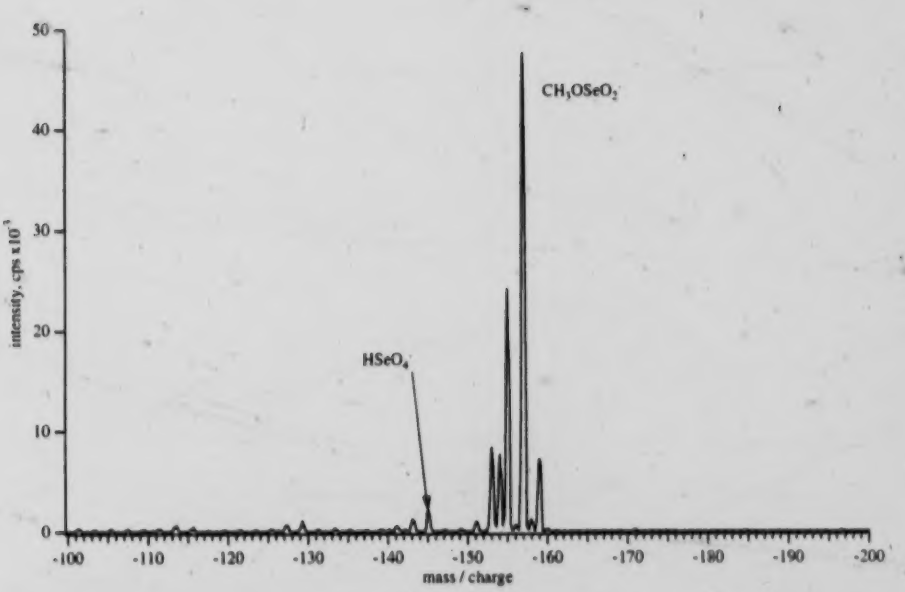

Figure 5.08 Mass spectrum of 0.1 mM sodium selenite and 0.3 mM sodium selenate in ethanol.

atmospheric related background peaks. This eliminates the possibility that selenate is first being reduced to selenite in these solvents, followed by conversion of selenite to the seleno-ester.

5.3.1.4 Analysis of a Mixture of Selenite and Selenate

A mass spectrum of a mixture of both anions present as their disodium salts is shown in Figure 5.09. Application of a relatively mild ΔV of –24 volts, resulted in a spectrum with the major peak at *m/z* –143, as predicted by the peak distribution in Figure 5.07. In order to evaluate the possibility of differentiating these species by varying sampling conditions, the effects on the mass spectrum of lowering ΔV to –19 and then to –14 volts, are shown in Figures 5.10a and 5.10b, respectively.

Reduction of ΔV to –19 volts resulted in the appearance of three clusters of poorly resolved peaks between *m/z* values of –85 and –110. The lone peak at *m/z* –93 corresponds to $CO_2(CH_3O^-)CH_3OH$, a background solvated peak routinely observed at mild sampling conditions. The cluster of peaks centred at m/z –99 matches the mass to charge ratio of a triply solvated, doubly charged selenate ion, $SeO_4^{2-}(H_2O)_3$. The double charge is predicted based on the position and separation of individual isotopes in the cluster as well as the occurrence of clusters on either side of the triply solvated species, separated by 9 *m/z* units. The nine *m/z* unit separation is also consistent with aqueous solvation of a doubly charged ion since the mass of water is 18 amu. Note that the isotope profile of the doubly hydrated selenate ion, centred at *m/z* –90, is skewed by the presence of oxalate impurity, $HC_2O_4^-$, in the test solution.

Further reduction in ΔV to –14 volts provides a clear picture of the origin of the original mass spectrum of Figure 5.09. From Figure 5.10b, the presence of two solvated ion distributions becomes apparent. The first is a doubly charged selenate distribution where the number of water ligands varies from 4 to 8, $SeO_4^{2-}(H_2O)_{4-8}$, while the second distribution consists of two sets of isotopes separated by 18 *m/z* units at –143 and –161. Notice that the peak profile at m/z –143 has changed

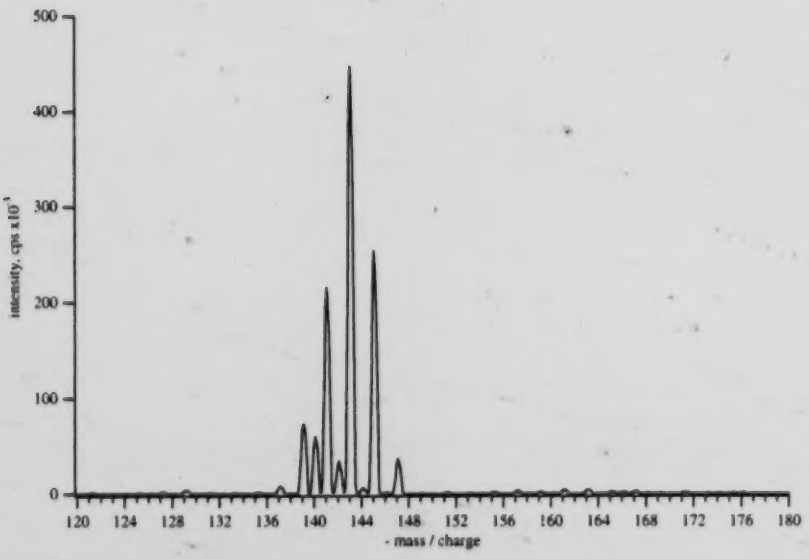

Figure 5.09 Mass spectrum of a mixture of 0.2 mM sodium selenite and sodium selenate in methanol, $\Delta V = -24$ volts.

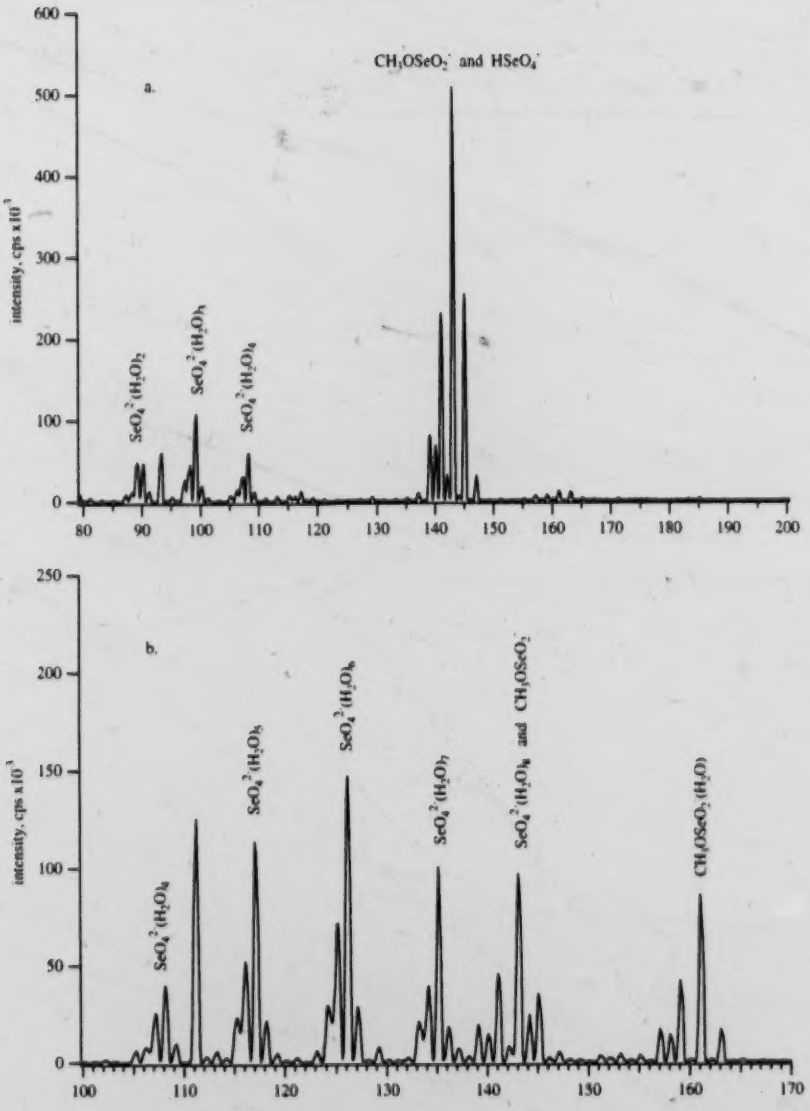

Figure 5.10 Electrospray mass spectra of a mixture of 0.2 mM sodium selenite and 0.2 mM sodium selenate in methanol with ΔV set to (a) –19 volts, (b) –14 volts.

significantly from that observed in Figure 5.10a. The second distribution is singly charged and is related to a narrow distribution of seleno-ester ions. The final two clusters of peaks in the spectrum are then assigned as $CH_3OSeO_2^-$ and $CH_3OSeO_2^-(H_2O)$. The lower degree of solvation of the seleno-ester may well be expected because of its lower relative charge density. At this mild collisional voltage it is possible to resolve the two selenium species by preserving solvation; identification of solvated selenate is also consistent with expected acid/base speciation.

5.3.1.5 Mass Spectral Dependence on Solution pH: Inorganic Selenium

Based on the pH dependent composition diagram for selenate shown in Figure 5.03b, the absence of solvated $HSeO_4^-$ in the Figure 5.10b is consistent with a solution pH greater than 4. The observation of biselenate in Figures 5.03 and 5.09 therefore reflects a shift in the relative proton affinities of water and selenate between the gas and condensed phases as desolvation proceeds, as given by equation 5.03.

$$SeO_4^{2-}(H_2O)_2 \rightarrow HSeO_4^- + OH^-(H_2O) \qquad 5.03$$

In this case, the doubly charged selenate ion is stable with as few as two solvating water molecules present. This differs from earlier investigations of sulfate [28, 29] in which proton transfer begins once the number of solvent molecules is reduced to four. The difference in behaviour between the sulfur and selenium analogues is due in part to the lower pK_a of bisulfate (1.99 *versus* 1.92 for biselenate), but the determining factor is the higher charge density of the sulfate compared to selenate ion.

5.3.1.6 High Energy Collisional Induced Dissociation

The results of applying harsh CID potentials to the original 0.2 mM mixture of selenite and selenate in methanol are shown in the mass spectra of Figure 5.11. Various oxo-selenium species that were not originally present in solution may be generated in the gas phase as well as the selenium radical ion at m/z –80 when ΔV is greater than –96 volts. The mechanism for production of these species from selenate

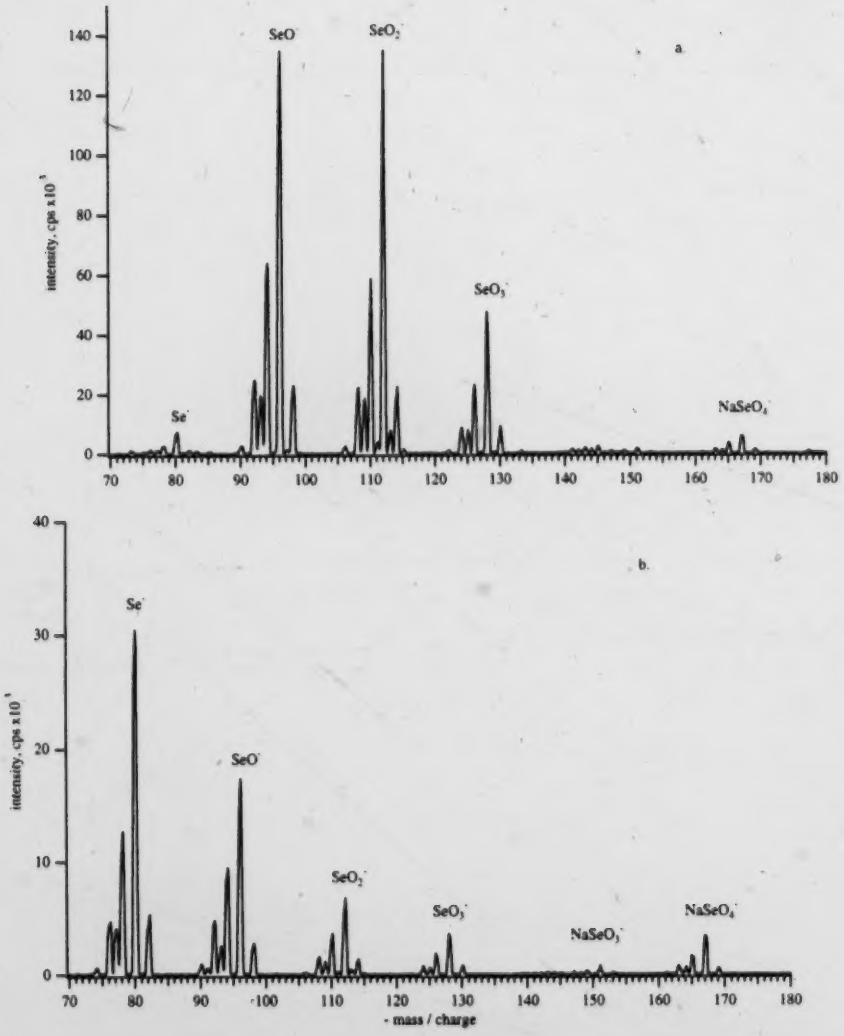

Figure 5.11 Electrospray mass spectra of a mixture of 0.2 mM sodium selenite and sodium selenate in methanol at high values of ΔV; (a) –96 volts and (b) –194 volts.

and the seleno-ester was found to be essentially equivalent after the initial dissociation. Collisional decomposition of selenate involves the initial loss of the hydroxyl group to form SeO_3^-, as given by:

$$HSeO_4^- + N_2 \rightarrow SeO_3^- + OH + N_2 \qquad 5.04$$

Similarly, the first step in the collisional dissociation of the methyl seleno-ester involves loss of the neutral methoxyl group to generate SeO_2^-:

$$CH_3OSeO_2^- + N_2 \rightarrow SeO_2^- + OCH_3 + N_2 \qquad 5.05$$

Further decomposition of the gas-phase oxo-selenium species follows a mechanism identical to that documented in Chapter 3 for halogenic oxo-anions.

$$SeO_x^- + N_2 \rightarrow SeO_{x-1}^- + O^- + N_2^+ \qquad 5.06$$

The appearance of $NaSeO_4^-$ and $NaSeO_3^-$ in the mass spectra of Figure 5.11 is unexpected since an Na-O ion-pairing interaction should be much weaker than the covalent Se-O bonds that are seen to experience extensive fragmentation at the CID potentials employed to acquire these spectra. Since these sodium adducts are not expected to survive such high energy collisions it is more reasonable to expect that they are formed within the collision region. Adduct formation between sodium and selenite or selenate in the expansion region is highly unlikely. A more plausible explanation for the occurrence of these sodium adduct ions may be the dissociation of poorly charged agglomerates of solution ions or "charged residues" as first proposed by Dole et al [30]. The dissociation of a simple charged residue of sodium selenate is written as equation 5.07.

$$Na_3(SeO_4)_2^- + N_2 \rightarrow NaSeO_4^- + Na_2SeO_4 + N_2 \qquad 5.07$$

Given the possible sizes of these charged residues, it is reasonable that their dissociation may only begin at high CID energies capable of sufficient acceleration of

heavy clusters for dissociation. Observation of $NaSeO_3^-$ in the spectra raises further questions about the formation of the methyl seleno-ester since the observation of this adduct is equivalent to the observation of free SeO_3^{2-} and Na^+ ions.

5.3.2 Organic Sulfur Compounds

The seleno-amino acids of interest in this work are essentially identical in structure and chemical properties to their sulfur containing amino acid analogues. However, they are much more expensive and less readily accessible. For these reasons, several preliminary experiments were performed with sulfur species, the results of which were then extended to selenium species. This approach to method development is a luxury not shared by an ICP source due to limitations in the analysis of sulfur on a low-resolution quadrupole mass spectrometer.

The determination of amino acids by electrospray requires that the acids be present in ionic form. Amino acids contain both acidic and basic groups and when their salts are dissolved in polar solvents they undergo intra-molecular acid-base reactions to exist primarily in the form of a dipolar ion or zwitterion with a net charge of zero. In sufficiently acidic solution (low pH) an amino acid may be protonated and thus exist as a cation; alternatively in basic solution (high pH) an amino acid may be deprotonated and exist as an anion. The amphoteric characteristic of amino acids give the analyst flexibility in choice of analysis as positive or negative ions; however, it also requires a firm understanding of solution pH and gas phase proton affinities. The effect of electrolysis on sample pH within the electrospray capillary and concentration effects within shrinking electrospray droplets must also be considered. Fractional composition diagrams of the two amino acids as a function of pH are given in Figure 5.12.

5.3.2.1 Methionine

Methionine contains two important functional groups, a strongly acidic carboxylic acid (pK_a= 2.20) and a basic amine (pK_a = 9.05). At pH values below 2.20 and greater than 9.05 the majority of methionine in solution will have a net positive or negative

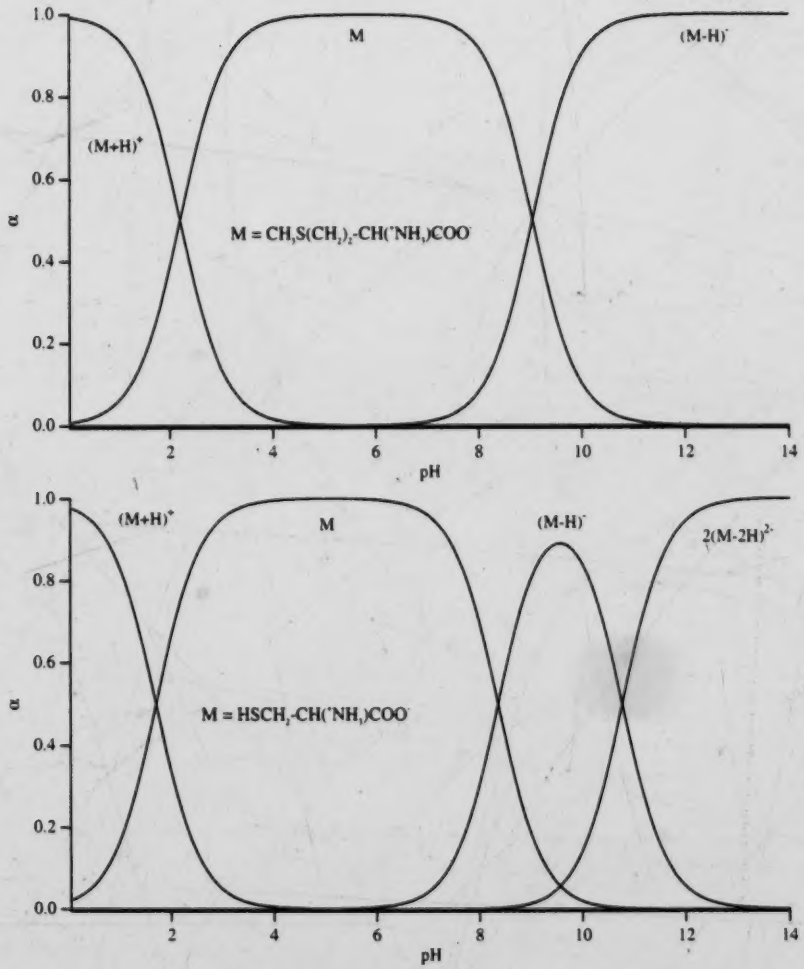

Figure 5.12 Fractional composition diagrams for (a) methionine and (b) cysteine as a function of pH.

charge, respectively. Intermediate pH values favour a neutral zwitterionic form of methionine in which the negative charge of the carboxyl group is compensated by the positively charged amine. Electrospray mass spectra of 0.1 mM methionine acquired using both negative and positive mode detection are shown in Figure 5.13. The negative ion spectrum is offset on the vertical axis by 5000 counts per second (cps). The two mass spectra are quite similar with the exception that the negative ion appears two mass units lower than the positive ion due to loss of two protons as shown in equation 5.08.

$$CH_3SC_2H_4-CH(NH_3^+)COOH \rightarrow CH_3SC_2H_4-CH(NH_2)COO^- + 2H^+ \quad 5.08$$

The two satellite peaks to the right of both base methionine peaks are due to the naturally abundant carbon-13 isotope. Although no external buffer, acid or base has been added to the solution, both ionic species are observed which is not expected from a solution of the neutral zwitterion with isoelectric point of pH 5.7.

5.3.2.2 Cysteine

There are three acidic protons on a molecule of cysteine, a strongly acidic carboxylic acid (pK_a= 1.71), a relatively basic sulfhydryl proton (pK_a = 8.36) and a basic amine (pK_a = 10.77). Like methionine, at pH values below 1.71 and greater than 8.36 the majority of cysteine in solution will have a net positive or negative charge, respectively. The exception to the case of methionine involves the dimerization of cysteine to form cystine *via* a sulfur bridge. The dimerization is an irreversible reaction that may occur at pH < 7 depending on the solution matrix. Electrospray mass spectra of 0.1 mM cysteine hydrochloride acquired using both negative and positive mode detection are shown in Figure 5.14. The negative ion spectrum is offset on the vertical axis by 5000 cps.

The two mass spectra are similar to that observed for methionine, but cysteine must only lose two of its three acidic protons to have an overall negative charge. It should

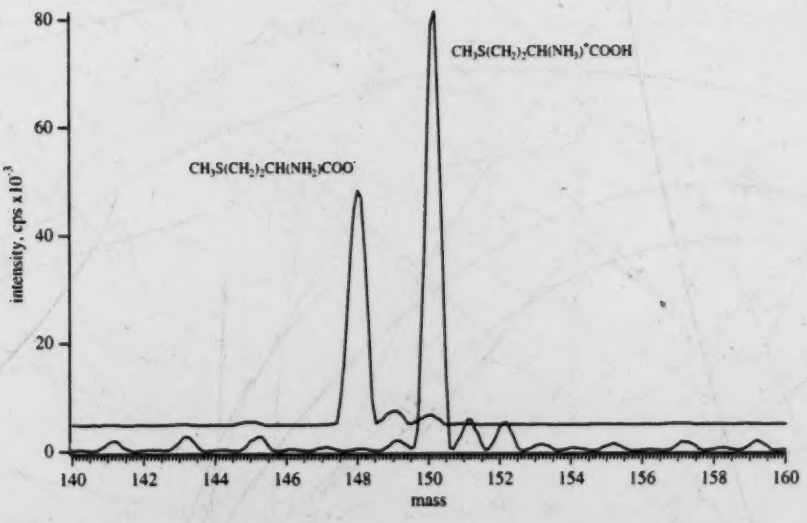

Figure 5.13 Negative and positive mode electrospray mass spectra of 0.1 mM methionine, $\Delta V = \pm 29$ volts.

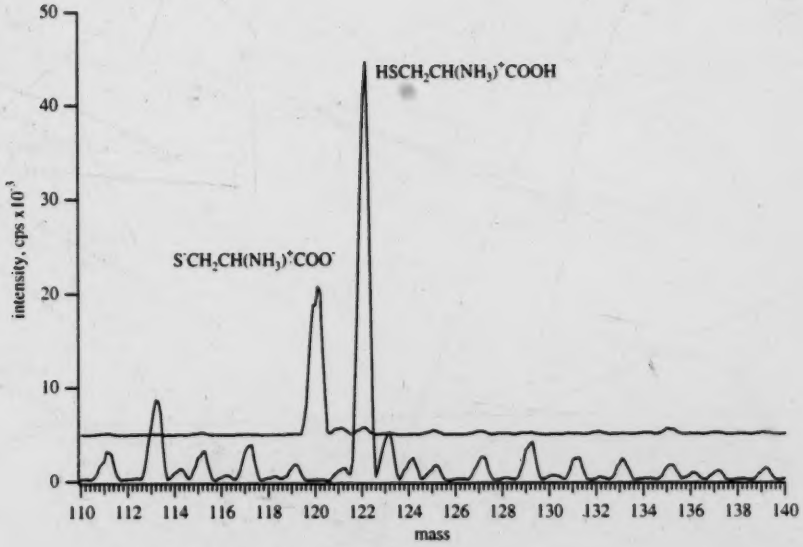

Figure 5.14 Negative and positive mode electrospray mass spectra of 0.1 mM cysteine hydrochloride, $\Delta V = \pm 29$ volts.

therefore be possible to generate anionic cysteine species at lower solution pH values than methionine. The pH dependent equilibrium between the cationic and anionic forms of selenium is given in equation 5.09.

$$HSCH_2 - CH(NH_3^+)COOH \rightarrow S^-CH_2 - CH(NH_3^+)COO^- + 2H^+ \qquad 5.09$$

The carbon-13 satellite peaks are less intense in this case because of lower carbon content in cysteine. Three more mass spectra of cysteine using negative ion detection are shown in Figure 5.15 in which different levels of sodium hydroxide have been added to the standard solutions. The first spectrum contains 0.1 mM cysteine and 0.1 mM sodium hydroxide. There are two cysteine related peaks observed in this spectrum, $(M-H)^-$ and $(M+Cl)^-$, where M is the neutral zwitterion, $HSCH_2$-$CH(NH_3^+)COO^-$. The chloride ion likely associates with the positively charged amine moiety, thereby neutralizing its positive charge and giving an overall species a charge of -1. The resulting spectrum from the addition of 0.2 mM NaOH, Figure 5.15b, demonstrates the observation of the cysteine dimer, cystine. Cystine is observed as a doubly charged ion at *m/z* –119, since the two sulfhydryl protons are lost in the sulfur bridge and the two amines are deprotonated at the resulting pH. Note that the intensity scale has also doubled in response to the change in alkalinity. A further increase in the level of sodium hydroxide to 0.35 mM results in more complete dimerization and another increase in the overall cysteine related signal intensity to approximately 220,000 cps, an almost fifteen-fold increase in intensity from the first spectrum. A diagram showing the various pH dependent forms of cysteine is given in Figure 5.16.

Cystine is also detected as a singly charged ion at *m/z* –239 in these solutions but at much lower intensities. Figure 5.17 shows mass spectra of 0.1 mM cysteine solutions with various levels of sodium hydroxide added. The intensity of singly charged cystine increases with increasing concentration of base added up to 0.25 mM. Above this level the intensity begins to drop; this is due to deprotonation of the second amine with increasing solution pH. The extent of gas phase proton transfer from water to

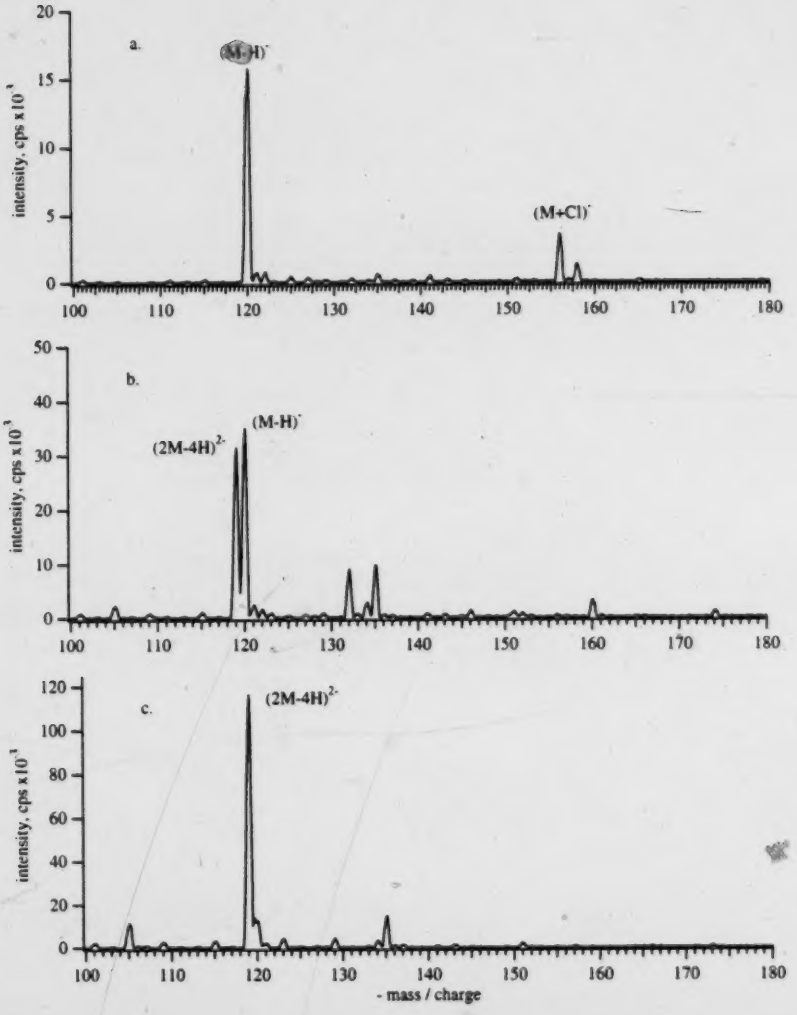

Figure 5.15 Mass spectra of 0.1 mM cysteine hydrochloride with varying levels of sodium hydroxide added; (a) 0.1 mM, (b) 0.2 mM and (c) 0.35 mM, $\Delta V = \pm 29$ volts.

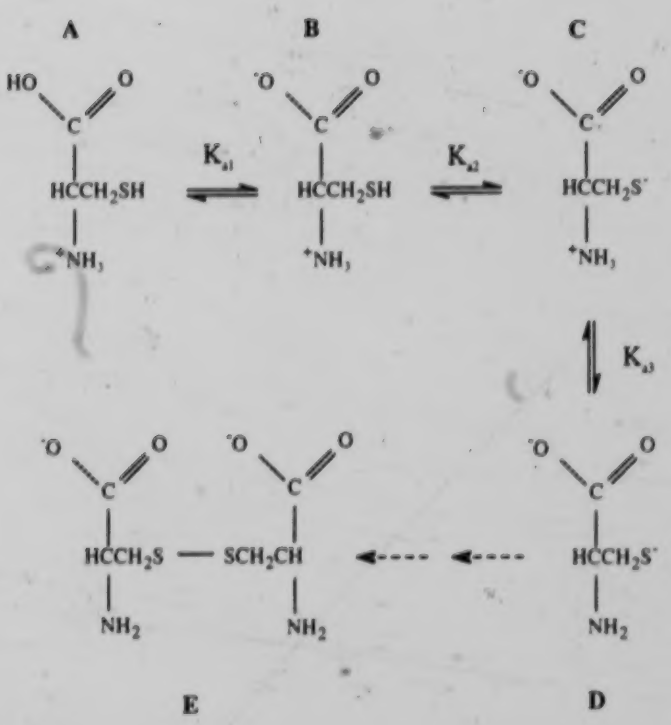

Figure 5.16 Diagram showing various forms of cysteine present in solution as a function of varying pH.

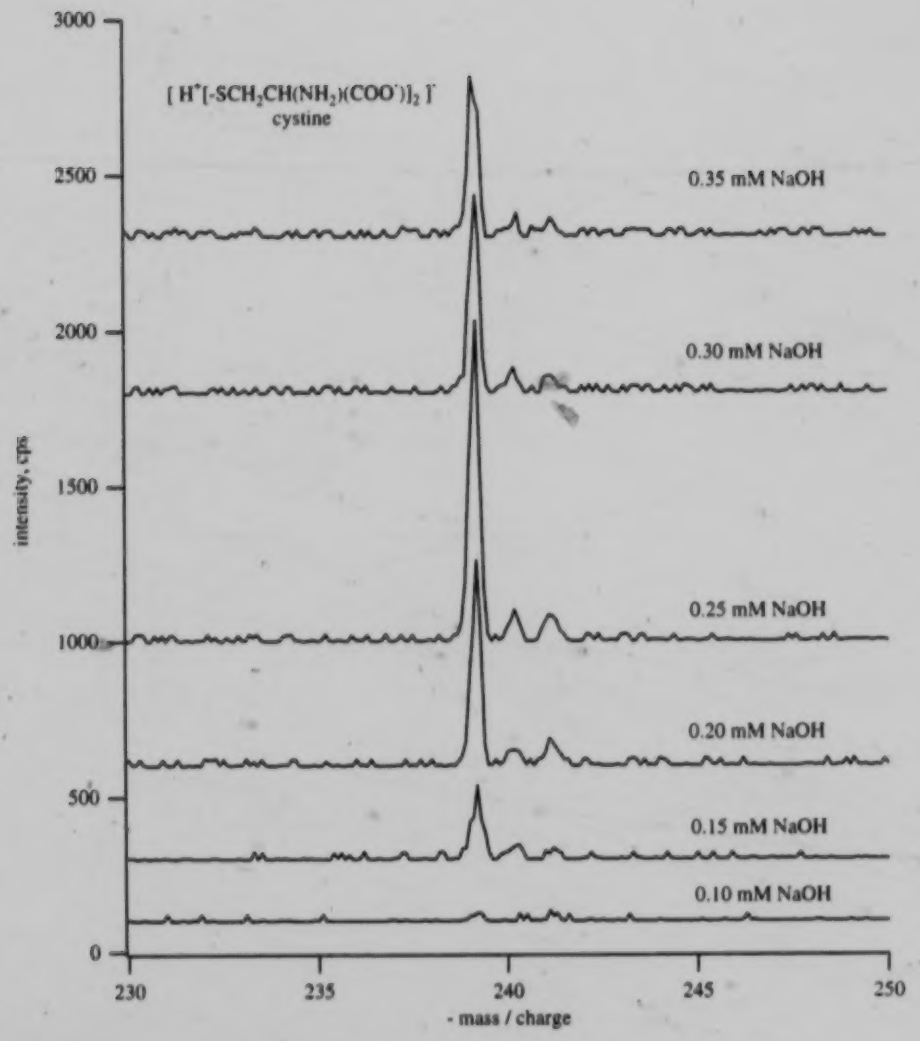

Figure 5.17 Mass spectra of 0.1mM cysteine hydrochloride with various levels of sodium hydroxide added.

divalent cystine is difficult to gauge, but it is certainly lower than for small inorganic sulfur and selenium oxo-anions.

5.3.3 Organoselenium Compounds: Seleno-Amino Acids

Fractional composition diagrams of the two seleno-amino acids as a function of pH are given in Figure 5.18. These diagrams are almost identical to pH dependent plots for methionine and cysteine with slight differences in K_a values. From these diagrams the options for detecting the two species by electrospray are clear. High acid concentrations will result in observation of cationic gas-phase species. Similarly, high concentrations of base will result in gas-phase anionic species. Selenocysteine is also subject to irreversible dimerization to selenocystine at high sample pH.

5.3.3.1 Selenomethionine

Mass spectra of 0.26 mM selenomethionine acquired using positive and negative ion mode detection are shown in Figures 5.19 and 5.20, respectively. Figure 5.19 consists of three plots. The first is a spectrum of selenomethionine over a wide mass range. In this spectrum two other selenium containing compounds are identifiable based on the characteristic isotope distribution. Plots 5.19b and 5.19c are expanded regions of Figure 5.19a for the two compounds, which turn out to be fragment ions of selenomethionine. The fragment at *m/z* 181 corresponds to the loss of the amine group while the fragment at *m/z* 152 represents the loss of the carboxylic acid functionality. The ΔV in this case was 34 volts. A decrease to 29 volts did not produce these fragment peaks. The complex isotopic pattern of selenium is advantageous in this example for identification of fragment ions as they are easier to distinguish in the spectrum than methionine, which is essentially mono-isotopic. The mass spectrum of the anionic form of selenomethionine is shown in Figure 5.20. A ΔV of –35 volts does not result in fragmentation of this ion. The same sample solution was used for both spectra and did not contain any external acid or base. However, the observed ions suggest widely different sample pH values. Even though both polarity ions can be observed without modification of sample pH, the addition of

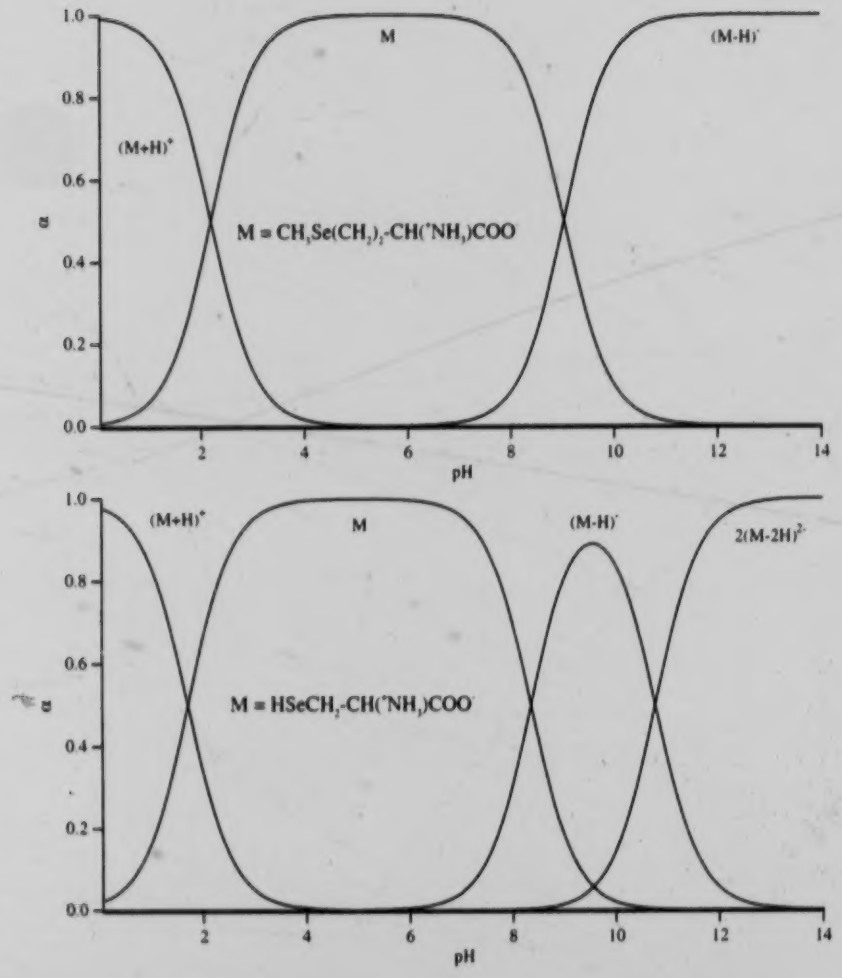

Figure 5.18 Fractional composition diagrams for (a) selenomethionine and (b) selenocysteine as a function of pH.

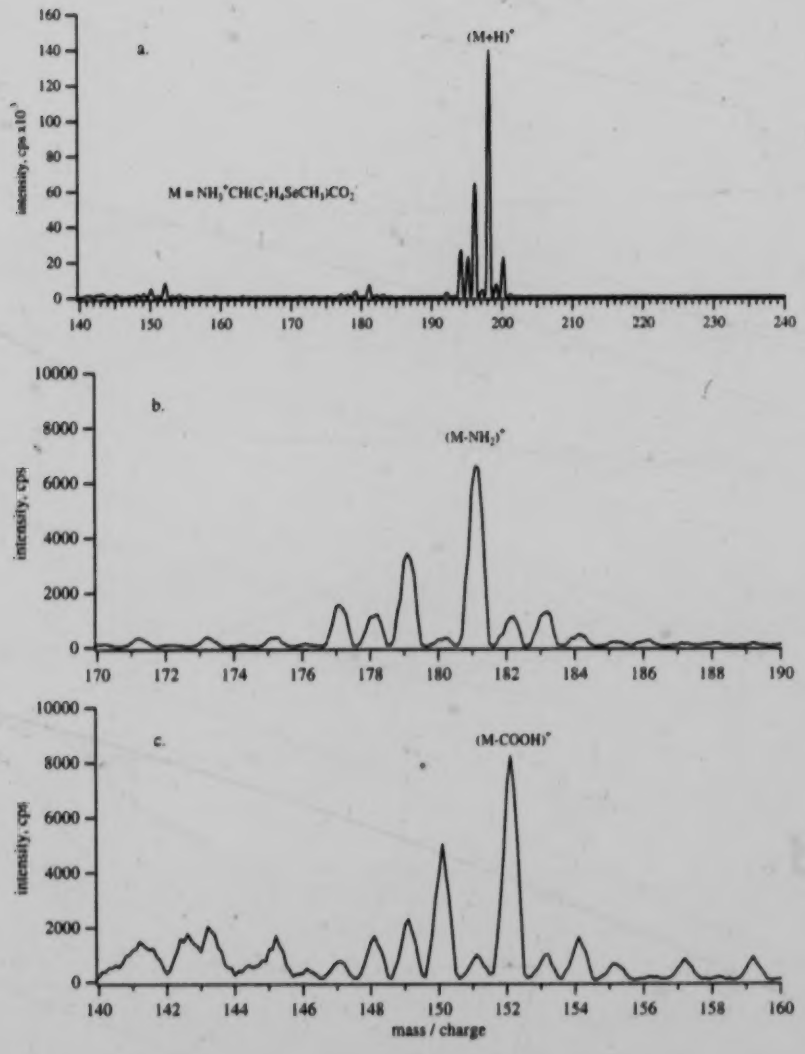

Figure 5.19 Mass spectra of (a) 0.26 mM selenomethionine and (b,c) fragment ions acquired with $\Delta V = 34$ volts

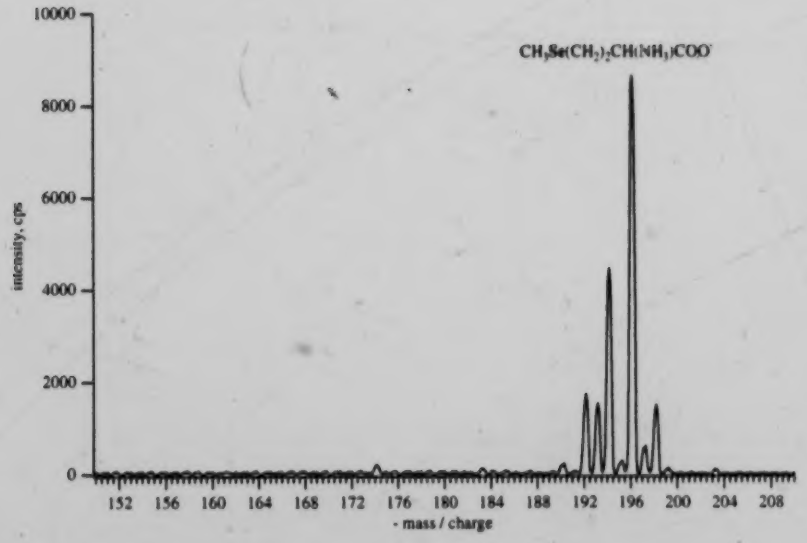

Figure 5.20 Negative ion mass spectrum of 0.26 mM selenomethionine in methanol, $\Delta V = -29$ volts.

moderate levels of acid or base does result in significant improvements in sensitivity. Figure 5.21 shows results from an experiment designed to study the effect of changes in acid or base levels on the speciation and intensity of selenomethionine related mass spectral peaks. Owing to difficulty associated with the definition of pH in methanolic solution the x-axis of these plots is labeled "[OH^-] added", the values to the left of center on the axis actually indicate concentrations of hydrochloric acid added while those to right correspond to the added concentrations of sodium hydroxide.

The first plot shows results from positive mode detection, two separate *m/z* values were monitored, corresponding to protonated and sodiated selenomethionine at 198 and 220, respectively. The effect of increasing the amount of hydrochloric acid (moving left of center) results in improved sensitivity up to 0.33 mM added HCl. Above this level of acid, the signal levels off and then decreases as the acid concentration exceeds 1 mM. The loss of sensitivity with high acid concentrations is expected based on quantitative results discussed in Chapter 3 for solutions of high conductivity. Space charge effects in the electrosprayed droplets and the mass spectrometer interface offset absolute increases in the levels of protonated selenomethionine at low pH. An increase in sodium hydroxide has detrimental effects on the protonated selenomethionine signal. The sodium adduct to the neutral zwitterion reaches a maximum at 0.2 mM NaOH and decays to zero with further increases. The decay of the sodium adduct is caused by the deprotonation of the zwitterion. No disodium adduct was detected at higher sodium hydroxide levels. Analysis of the same solutions by negative ion electrospray results in the plot in Figure 5.21b. This plot is essentially a mirror image of the positive mode experiment. The sensitivity of the anionic selenomethionine species is decreased approximately three-fold. A chloride adduct is observed at mildly acidic conditions while the deprotonated selenomethionine species reaches a maximum at approximately 0.5 mM added sodium hydroxide followed by similar suppression of signal. A schematic of the various species involved in the gas-phase selenomethionine equilibria is given in Figure 5.22. Species A, B and C represent three pH dependent condensed phase species. Neutral species D and E are possible sources of signal suppression observed

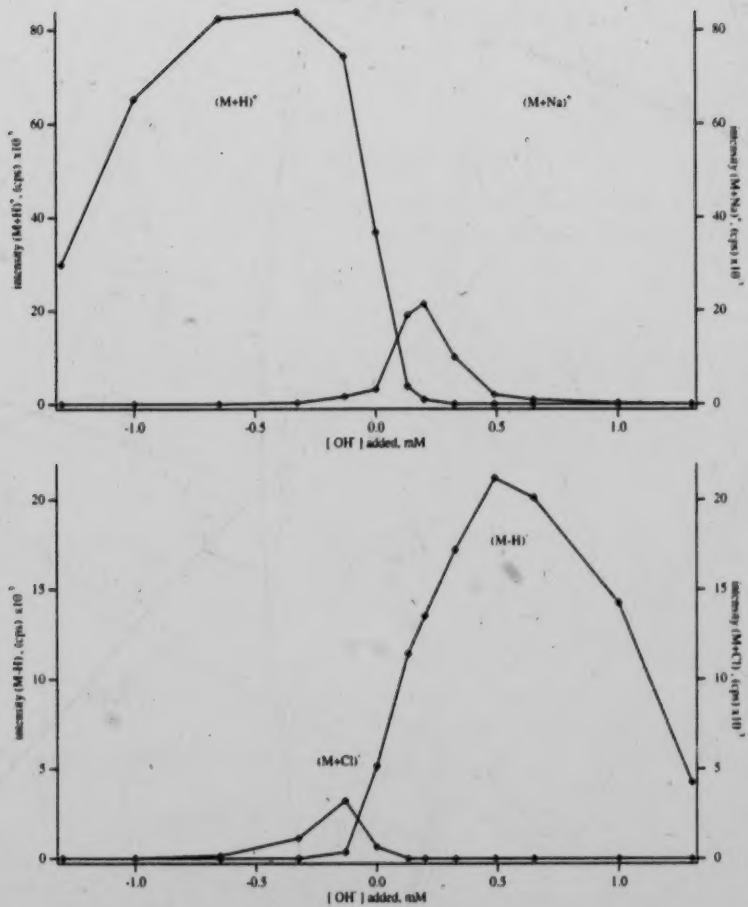

Figure 5.21 Effect of hydrochloric acid and sodium hydroxide on the determination of selenomethionine by (a) positive and (b) negative mode electrospray mass spectrometry.

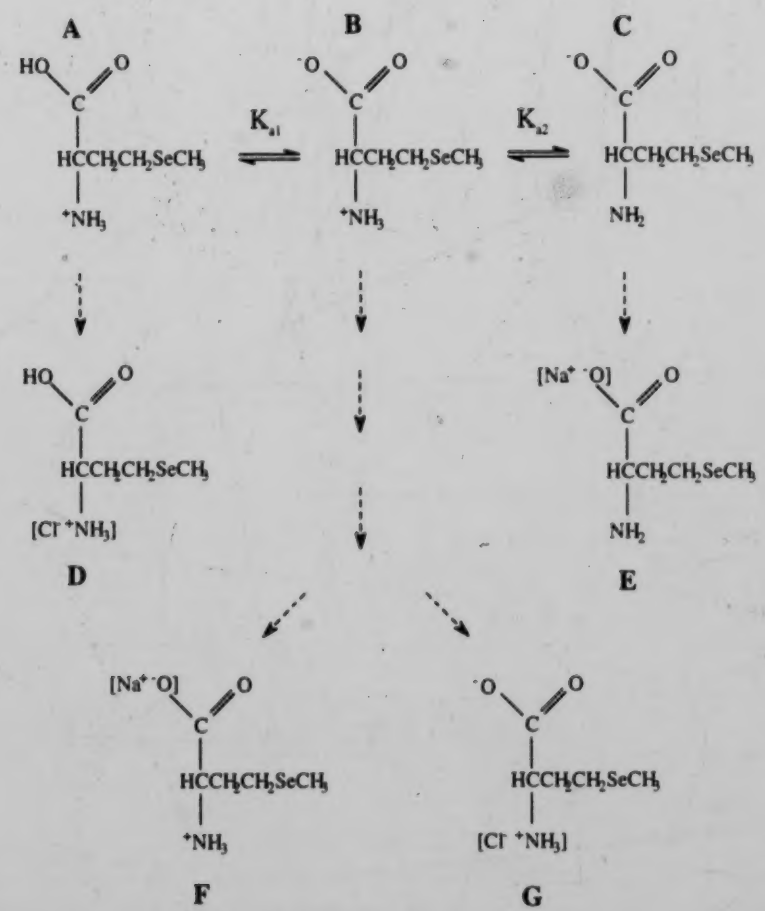

Figure 5.22 Diagram depicting various forms of selenomethionine present in solution (A,B,C) and in the gas-phase (D,E,F,G) as a function of varying aqueous solution pH.

at high acid and base concentrations and F and G are charged sodium and chloride adducts as observed in the mass spectra.

5.3.3.2 Selenocysteine

A positive ion mass spectrum of 0.22 mM selenocysteine is shown in Figure 5.23. In order to stabilize selenocysteine in the original stock solution, the pH was adjusted to 2.0 with the addition of hydrochloric acid. Subsequent dilution of this solution in methanol and addition of up to 1 mM sodium hydroxide was insufficient to generate electrospray mass spectra of anionic selenocysteine or selenocystine. The reason for the inability to produce a spectrum in the negative ion mode is unclear; the same difficulty has also been noted by Crews et al. [3].

5.4 Conclusions

Direct speciation of inorganic and organic forms of selenium by electrospray mass spectrometry has been demonstrated. A disadvantage of using methanol for determination of selenium is the reaction of selenite to form a methyl seleno-ester, which interferes with detection of selenate. Other disadvantages of ESMS that are not restricted to selenium include alteration of solution acidity, and increased potential for formation of ion adducts in low dielectric strength solvents. Dilution of aqueous samples by 10 to 100-fold in methanol also compromises absolute detection capabilities.

It is not clear at this stage as to the relative contributions of the methanolic dilution, the electrospray mechanism and the transfer of analyte to the gas-phase on the observed differences in the organo-sulfur and selenium species observed by mass spectrometry and those originally believed present in aqueous solution. However, the observation of both cationic and anionic forms of cysteine, methionine and selenomethionine in the same solution without addition of external acid or base suggests contributions from pre-concentration of protons or hydroxide within evaporating droplets.

Further development of selenium speciation capabilities by electrospray is warranted since it has the potential to provide unambiguous species identification which may be used with ICP for characterizing new forms of selenium in biological matrices. More importantly, however, is to first develop a sensitive and stable method for the electrospray of purely aqueous solutions, especially for generation of negatively charged ions. This goal is the focus of the following chapter.

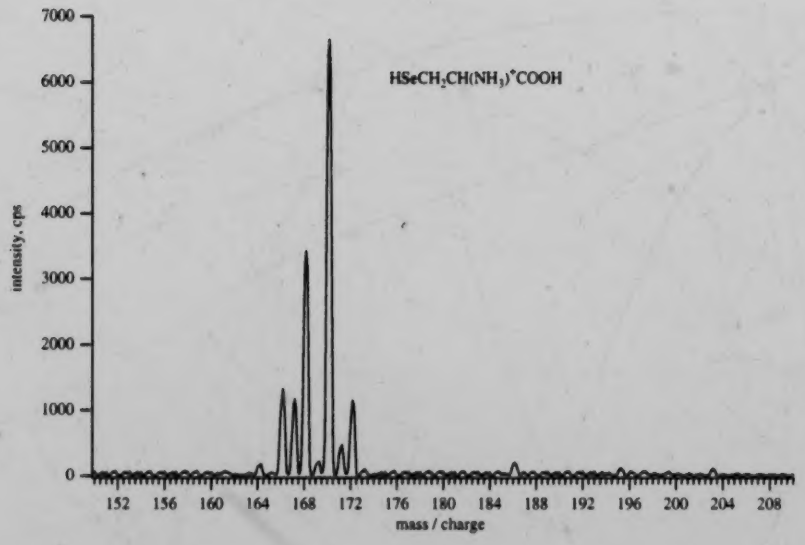

Figure 5.23 Positive mode electrospray mass spectrum of 0.22 mM selenocysteine.

5.5 References

1. Robberecht, H.; Van Greiken, R., *Talanta*, **1982**, 29, 823-844.

2. Cutter, G. A., *Anal. Chem.*, **1985**, 57, 2951-5.

3. Crews, H. M.; Clarke, P. A.; Lewis, D. J.; Owen, L. M.; Strutt, P. R.; Izquierdo, A., *J. Anal. At. Spectrom.*, **1996**, 11, 1177-82.

4. De-qiang, Z.; Han-wen, S.; Li-li, Y., *Fres. J. Anal. Chem.*, **1997**, 359, 492-6.

5. Emteborg, H.; Bordin, G.; Rodriguez, A. R., *Analyst*, **1998**, 123, 245-53.

6. Shapira, J. R. *Organic selenium compounds. Their chemistry and biology.*; Wiley Interscience: New York, 1971.

7. Shibata, Y.; Morita, M.; Fuwa, K., *Adv. Biophys.*, **1992**, 28, 31.

8. Kolbl, G.; Lintschinger, J.; Kalcher, K.; Irgolic, K. J., *Mikrochim. Acta*, **1995**, 119, 113-27.

9. Geurin, T.; Astruc, A.; Astruc, M.; Batel, A.; Borsier, M., *J. Chromatogr. Sci.*, **1997**, 35, 213-20.

10. Cai, Y.; Cabanas, M.; Fernandez-Turiel, J. L.; Abalos, M.; Bayona, J. M., *Anal. Chim. Acta*, **1995**, 314, 183-92.

11. Bird, S. M.; Uden, P. C.; Tyson, J. F.; Block, E.; Denoyer, E., *J. Anal. At. Spectrom.*, **1997**.

12. Bryce, D. W.; Izquierdo, A.; Castro, M. D. L. d., *J. Anal. At. Spectrom.*, **1995**, 10, 1059-63.

13. Johansson, K.; Andersson, O.; Olin, A., *Ananlyst*, **1995,** 120, 423-9.

14. Jakubowski, N.; Thomas, C.; Stuewer, D.; Dettlaff, I.; Schram, J., *JAAS*, **1996,** 1023-1029.

15. Furuta, N.; Shinofuji, T., *Fresenius J. Anal. Chem.*, **1996,** 355, 457-60.

16. Caldwell, K. A.; Tappel, A. L., *J. Chromatogr.*, **1968,** 32, 635.

17. Hagege, A.; Troyer, C.; Grasserbauer, M.; Leroy, M. J. F., *Mikrochim. Acta*, **1997,** 127, 113-8.

18. Tan, S. H.; Horlick, G., *Appl. Spectrosc.*, **1986,** 40, 445-59.

19. Houk, R. S., *Anal. Chem.*, **1986,** 58, 97A-105A.

20. Platzner, I.; Sala, J. V.; Mousty, F.; Trincherini, P. R.; Polettini, A. L., *J. Anal. Atom. Spec.*, **1994,** 9, 719-26.

21. Hill, S. J.; Ford, M. J.; Ebdon, L., *J. Anal. Atom. Spec.*, **1992,** 7, 1157-65.

22. Krushevska, A.; Kotrebai, M.; Lasztity, A.; Barnes, R. M.; Amarasiriwardena, D., *Fres. J. Anal. Chem.*, **1996,** 355, 793-800.

23. Goossens, J.; Vanhaecke, F.; Moens, L.; Dams, R., *Anal. Chim. Acta*, **1993,** 280, 137-43.

24. Olivas, R. M.; Quetel, C. R.; Donard, O. F. X., *J. Anal. At. Spectrom.*, **1995,** 10, 865-70.

25. Delves, H. T.; Sieniawska, C., *JAAS*, **1997,** 12, 387-9.

26. Yoshinaga, J.; Shirasaki, T.; Oishi, K.; Morita, M., *Anal. Chem.*, **1995,** 67, 1568-74.

27. Brown, P. G.; Davidson, T. M.; Caruso, J. A., *J. Anal. At. Spectrom.*, **1988,** 3, 763-9.

28. Stewart, I. I.; Barnett, D. A.; Horlick, G., *J. Anal. At. Spectrom.*, **1996,** 11, 877-86.

29. Blades, A. T.; Kebarle, P., *J. Am. Chem. Soc.*, **1994,** 116, 10761-6.

30. Dole, M.; Mack, L. L.; Hines, R. L.; Mobley, R. C.; Ferguson, L. D.; Alice, M. B., *J. Chem. Phys.*, **1968,** 49, 2240-9.

Chapter 6

Aqueous Electrospray Mass Spectrometry

6.1 Introduction

Electrospray ionization for the purpose of mass spectrometric analyses may be easily achieved using solvents such as methanol or acetonitrile. However, the extension of electrospray to aqueous samples is desirable from an analytical standpoint since water is the primary solvent for ionic analytes and the natural medium for environmental and life processes. The main reason for the lack of aqueous ESMS applications is the difficulty in establishing true electrostatic nebulization of water in the absence of a corona discharge. True ES nebulization is defined by the presence of a stable Taylor cone as described in the introductory chapter. Smith [1] observed that the onset potential for electrospray of a liquid increases with the square root of surface tension. Because of this dependence, the electric field necessary for the onset of a stable Taylor cone of water often exceeds that required for the ionization of air.

Sample and Bollini [2] reported electrostatic atomization of distilled water, which they described as "harmonic electrical spraying". The measured droplet diameters (d = 140-429 μm) were much larger than what may easily be desolvated and sampled in an ordinary mass spectrometer interface. Chowdhury and Chait [3] reported stable spray of aqueous solution using sharpened capillaries. In their report, the authors stated that by decreasing the outer radius of the capillary tip, the onset of stable electrospray could be achieved at absolute potentials lower than that leading to the discharge condition. Contrary to the authors' premise, it is the magnitude of the electric field, not the applied voltage that leads to discharge. Despite a reduction in the thickness of the capillary walls the electric field required for discharge or to establish a stable Taylor cone does not vary. The dependence of electric field on applied voltage and capillary radius is expressed as equation 6.01.

$$E \approx \frac{2V}{r_c \ln(4d/r_c)} \qquad 6.01$$

In addition, the authors describe the performance of their sharpened capillaries for aqueous nebulization; however, the spectra presented contained a minimum of 1%

acetic acid. Attempts to reproduce their observations in this laboratory for inorganic analytes were unsuccessful.

Kebarle et al. [4, 5] investigated a different approach to achieve aqueous electrospray without a discharge. Rather than modifying the ES source, they modified the electric stability of the ambient atmosphere by replacing air with sulfur hexafluoride gas, SF_6. Sulfur hexafluoride helps prevent the electron avalanche formally known as a corona discharge by quickly scavenging free gas-phase electrons. Improvements in analyte sensitivity and signal stability were observed for both positive and negative ion modes (PIM and NIM) of electrospray of aqueous solutions with the addition of SF_6 gas. However, sensitivity was lower by a factor of four in water relative to methanol. The difference in sensitivity was attributed to larger droplets and lower efficiency of ion formation from charged water, relative to methanol, droplets. The cost and availability of SF_6 gas is also a limiting factor to its application.

Recently, Wilm and Mann [6] characterized what they referred to as a nanoelectrospray ion source. It differs significantly from conventional electrospray sources in dimensions and performance. Capillaries of borosilicate glass (1.2 mm dia.) were pulled at one end and coated with gold to give a spraying orifice of 1-2 μm diameter. The bulk of the glass capillary served as a sample reservoir. The nano-ES source was operated in the absence of an external pump at flow rates (20 nL/min) dictated by the electrospray process. The low flow rate and small spraying orifice resulted in very small droplet sizes for various solvents, including water, and for buffer compositions not accessible to conventional ES sources.

The latest development in electrospray needle design is based on charge separation within a fused silica capillary by dc induction using a concentric cylindrical capacitor. Wang and Hackett [7] report production of gas phase ions from aqueous solution without application of an external high voltage, thus eliminating the risk of corona discharge. Their design consists of a concentric arrangement of a charged platinum wire inside a fused silica capillary all surrounded by a grounded cylindrical electrode. As liquid is pumped through the silica capillary, charge separation occurs radially within the silica capillary; and redox reactions responsible for charge neutrality are

thought to occur at the central platinum electrode. Results are preliminary and further detailed investigation is necessary to characterize and evaluate the performance of this design. However, the combination of low sample flow rates (50 – 500 nL/min) and isolation of the high voltage from atmosphere appears to result in small, highly charged aqueous droplets in the absence of a discharge.

Ionspray, an alternative to conventional electrospray for aqueous nebulization employs a flow of nitrogen gas concentric to the charged ES capillary to assist disruption of the liquid surface. A disadvantage of ionspray is the absence of a stable Taylor cone mode since pneumatic nebulization results in characteristically broader droplet size distributions with larger mean diameters than strict electrostatic nebulization. The implications of using ionspray for mass spectrometry are poorer sensitivity due to lower ion liberation efficiencies from droplets of lower charge density, strong mass spectral dependence on the relative position of the source, and high levels of ion pairs or adducts [8].

In this study, electrostatic nebulization of aqueous solutions of inorganic salts is observed directly from a fused silica capillary. Electrical contact to the sample solution is made at the syringe and a sheath electric field is applied concentric to the spraying tip to accelerate charged droplets into the MS interface region and reduce surface wetting of the ES needle. Preliminary results are presented for monovalent potassium, divalent cobalt and trivalent lanthanum ions in water.

6.2 Experimental

6.2.1 Aqueous Electrospray Design

The new electrospray needle design is depicted in Figure 6.01. A 20 cm length of fused silica capillary, FSC, was used as both the sample transfer line and the spraying

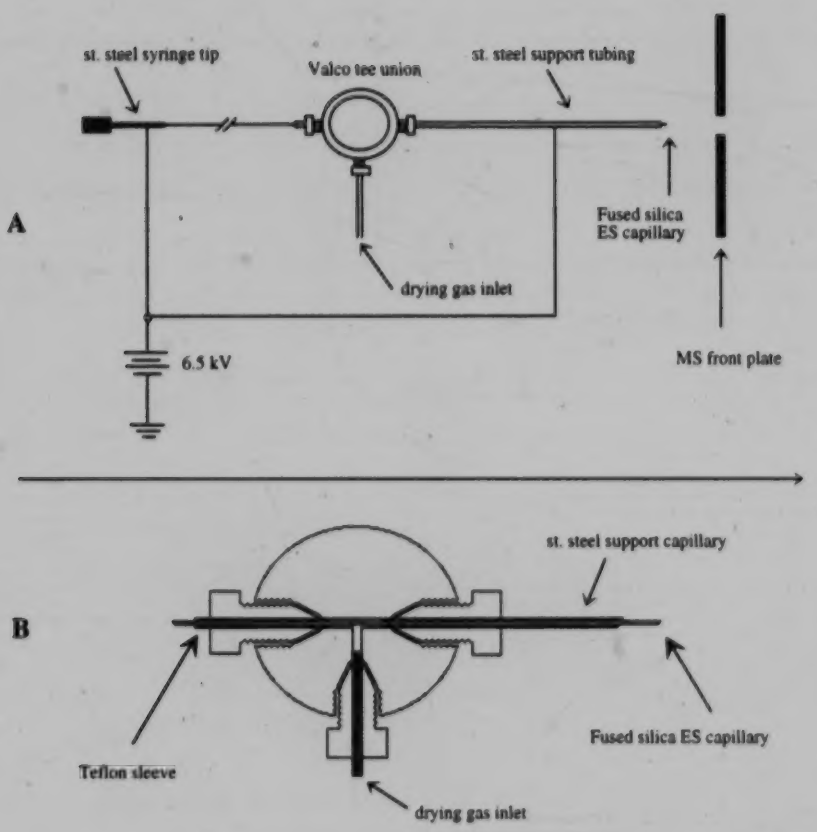

Figure 6.01 (A) Modified electrospray design and (B) expanded view of the plumbing within the Valco tee union.

capillary. The FSC had dimensions of 141 μm o.d. x 40 μm i.d. and was coated with a 17 μm thick layer of polyimide. A tee union supplied by Valco (Houston, TX) was used to hold the silica capillary in a fixed position inside a stainless steel support capillary (1/16" x 250 μm x 10 cm). The left port of the tee was lined with a flexible Teflon insert that when tightened held the FSC firmly in place and formed an airtight seal. The bottom port was used for introduction of a low flow of dry helium, concentric to the ES capillary. The gas flow was not used for external nebulization, rather to dry the outer wall of the capillary after rinsing the system with sample. The gas flow was stopped prior to collection of mass spectra since its flow was observed to be detrimental to both signal stability and sensitivity. The right port of the tee was used to hold the steel support capillary. There was no contact between solution in the capillary and the concentric steel support. A potential of 6.5 kvolts was applied directly to the steel capillary resulting in the formation of a "sheath" electric field. A similar potential was applied to the sample *via* a stainless steel luer adapter at the syringe. An expanded view of the electrospray capillary tip and support capillary is shown in Figure 6.02.

The connection between the sample syringe and the FSC is depicted in Figure 6.03. Teflon sleeves were mounted inside both 1/16" nuts of the internal union. The capillary passed through the union uninterrupted, held in place by the 250 μm i.d Teflon insert on the right side of the union. After loading the sample syringe, the FSC is inserted into the steel needle of the luer adapter, the steel needle is simultaneously inserted through the 1 mm Teflon insert on the left side of the union and sealed by tightening the nut. Sample is then pumped through the FSC to the spray with minimal mixing. The sample flow rate for this setup was 0.75 μL/min compared to 2.0 μL/min with the stainless steel ES capillary.

There are three important differences to note between the conventional ES source described in Chapter 2 and the new ES design detailed here. The use of a non-conductive fused silica capillary as a spray tip diminishes the risk of electric discharge, much like the design of Wang and Hackett [7]. The smaller diameter of the

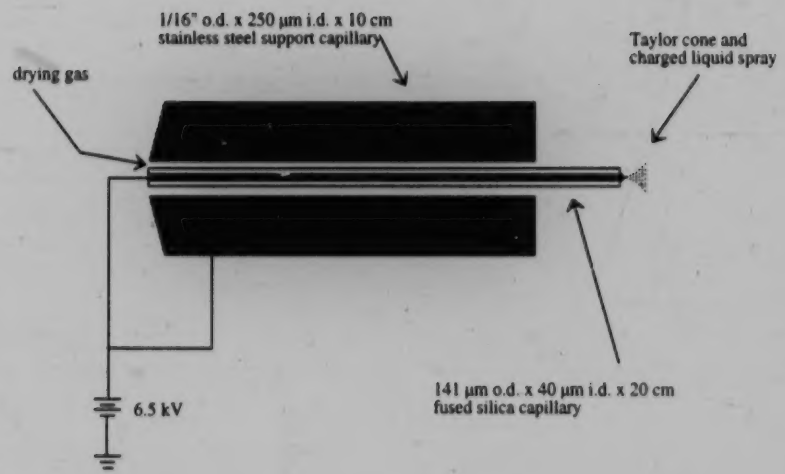
1/16" o.d. x 250 µm i.d. x 10 cm
stainless steel support capillary
Taylor cone and
charged liquid spray
drying gas
6.5 kV
141 µm o.d. x 40 µm i.d. x 20 cm
fused silica capillary

Figure 6.02 Expanded view of the electrospray tip and support capillary arrangement.

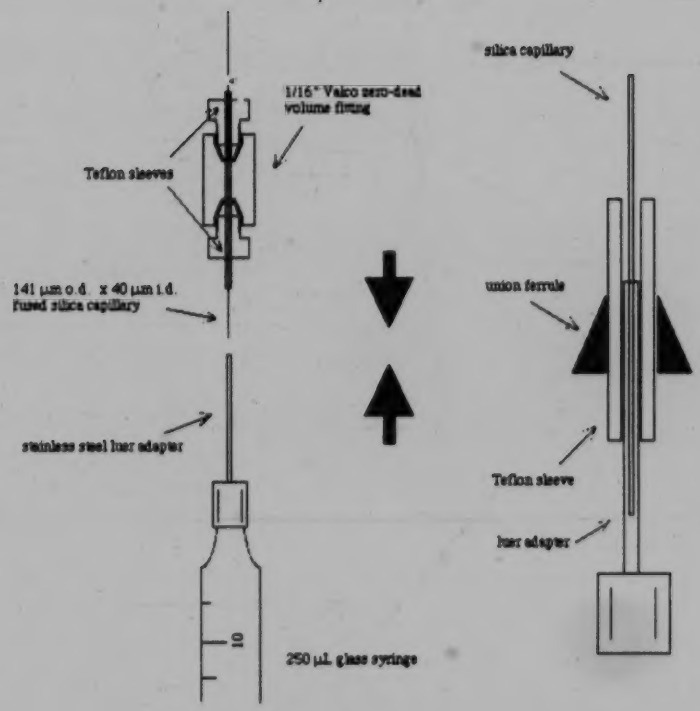

Figure 6.03 The syringe to fused silica capillary connection.

silica capillary reduces the amount of solvent to be electrically nebulized per unit time and results in smaller Taylor cone dimensions and droplet sizes. Thirdly, the potential applied to the solution and support capillary is greater than those observed to cause discharge in conventional ES experiments. Advantages of the silica capillary not directly related to its ES characteristics include that it may be more easily positioned and replaced than stainless steel. Rinse volumes are reduced because of improved plumbing at the syringe connection and the spraying tip. Memory effects were observed due to adsorption of cations, especially protons and sodium ions, to negatively charged sites on the capillary walls.

6.3 Results and Discussion

All of the preliminary results reported here have been acquired using positive ion mode since discharge does not occur as readily for positive as for negative voltages, presumably because the ES needle is electron deficient in the positive case. Ultimately, the goal of this design modification is to target negative ions in aqueous solution.

In terms of electrospray mass spectrometry, metal ions may be divided into three general classes based on their valency. Monovalent metal ions are generally of the least concern because of the simplicity of their gas phase chemistry. Divalent and trivalent metal ions generate much more interest. In subsequent sections, mass spectra acquired in purely aqueous solution of representative metal ions from each of these three classes are presented.

6.3.1 Operating Parameters

To date, few parametric investigations of this source have been undertaken, but a few points of particular concern will be highlighted. The position of the silica capillary relative to the stainless steel support sheath appears to be very important. When the capillary is extended more than two mm from the steel, liquid accumulates on the capillary and is liberated periodically in the form of large droplets visible to the naked eye. When the capillary does not protrude far enough from the stainless steel (< 1 mm) liquid migrates along the outer silica capillary wall and collects at the stainless

steel tube. This second phenomenon may be rationalized by the possibility that the electric field between the liquid at the spray tip and the steel sheath (V_{up}, 6.5 kV, <1 mm) may be greater than that from the spray tip to the mass spectrometer front plate (V_{up}, 600 V, 5 mm). The potential at the spray tip, V_{up}, can not be measured but will be less than 6.5 kV by an amount equal to the IR drop over the length the capillary. This could result in negative ions in solution being drawn to the stainless steel sheath rather than spray of positively charged droplets to the MS interface. Unfortunately, this behavior is not expected to be consistent over a range of sample concentrations since the absolute potential at the capillary tip will depend on the conductivity of the sample. For the 20 cm silica capillary it was necessary to use electrolyte concentrations ten-fold greater than those used with the conventional set-up to maintain a stable spray. Optimization of the needle-to-front-plate separation distance was also complicated due to the change in relative electric field between the capillary-front plate and capillary-sheath regions.

6.3.2 Lithium and Potassium Chloride

ES mass spectra of 1 mM lithium chloride and potassium chloride with a sampling plate to skimmer potential gradient, ΔV, of 18 volts (skimmer voltage = 9 volts) are shown in Figure 6.04. In the first spectrum there are two distributions of solvated ions, $Li(H_2O)^+_{2\text{-}13}$, and $H(H_2O)^+_{2\text{-}13}$. Similar distributions are observed for potassium: $K(H_2O)^+_{1\text{-}13}$ and $H(H_2O)^+_{2\text{-}15}$. The extent of solvation of both lithium and potassium in methanolic solution has been observed previously [9]. The maximum number of molecules of methanol observed in clusters acquired under mild conditions was five and four for lithium and potassium, respectively. The higher degree of solvation in aqueous solution is expected based on stronger ionic solvent properties of water.

The origin of the hydrated protons observed in these spectra is likely the acidic silanol groups on the capillary wall. The capillary was rinsed with 10 mM hydrochloric acid solution prior to spraying the 1 mM solutions of lithium and potassium. Removal of protons from the capillary wall could easily account for charge neutrality without the

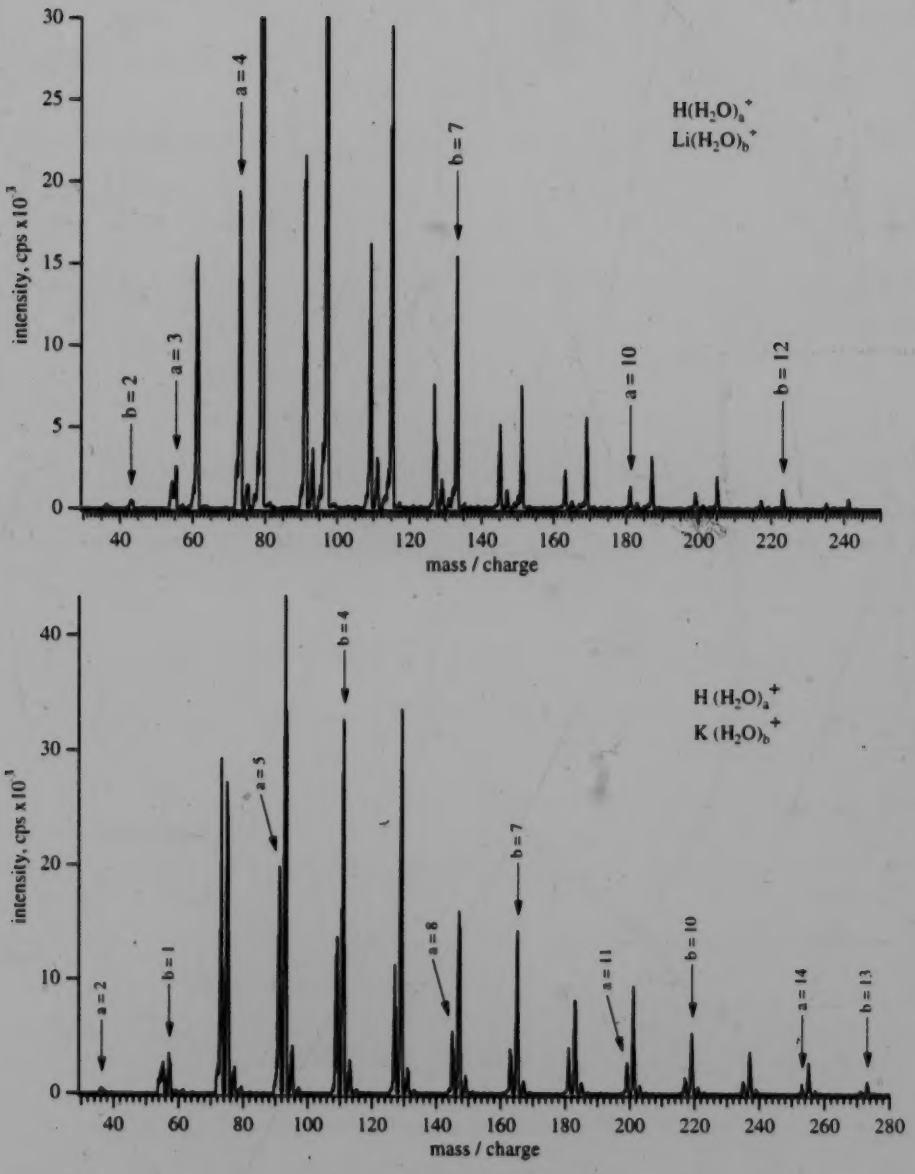

Figure 6.04 Mass spectra of (a) 1 mM lithium chloride and (b) 1 mM potassium chloride in distilled, deionized water, ΔV = 18 volts.

requirement for electrochemical oxidation of solvent or impurities at a metal surface. If this is the case, temporal stability of electrospray from silica might be expected as protons become depleted from the surface. Periodic conditioning of the capillary with acid may be required for optimal performance.

A mass spectrum generated for 1mM KCl by increasing ΔV to 193 volts is shown in Figure 6.05a. Aside from sodium that is present as impurity in the potassium salt, the dominant background ions in the spectrum are related to nitrogen. Bare elemental nitrogen is observed at *m/z* 14 along with CN^+, N_2^+, HN_2^+ and NO^+, at m/z 26, 28, 29 and 30, respectively. This spectrum is very simple compared to a background Ar-ICP spectrum, but the high sampling energy results in a substantial loss in analyte sensitivity from the spectrum in Figure 6.04b. An expanded view of the background from 10 to 70 mass units is shown in Figure 6.05b.

6.3.3 Cobalt Bromide

The ES mass spectrum of 1 mM cobalt (II) bromide with ΔV = 55 volts is shown in Figure 6.06. A range of solvent-clustered cobalt ions, $Co(H_2O)_n^{2+}$, is observed with n from 4 to 13. Note that the potential is much higher than that used to generate spectra from solutions of lithium and potassium. Larger cobalt ion clusters were not detected by lowering the sampling potential further, instead the spectra were dominated by a solvated proton distribution similar to those observed in Figure 6.04. Some protonated water clusters ($H^+(H_2O)_{3\text{-}5}$, *m/z* = 55, 73, 91) are observed in this spectrum, but the distribution has been shifted far to the left (i.e. lower mass) by the higher sampling plate voltage. Similar spectra have been reported for doubly charged metal ions in binary mixtures of methanol and water [10, 11] but at much lower collisional voltages.

Despite the high electrolyte concentration of 1 mM, no solvated metal-counter ion clusters, $CoX(H_2O)_n^+$, (where X = counterion) are observed in this spectrum, unlike those routinely observed in 0.1 mM methanolic solutions of multiply charged metals. Observation of such clusters as $Co^{2+}(H_2O)_{13}$, therefore suggest that individual ions are well separated in

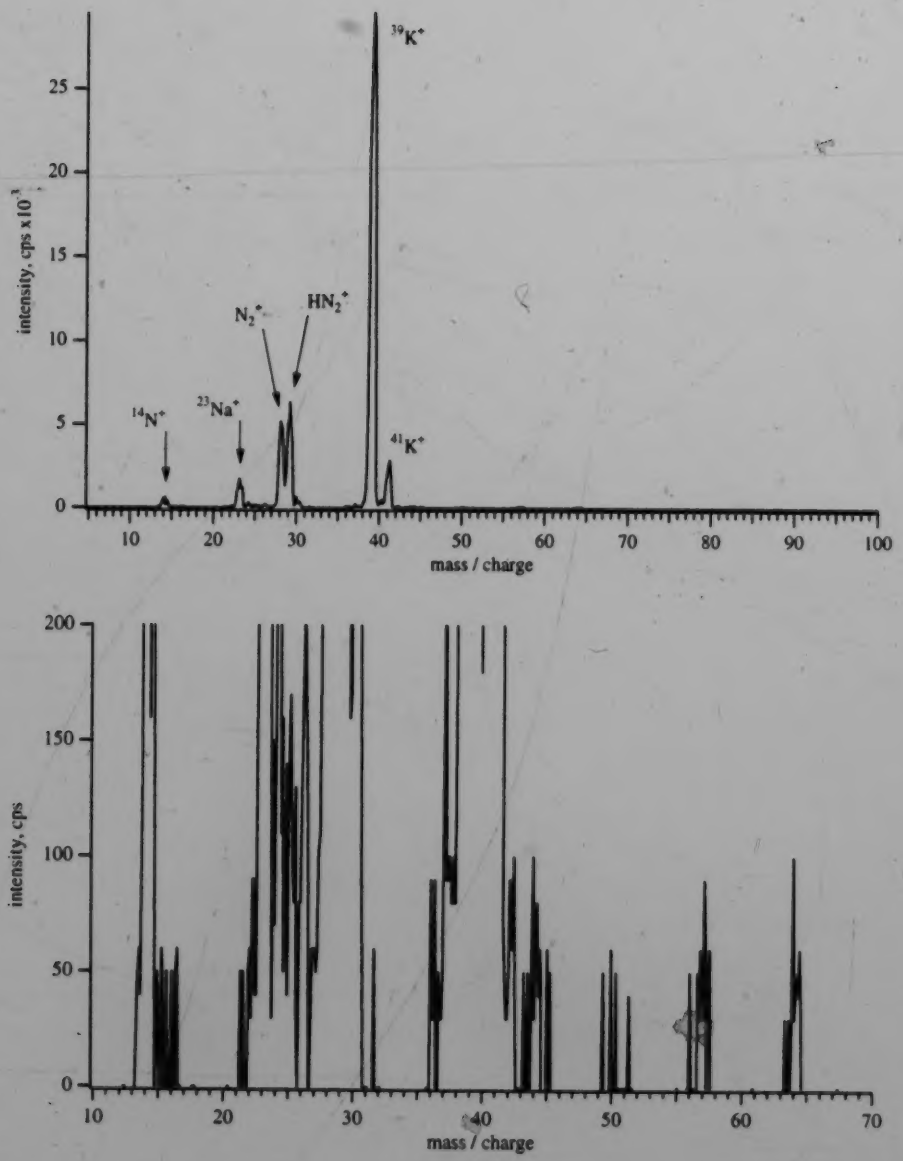

Figure 6.05 (a) Mass spectra of 1 mM potassium chloride in distilled, deionized water, (ΔV = 193 volts) (b) an expanded spectrum for the 10 to 70 *m/z* range.

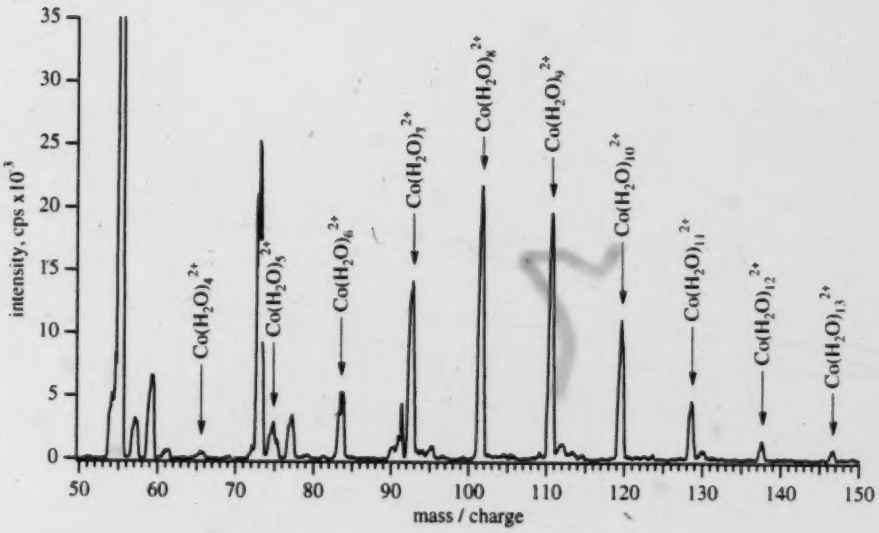

Figure 6.06 Mass spectrum of 1 mM cobalt bromide in distilled, deionized water, (ΔV = 55 volts).

solution at this concentration. Once this source is successfully extended to negative ions it will be interesting to look for anionic metal halide complexes, similar to those detected in methanol in Chapter 3. One may speculate that species indicative of gas-phase ionic interactions such as $CaCl_3^-$ will be less likely when spraying water, which is better able to individually solvate ions than a lower dielectric medium like methanol.

6.3.3 Lanthanum Nitrate

Mass spectra of 1 mM lanthanum nitrate acquired with ΔV settings of 73 and 293 volts are shown in Figure 6.07. Three distributions of solvated lanthanum ions can be identified in this spectrum: $LaOH^{2+}(H_2O)_{0\text{-}12}$, $LaNO_3^{2+}(H_2O)_{3\text{-}10}$ and $La^{3+}(H_2O)_{16\text{-}25}$. This spectrum marks the first reported observation of a trivalent metal ion with an aqueous solvation sheath in the gas phase. Note that every third solvated La^{3+} ion, i.e. $La^{3+}(H_2O)_{15,\ 18,\ 21\ and\ 24}$ overlaps with every second solvated lanthanum nitrate adduct, $LaNO_3^{2+}(H_2O)_{4,\ 6,\ 8\ and\ 10}$. The origin of lanthanum hydroxide may be either gas phase charge separation or hydrolysis of lanthanum in solution, as written in equations 6.02 and 6.03.

$$La(H_2O)_{16}^{3+} + N_2 \rightarrow LaOH^{2+}(H_2O)_{14} + H_3O^+ + N_2 \qquad 6.02$$

$$La(H_2O)_6^{3+} + N_2 \rightarrow LaOH^{2+}(H_2O)_5 + H_{aq}^+ \qquad 6.03$$

If it is assumed that in solution lanthanum is hexa-coordinate, i.e. there are six water molecules in the inner coordination sphere of lanthanum, the hydrolysis reaction may be written for the hexa-aquo ion with the loss of a proton. With the hexa-coordinate nature of lanthanum in mind, the definition of an ion-solvent cluster or complex begs attention. Is a triply charged lanthanum ion that is solvated by 25 water molecules in the gas phase, shown in Figure 6.07, a coordinated ion-solvent cluster or a nano-droplet? At what stage does condensed phase chemistry end and gas phase chemistry begin?

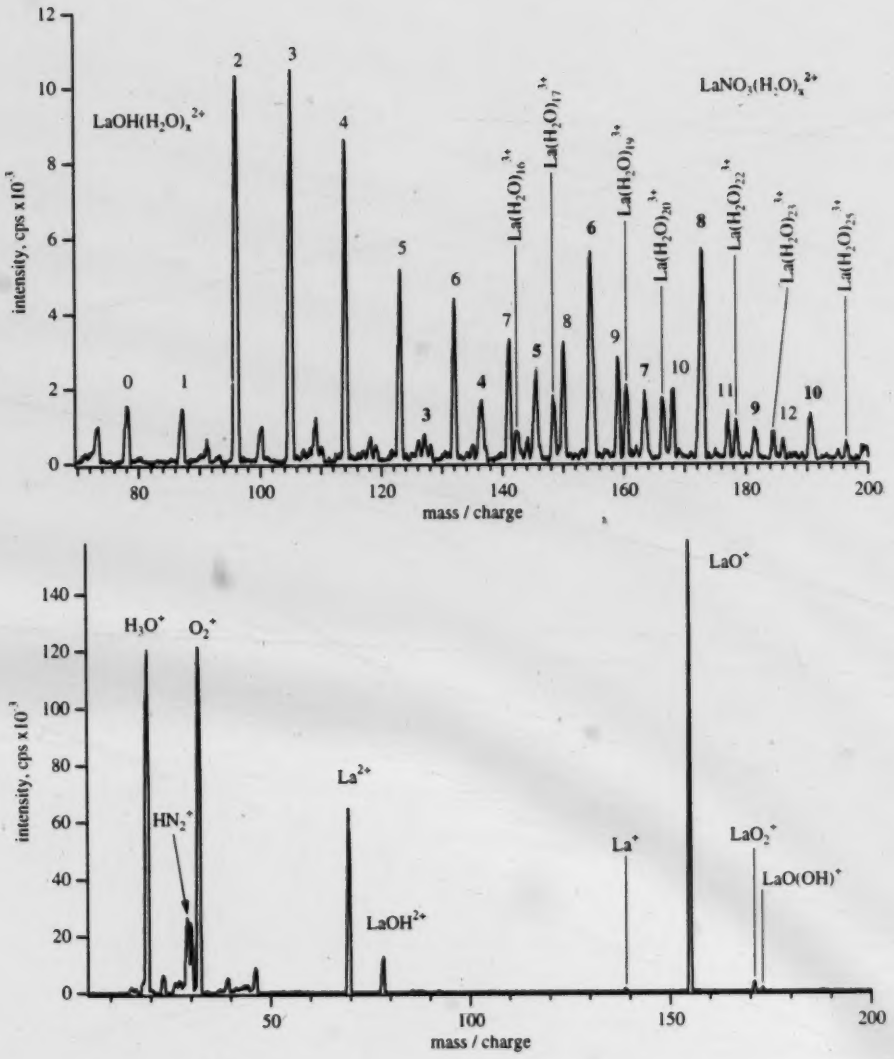

Figure 6.07 Mass spectra of 1 mM lanthanum nitrate in distilled, deionized water at ΔV settings of (a) 73 and (b) 293 volts.

An increase in the ΔV to 293 volts results in a reduction of the complexity of the spectrum. Several lanthanum species may be identified, but the dominant ions are La^{2+} and LaO^+ at *m/z* 69.5 and 155, respectively. Several background ions are observed at *m/z* < 50. There are some distinct differences between this background and that observed in Figure 3.04 for a potassium matrix. In Figure 3.04, no protonated water, H_3O^+, or oxygen, O_2^+, was observed in the spectrum. At 300 volts sampling potential these two species should be efficiently dissociated, but in this case they are not formed until late in the collision region. The origin of the proton in this spectrum is not from the capillary walls, free acid in solution or the relatively gentle gas phase charge separation given in equation 6.02, but rather from the following energetic reaction.

$$LaOH(H_2O)^{2+} + N_2 \rightarrow LaO^+ + H_3O^+ + N_2 \qquad 6.04$$

A mechanism for the formation of O_2^+ by collisional dissociation of a lanthanum species is not as clear and attempts to assign one would be based on solely on speculation. It is important to remember that the precursors to all of the CID products observed in this spectrum were small charged droplets sampled from the electrospray plume into the mass spectrometer interface. The level of solvation may vary broadly between ions and in turn so may the collisional path they follow to reach complete desolvation. This may explain the variety of species present in Figure 6.07, but complete delineation of all collision pathways is not likely possible.

6.4 Conclusions

Preliminary results using a modified electrospray needle for the generation of ES mass spectra from aqueous solutions are promising. Observation of solvated distributions of lithium, potassium, cobalt and lanthanum derived from 1mM concentrations of their inorganic salts was achieved without generation of discharge species. Several fundamental investigations of this design remain to be performed including the interdependencies of electrolyte concentration, length of fused silica capillary, and applied voltage on the apparent voltage at the floating ES capillary tip. The relation between the sheath and ES voltages must also be examined in detail.

Some contribution to the ES process may be expected from electroosmotic and electrophoretic processes within the capillary; their relative contributions will likely vary with solution properties and sample flow rates.

Ultimately, the extension of this source to production of negative ions is the goal to be accomplished, but several interesting results have been observed for simple metal cations in aqueous solution. Use of this capillary arrangement has resulted in significant improvement in the stability of both negative and positive ion modes using methanolic solution over the original stainless steel design. Memory effects caused by insufficient rinsing of the original ES source have also been greatly reduced.

6.5 References

1. Smith, D. P. H., *IEEE Trans. Ind. Appl.*, **1986,** IA-22, 527-35.

2. Sample, S. B.; Bollini, R., *J. Colloid Sci.*, **1972,** 41.

3. Chowdhury, S. K.; Chait, B. T., *Anal. Chem.*, **1991,** 63, 1660-4.

4. Wampler, F. M.; Blades, A. T.; Kebarle, P., *J. Am. Soc. Mass. Spectrom.*, **1993,** 4, 289-95.

5. Ikonomou, M. G.; Blades, A. T.; Kebarle, P., *J. Am. Soc. Mass. Spectrom.*, **1991,** 2, 497-505.

6. Wilm, M.; Mann, M., *Anal. Chem.*, **1996,** 68, 1-8.

7. Wang, H.; Hackett, M., *Anal. Chem.*, **1998,** 70, 205-12.

8. Olesik, J. W.; Thaxton, K. K.; Olesik, S. V., *J. Anal . At. Spectrom.*, **1997,** 12, 507-16.

9. Agnes, G. R. PhD Thesis, Unversity of Alberta, Edmonton, Alberta, 1994.

10. Blades, A. T.; Jayaweera, P.; Ikonomou, M. G.; Kebarle, P., *Int. J. Mass. Spectrom. Ion. Proc.*, **1990,** 102, 251-67.

11. Blades, A. T.; Jayaweera, P.; Ikonomou, M. G.; Kebarle, P., *J. Chem. Phys.*, **1990,** 92, 5900-6.

Chapter 7

Conclusions

7.1 Summary

The earliest investigations of elemental analysis by electrospray highlighted the potential of generating gas-phase multivalent metal ions and detecting them by mass spectrometry. The unique nature of electrospray, whereby solution ions are stabilized by solvation during transfer to the gas phase at atmospheric pressure, seemed well suited to this goal. The ability to generate solvated metal clusters and then sequentially remove solvent in a collision cell provided many new insights into both solution and gas-phase thermodynamic equilibria. However, the pursuit of valence state speciation of metals quickly faded upon the realization that regardless of the energy of the ion source it is not possible to generate metal ions in their original multivalent charge state in the absence of a stabilizing solvent sheath or ligand. In addition, the energy available *via* collision induced dissociation in the atmospheric pressure interface is often insufficient to dissociate solvent derived metal oxides. At best it was possible to generate a spectrum of charge reduced metal ions, similar in appearance to that observed by ICP-MS, but sensitivities were poor because of defocusing in the high energy collision interface.

The state of the art of elemental analysis by ESMS in 1994, the year in which these studies were begun, was clearly shifting away from the development of a universal analysis method and towards niche applications, for use in a complementary role to other atomic sources. At the time there were two factors that formed the basis for targeting analysis of anions by ESMS. The first factor is that as a group, the nonmetals pose the most difficulty for analysis by classical atomic spectroscopy and these elements exist predominantly in anionic forms in solution. The second factor was that lower energies are required for gas-phase charge reduction of anionic gas phase ions, which should result in better sampling and detection capabilities. The difference in energy is caused by the fact that generation of bare M^+ ions requires dissociation of solvent derived metal oxide bonds, whereas the formation of HXO_4^- (where X = As, S, Se..) from a divalent oxo-anion, XO_4^{2-}, involves proton transfer from a solvent molecule.

Use of negative ion mode, NIM, detection to determine monovalent halogen ions is analogous to determination of alkali metals using positive ion mode, PIM, but it is more difficult because of a greater tendency of the source to discharge. The investigation of halogen quantitation had several important implications for later studies of more complex anionic species. One of the most valuable results of the halogen investigation was the definition of stable ES operating parameters that could be used to generate reproducible anionic mass spectra on both a short and long-term basis. The role of CID in the atmospheric pressure interface was evaluated and settings were optimized to ensure complete analyte desolvation without altering speciation of oxo-anionic forms of chlorine, bromine and iodine. The degree of analyte solvation observed in mass spectra acquired with gentle CID conditions was greatest for ions of highest charge to radius ratio. Potential gradients, ΔV, in excess of 30 volts were required to desolvate fluoride ions while bare iodide was detected with gradients as low as 9 volts.

Linear calibration plots were established for fluoride, chloride, bromide, iodide, chlorate, perchlorate, bromate and iodate with the addition of 0.1 mM levels of inert electrolyte, which acted to stabilize the ES process. The signal from the stabilizer ion was also used as an internal standard to correct for analyte suppression or enhancement caused by changes in total electrolyte concentration or solvent composition. Limits of detection for these ions were in the part-per-billion range in methanol; necessary dilution of aqueous samples compromised absolute detection limits in water by at least an order of magnitude. Potential metal ion interferences were observed but not extensively examined; these may lead to erroneous quantitation and should be investigated further. Suppression of fluoride intensity by cationic surfactant could not be corrected for by internal standardization, but reliable determination of fluoride in commercial mouthwash samples was achieved by both standard additions and matrix matching.

Several advantages of NIM analysis for determination of metals as anionic EDTA complexes were reported in Chapter 4. EDTA was the complexing agent of choice because it was known to form stable complexes with several different metal ions. Divalent metal ions generate doubly charged complexes, which can be observed

directly in the mass spectrum, or protonated by either decreasing solution pH or *via* collisions with water in the sampling interface, and observed as monovalent ions. Preservation of divalent complexes was necessary in order to lower the mass to charge ratio such that they could be detected on the ELAN Model 250 mass spectrometer. Determination of complexes of trivalent metal ions was limited to using a SCIEX API-100 LCMS. The importance of the role of CID in sampling of singly and doubly charged ions became apparent when using the latter instrument. An increase in CID energy when sampling divalent, uncomplexed EDTA, H_2Y^{2-}, was observed to result in efficient charge reduction by proton transfer to produce H_3Y^- in the mass spectrum. Low CID energies also resulted in observation of large singly charged agglomerates of Al-EDTA complexes and sodium nitrate. Several ionic fragments of EDTA could be generated when the CID potential, ΔV, was increased beyond 50 volts.

The simultaneous characterization of anionic and "cationic" solution composition renewed interest in ESMS as a one-stop elemental analysis technique. A detailed interpretation of complexation equilibria was complicated by the electrospray solvent limitation, but quantitative complexation of calcium was verified by a simulated water hardness titration using MS detection. The titration endpoint was marked by detection of free indicator ion and leveling off of Ca-EDTA intensity with further additions of EDTA.

Speciation of inorganic (selenate and selenite) and organic (selenomethionine and selenocysteine) forms of selenium was presented in Chapter 5. Selenate ion was detected as monovalent biselenate, despite the fact that it is a weak conjugate base in solution, due to proton transfer in the gas phase. Selenite reacted with methanol in solution to produce a methyl seleno-ester; and a similar reaction was observed for sulfite with methanol. Confirmation of the seleno-ester formation was achieved by ESMS in deuterated methanol, ethanol, and isopropyl alcohol solvents. All of the selenium species targeted had acid/base properties, but the zwitterionic character of seleno-amino acids adds further complication to their determination. Mass spectra acquired using NIM and PIM for selenomethionine, selenocysteine and their sulfur

containing analogues were very similar, but positive mode detection was more sensitive.

The underlying theme that became apparent during the studies of metal complexation by EDTA and selenium speciation was the difficulty associated with the interpretation of results derived from non-aqueous solution. Extension of electrospray to aqueous solutions was the focus of the work presented in Chapter 6. A simple modification of the electrospray source employing a sheath electric field around a small diameter fused silica capillary resulted in sensitive detection of triply charged lanthanum with an aqueous solvation sphere. Extension of this source to NIM operation has not yet been achieved.

7.2 Future Work

The first task at hand is to characterize the operational parameters of the modified electrospray source described in Chapter 6 for PIM and NIM operation with aqueous solvents. Reliable characterization of ES functioning modes will require comparison of mass spectrometric ion current, visual observation of the spraying tip and construction of ES current to applied voltage plots, preferably simultaneously. In the event that this source can not be successfully used for NIM operation, other approaches for aqueous electrospray must be pursued, a possible candidate is the design recently described by Wang and Hackett [1] and discussed in Section 6.1. Other developments and areas for further study may be divided into three general categories: (1) instrument modifications, (2) qualitative analysis and (3) quantitative analysis/method development. Some suggestions in each of these categories follow.

7.2.1 Instrument Modifications

The Perkin Elmer/SCIEX ELAN Model 250 is a first generation mass spectrometer designed for use with an inductively coupled plasma source. This mass spectrometer is not only outdated for ICP operation, but also has several limitations for use with an electrospray source. A few of the limitations include a restrictive mass range, poor entrance ion optics, slow data acquisition and inflexible software. Realistically, the

most efficient means to overcome these limitations, though not necessarily the easiest solution, is instrument replacement.

Other less drastic modifications, which would improve the overall performance of the ELAN 250 system, include changes to the atmospheric pressure interface. An increase in the size of the sampling plate orifice combined with an increase in the pumping capacity of the first vacuum region may result in more efficient sampling of the ES ion current and alleviation of space charge effects. Increased pump capacity may be achieved with an upgrade to the Edwards Model 18 roughing pump or addition of a turbomolecular pump. Addition of an optical imaging microscope for on-line visual monitoring of electrospray operation would also be an immensely valuable diagnostic tool. Finally, the design and application of a reliable flow injection interface for sample introduction is long overdue.

7.2.2 Qualitative Analysis

The fastest developing trend in inorganic electrospray is as a characterization tool for synthetic chemistry. High molecular weight inorganic catalysts and pigments are ideally suited for ESMS detection. This class of analyte unfortunately requires a higher mass range than is currently available in our laboratory. Air and water sensitive compounds also represent a potentially broad class of analytes that may be characterized by ESMS in polar, non-aqueous solvents under a dry nitrogen atmosphere. Qualitative identification of metal speciation in environmental samples or aged solutions is becoming of increasing interest, particularly for metals that readily hydrolyze and exhibit varying degrees of oxo-anionic polymerization depending on solution conditions, such as chromium, molybdenum and tungsten.

7.2.3 Quantitative Analysis

There is plenty of potential for quantitative analysis and sample specific method development for determination of low molecular weight anions in aqueous solution. The effect of aqueous sample pH on analytes with acid/base properties needs to be investigated further. Metal complexation in the presence of multiple ligands and organic acids is an interesting area that has direct implications on bioavailability and

transport of metals in environmental samples. EDTA and other ligands may be used to evaluate relative complex strengths and as potential masking agents for interference free determination of anions. Simultaneous determination of free and hydrolyzed forms of the same metal using complexation e.g. Cr(III) as Cr(EDTA)$^-$ and Cr (VI) as $HCr_2O_7^-$ is also a potential avenue for investigation.

7.3 References

1. Wang, H.; Hackett, M., *Anal. Chem.*, **1998**, 70, 205-12.